Summer 2015

Small signal modeling and analysis of microgrid systems

Md. Rasheduzzaman

SMALL SIGNAL MODELING AND ANALYSIS OF MICROGRID SYSTEMS

by

MD. RASHEDUZZAMAN

A DISSERTATION

Presented to the Graduate Faculty of the

MISSOURI UNIVERSITY OF SCIENCE AND TECHNOLOGY

In Partial Fulfillment of the Requirements for the Degree

DOCTOR OF PHILOSOPHY

in

ELECTRICAL ENGINEERING

2015

Approved by

Dr. Jonathan Kimball, Advisor
Dr. Mariesa Crow
Dr. Mehdi Ferdowsi
Dr. Pourya Shamsi
Dr. Bruce McMillin

PUBLICATION DISSERTATION OPTION

This dissertation has been prepared in the form of four papers.

Pages 9–40 have been published as *An Accurate Small-Signal Model of Inverter-Dominated Islanded Microgrids Using dq Reference Frame*, IEEE Journal of Emerging and Selected Topics in Power Electronics, vol. 2, no. 4, December 2014 with Md. Rasheduzzaman, Jacob A. Mueller, and Jonathan W. Kimball.

Pages 41–64 have been submitted as *Reduced Order Small-Signal Model of Microgrid Systems – Part I*, IEEE Transaction on Sustainable Energy (2015), with Md. Rasheduzzaman, Jacob A. Mueller, and Jonathan W. Kimball.

Pages 65–89 have been submitted as *Reduced Order Small-Signal Model of Microgrid Systems – Part II*, IEEE Transaction on Sustainable Energy (2015), with Md. Rasheduzzaman, Jonathan W. Kimball, and Jacob A. Mueller.

Pages 90–104 have been published as *Markov jump linear system analysis of microgrid stability*, American Control Conference (ACC), 2014, with Md. Rasheduzzaman, Tamal Paul, and Jonathan W. Kimball.

ABSTRACT

This dissertation focuses on small-signal modeling and analysis of inverter based microgrid systems. The proposed microgrid consists of two microsources placed on two different buses. The buses are connected using a distribution feeder with some impedance. The proposed microgrid can operate with the grid support, or without the grid support. When operated without the grid support, the standalone system's microsources participate in controlling the system voltage and frequency. For a non-inertia source, such as the inverter, the load perturbations play an important role in system dynamics. In paper-I, such complex system was studied.

In the grid-tied mode, the microsources share the load demand with other sources that are present in the main grid. The control algorithm for such system is much simpler than that of the islanded system. However, when aggregated in multi-bus system, prohibitively higher order state-space models are formed. In paper-II, a reduced order modeling of such systems was considered. Singular perturbation method was applied to identify the two time-scale property of the system. In paper-III, a similar approach was taken to develop a reduced order model of the islanded system that was developed in paper-I. Application of such reduced order models were illustrated by using them to simulate a modified IEEE-37 bus microgrid system.

The islanded microgrids system's stability is characterized in paper-IV by the Markov Jump Linear System Analysis. Conservative bounds on the expected value of the state were determined from a combination of the Markov process parameters, the dynamics of each linear system, and the magnitude of the impulses. The conclusions were verified with the simulation results.

ACKNOWLEDGMENTS

I would like to express my sincere appreciation to my advisor, Dr. Jonathan Kimball, for his guidance, encouragement, and support throughout the course of this work. I am grateful that Dr. Kimball has spent a significant amount of time from his busy schedule to advice me to successfully complete this dissertation. I gratefully thank my Ph.D. committee members Dr. Mariesa Crow, Dr. Mehdi Ferdowsi, Dr. Pourya Shamsi, and Dr. Bruce McMillin for enlightening discussions and suggestions.

It has been a great pleasure to work with Jacob Mueller. His constant efforts in improving the hardware test bed have made the laboratory setup an ideal tool for graduate research. I would also like to thank my fellow students in the power lab. Special thanks go to my parents, my brother and my wife for their continuous support in chasing my dreams.

TABLE OF CONTENTS

SECTION

LIST OF ILLUSTRATIONS

LIST OF TABLES

SECTION

1. INTRODUCTION

1.1. MOTIVATION AND OUTCOME OF THE RESEARCH

Distributed energy sources (DERs) such as solar, wind, fuel cells etc. are now considered to be viable alternatives for conventional fossil fuel based generation systems to address the environmental concerns. As the national grid gets ready for integrating the renewable energy sources as a part of modernizing the current grid architecture, the need for microgrids has never been more obvious. Microgrids can facilitate the grouping of these sources into smaller subsets which are easier to manage and operate. As an added advantage, the system reliability may be improved by islanding and operating these smaller subsets of the power system.

Although the autonomous grids have been around for many decades, the concept of a microgrid [1] is still new and requires some attention before they could be implemented successfully in the power grid. Olivares et al. has described microgrid as a cluster of loads with DER units and Energy Storage Systems (ESS) connected to the distribution grid at the point of common coupling (PCC) [2]. The microgrids became more popular in the recent past when the use of small-scale renewable energy sources, such as solar-Photovoltaic (PV) and wind power, increased in the main grid [3]. The number of microgrids has increased over the last 10 years not only in Europe but also in US. A research report shows that, there are currently 219 operational, under construction, or planned microgrid projects in US [4].

A microgrid can operate in grid-tied mode or in islanded mode. An existence of the PCC terminal in the microgrid network means that the microgrid supports both modes of operation. When transitioning from islanded to grid-tied operation, the coordination

between the microsource and ESS generation, the PCC breaker and the power grid is done using the central controllers [5]. However, a lower level microsource controller is responsible for the output power generation. In grid-tied mode, the microsource controller controls the active and reactive power output, which is proportional to a reference. The reference power could be determined by the central controller, the Maximum Power Point Tracker (MPPT) or by the user. In most cases, the DER does not participate in supplying the reactive power to the main grid. However, at times there might be a requirement of bus voltage regulation in the events of intermittent faults. In an islanded mode of operation, the microsource controller's primary objectives are to maintain the standard voltage and frequency level throughout the system. In the process, the DERs participate in system's load sharing. Several power-sharing control algorithms such as droop control, model predictive control, and multi-agent based control exists. However, the droop based DER operation is the most simple and well-understood method that is studied in several scholarly articles [6, 7, 8, 9, 10].

In the power systems network, generating units such as synchronous machines have been used for over a century as a reliable means of power-supply. However, with the continuous growth in interest in renewable energy sources, and modernization of the current grid structure, power electronics based generating units are not too far from dominating the generating stations. These power electronics converters lack inertia. Under constant load perturbation, these low inertia units can result in frequency deviations and affect the overall system's stability [2].

Development of the mathematical models of microgrids is required to understand the system characteristics e.g. dynamic response analysis, stability analysis, modeling the parameter uncertainty, effect of the load perturbation etc. Mathematical models allow engineers to determine the eigenvalues of the system. The system states associated with the eigenvalues with dominant dynamic characteristics can be isolated using the participation factor analysis. The model gives insight to the individual system parameters governing the

system response. Another important aspect of the mathematical model is, these models can be used to perform the power flow analysis of the islanded microgrid system [11]. The conventional power flow algorithms fail to converge in a case like this due to the absence of the slack bus.

The primary motivation behind this work is to model the microgrid systems and address the inaccuracies that existed in the previous works in developing the models of the inverter-based systems. The model presented in this dissertation is more accurate and suitable for industry applications. In developing the model, all the circuit parasitic elements are considered. Models are developed for both the grid-tied and the islanded system. The controller operations are investigated in the Matlab/Simulink platform and their mathematical models are formulated in the time domain. To find the eigenvalues, the non-linear equations are linearized against a stable operating point. These linearized equations are used to form the small-signal state space model of the system.

However, the mathematical model with higher accuracy tend to include all the parasitic elements of the circuit. Such model contains both the slow and fast dynamics. This makes the system "stiff" and difficult to simulate. The mathematical model of a multibus microgrid become much time-consuming when this stiff model is simulated. The literature survey shows that, a very few work has been accomplished to reduce the order of the inverter based microgrids. An attempt has been made to address this issue in this dissertation.

A simulation based study on the reduced order small-signal model of dc microgrids was presented in [12]. The model is inapplicable to an ac system, where the dynamics of PLL is important in determining the system stability. In [13], an ac microgrid was modeled with all the parasitic elements, which made the model difficult for simulation in a multi-bus system. The proposed reduced order model in this paper alleviates this problem. A simplified converter modeling for application in microgrid was discussed in [14]. The model is applicable to peak current-mode control algorithm only. Also, the output coupling filter, which is important for harmonics rejection, was ignored in the model.

The microgrid model in [15] was used for dynamic stability analysis. The model is unsuitable for a microgrid which is dominated by the inverter based DERs. In [16], a reduced order mathematical model of the ac microgrid was presented based on the droop control gains only. The voltage controllers were completely ignored assuming that they have faster dynamics. For a stable operation of the DER, the inner loop is designed faster than the outer loop. As a result, the voltage controller can not be ignored in reduced order modeling, which is shown in this paper. Also, the model was claimed to be a lower computational burden for simulation. However, no time comparison data was presented to show the effectiveness of the reduced model. In this paper, a time comparison between the full order model and the reduced order model of a multi-bus microgrid is presented. The comparison shows that, the reduced order model is a lower computational burden for the simulator.

A review of model order reduction methods was presented in [17]. The reduction methods are divided into three types: Singular value decomposition (SVD) based methods, Krylov based methods, and iterative methods combining aspects from both SVD and Krylov methods. Of these methods, the singular value decomposition method is the most popular [18, 19]. In SVD, the system is first balanced based on the controllability and observability grammians and then the determination of the number of important states is made based on the Hankel singular values (HSV) [20]. However, this method works only with the linearized model. Also, the system's model order can not be reduced without using the expensive grammian routines. The SVD methods are heavily dependent on the input-output relationship of the system too. To overcome these challenges, the singular perturbation method is considered for model order reduction in this work. The slow and the fast system states are determined from the model parameters, which eliminates the need for determining the controllability and the observability grammians.

The islanded system's stability in light of the load perturbation becomes an important issue as the DER inverters lack inertia. Literature review shows different techniques for

determining the system's stability criteria. A method for computing the small-signal stability boundaries for large scale power systems was presented in [21]. In [22], the dynamic stability of the isolated power system was discussed. Synchronous machines were considered to model the system in those papers, which includes the rotor inertia. An impedance-based stability analysis was done for the inverter based microgrids in [23, 24]. Only the grid-tied converters were considered in those papers where the grid dynamics were ignored by setting it as a constant voltage source. As a result, the impedance-based method becomes difficult to apply in an islanded system. The stability of an isolated microgrid system was evaluated in [25] using the Nu-gap method. The stability study considered the load variation. The system was modeled assuming that the filter capacitor was lumped with the load capacitance and the grid-side inductance was lumped together with the inverter side inductance. Instead of using the conventional small-signal models, microgrid stability in the global/semi-global sense was discussed in [26] based on the polynomial Lyapunov function. A two-point estimate based method for probabilistic analysis of the small-signal stability of microgrid was discussed in [27]. However, the method was only applicable to the grid-tied system. In this work, islanded microgrids are modeled as linear switched systems, where the state jump influences in determining the stability of the overall system. The bounds on the state jumps are used as a measurable factor to determine switched system's stability. This bound was investigated using the Markov Jump Analysis.

1.2. CONTRIBUTION TO DATE

This dissertation reports modeling and analysis of a microgrid system operated in two different modes: grid-tied and islanded. Mathematical models are developed for a two bus microgrid system. These models are extended to a multi-bus system. The system dynamics obtained from the simulation, and the mathematical models are verified against the results obtained from the hardware setup. For accelerated simulation, the multi-bus

microgrid is modeled using singular perturbation method. Reduced order models are implemented in a modified IEEE-37 bus microgrid system. Islanded system's stability is investigated using the Markov Jump Analysis for Linear Systems.

In paper I, a two bus islanded microgrid system is modeled and analyzed. The small-signal model is verified using hardware test-bed results. System's oscillatory modes are identified for future use in the reduced order models. In paper II, a grid-tied system is modeled and then the order of the system is reduced using singular perturbation approach. The accuracy of the model is verified using the results obtained from the experimental testbed. The reduced model is used in an IEEE-37 bus microgrid system. In paper III, the oscillatory modes obtained from paper 2 are divided into two groups: fast oscillatory and slow oscillatory modes. Fast modes are discarded keeping only the slow eigenvalues of the system using singular perturbation technique. A reduced order model of the islanded microgrid system is found. An algorithm has been developed for model order reduction of such systems. The performance of the proposed algorithm has been tested in an IEEE-37 bus microgrid system. In paper IV, the small-signal model obtained from paper I is used to determine the bounds of the state jumps for stability analysis using Markov Jump Linear System (MJLS) Analysis. A correspondence is established between an islanded microgrid and an impulsive MJLS.

1.3. REFERENCES

[1] N. Hatziargyriou, H. Asano, R. Iravani, and C. Marnay, "Microgrids," *IEEE Power Energy Mag.*, vol. 5, no. 4, pp. 78–94, Jul. 2007.

[2] D. E. Olivares, A. Mehrizi-Sani, A. H. Etemadi, C. A. Canizares, R. Iravani, M. Kazerani, A. H. Hajimiragha, O. Gomis-Bellmunt, M. Saeedifard, R. Palma-Behnke, G. A. Jimenez-Estevez, and N. D. Hatziargyriou, "Trends in Microgrid Control," *IEEE Trans. Smart Grid*, vol. 5, no. 4, pp. 1905–1919, Jul. 2014.

[3] L. Junfeng, B. Lohani, E. M. Galàn, P. Monga, P. Mubiru, N. Nakicenovic, K. Nassiep, R. Pachauri, W. Palz, H. Pelosse, and others, "Renewable Energy Policy Network for the 21st Century," Tech. Rep. 2010, REN21.

[4] M. Shahidehpour and S. Pullins, "Is the Microgrid Buzz Real?," *IEEE Electrification Mag.*, vol. 2, no. 1, pp. 2–5, Mar. 2014.

[5] M. Rasheduzzaman, S. N. Bhaskara, and B. H. Chowdhury, "Implementation of a microgrid central controller in a laboratory microgrid network," in *North American Power Symposium (NAPS)*, 2012, pp. 1–6.

[6] K. De Brabandere, B. Bolsens, J. Van den Keybus, A. Woyte, J. Driesen, and R. Belmans, "A Voltage and Frequency Droop Control Method for Parallel Inverters," *IEEE Trans. Power Electron.*, vol. 22, no. 4, pp. 1107–1115, Jul. 2007.

[7] C. K. Sao and P. W. Lehn, "Autonomous load sharing of voltage source converters," *IEEE Trans. Power Deliv.*, vol. 20, no. 2, pp. 1009–1016, Apr. 2005.

[8] P. Piagi and R. H. Lasseter, "Autonomous control of microgrids," in *IEEE Power Engineering Soc. General Meet.*, 2006, p. 8.

[9] F. Gao and M. R. Iravani, "A Control Strategy for a Distributed Generation Unit in Grid-Connected and Autonomous Modes of Operation," *IEEE Trans. Power Deliv.*, vol. 23, no. 2, pp. 850–859, Apr. 2008.

[10] F. Katiraei, M. R. Iravani, and P. W. Lehn, "Micro-grid autonomous operation during and subsequent to islanding process," *IEEE Trans. Power Deliv.*, vol. 20, no. 1, pp. 248–257, Jan. 2005.

[11] M. M. A. Abdelaziz, H. E. Farag, E. F. El-Saadany, and Y. A.-R. I. Mohamed, "A Novel and Generalized Three-Phase Power Flow Algorithm for Islanded Microgrids Using a Newton Trust Region Method," *IEEE Trans. Power Syst.*, vol. 28, no. 1, pp. 190–201, Feb. 2013.

[12] S. Anand and B. Fernandes, "Reduced-Order Model and Stability Analysis of Low-Voltage DC Microgrid," *IEEE Transactions on Industrial Electronics*, vol. 60, no. 11, pp. 5040–5049, Nov. 2013.

[13] A. Radwan and Y. Mohamed, "Modeling, Analysis, and Stabilization of Converter-Fed AC Microgrids With High Penetration of Converter-Interfaced Loads," *IEEE Transactions on Smart Grid*, vol. 3, no. 3, pp. 1213–1225, Sep. 2012.

[14] T. Pavlovic, T. Bjazic, and Z. Ban, "Simplified Averaged Models of DC-DC Power Converters Suitable for Controller Design and Microgrid Simulation," *IEEE Transactions on Power Electronics*, vol. 28, no. 7, pp. 3266–3275, Jul. 2013.

[15] X. Tang, W. Deng, and Z. Qi, "Investigation of the Dynamic Stability of Microgrid," *IEEE Transactions on Power Systems*, vol. 29, no. 2, pp. 698–706, Mar. 2014.

[16] S. Iyer, M. Belur, and M. Chandorkar, "A Generalized Computational Method to Determine Stability of a Multi-inverter Microgrid," *IEEE Transactions on Power Electronics*, vol. 25, no. 9, pp. 2420–2432, Sep. 2010.

[17] A. C. Antoulas and D. C. Sorensen, "Approximation of large-scale dynamical systems: An overview," *App. Math. Comp. Science*, vol. 11, no. 5, p. 1093–1122, 2001.

[18] X. Xu, R. M. Mathur, J. Jiang, G. J. Rogers, and P. Kundur, "Modeling of generators and their controls in power system simulations using singular perturbations," *Power Syst., IEEE Trans.*, vol. 13, no. 1, p. 109–114, 1998.

[19] N. Monshizadeh, H. L. Trentelman, and M. K. Camlibel, "A simultaneous balanced truncation approach to model reduction of switched linear systems," *IEEE Trans. Autom. Control*, vol. 57, no. 12, pp. 3118–3131, Dec. 2012.

[20] J. Hahn and T. F. Edgar, "An improved method for nonlinear model reduction using balancing of empirical gramians," *Comp. Chem. Eng.*, vol. 26, no. 10, p. 1379–1397, 2002.

[21] C. Li and Z. Du, "A Novel Method for Computing Small-Signal Stability Boundaries of Large-Scale Power Systems," *IEEE Transactions on Power Systems*, vol. 28, no. 2, p. 877–883, 2013.

[22] S. Leva, "Dynamic Stability of Isolated System in the Presence of PQ Disturbances," *IEEE Transactions on Power Delivery*, vol. 23, no. 2, p. 831–840, 2008.

[23] J. Sun, "Impedance-Based Stability Criterion for Grid-Connected Inverters," *IEEE Transactions on Power Electronics*, vol. 26, no. 11, p. 3075–3078, 2011.

[24] T. Kato, K. Inoue, H. Kawabata, "Stability analysis of a grid-connected inverter system," *Control and Modeling for Power Electronics (COMPEL), 2012 IEEE 13th Workshop on* , vol., no., pp.1,5, 10-13 June 2012.

[25] A. Alfares and A. Sayed-Ahmed, "Analysis and assessment of microgrid stability using the Nu gap approach," *Energy Conversion Congress and Exposition (ECCE), 2014 IEEE* , vol., no., pp.2676,2683, 14-18 Sept. 2014.

[26] S.K. Mazumder, C. Bhandari, S. Rajoria, E. Pilo de la Fuente, "Polynomial Lyapunov function based stability analysis of microgrid," *Power Electronics, Drives and Energy Systems (PEDES), 2014 IEEE International Conference on*, vol., no., pp.1,6, 16-19 Dec. 2014.

[27] X. Xu, T. Lin and X. Zha, "Probabilistic Analysis of Small Signal Stability of Microgrid Using Point Estimate Method," *Sustainable Power Generation and Supply, 2009. SUPERGEN '09. International Conference on*, vol., no., pp.1,6, 6-7 April 2009.

PAPER

I. AN ACCURATE SMALL-SIGNAL MODEL OF INVERTER-DOMINATED ISLANDED MICROGRIDS USING *dq* REFERENCE FRAME

Md. Rasheduzzaman, Jacob A. Mueller, and Jonathan W. Kimball

Department of Electrical and Computer Engineering

Missouri University of Science & Technology, Rolla, MO 65409

ABSTRACT— In islanded mode operation of a microgrid, a part of the distributed network becomes electrically separated from the main grid, while loads are supported by local sources. Such distributed energy sources (DERs) are typically power electronic based, making the full system complex to study. A method for analyzing such a complicated system is discussed in this paper. A microgrid system with two inverters working as DERs is proposed. The controllers for the inverters are designed in the *dq* reference frame. Nonlinear equations are derived to reflect the system dynamics. These equations are linearized around steady state operating points to develop a state-space model of the microgrid. An averaged model is used in the derivation of the mathematical model, which results in a simplified system of equations. An eigenvalue analysis is completed using the linearized model to determine the small-signal stability of the system. A simulation of the proposed microgrid system consisting of two inverter based DERs, passive loads, and a distribution line is performed. An experimental test bed is designed to investigate the system's dynamics during load perturbation. Results obtained from the simulation and hardware experiment are compared to those predicted by the mathematical model in order to verify its accuracy.

Index Terms— Microgrid, small-signal model, reference frame, switched system

1.1. INTRODUCTION

Significant efforts are underway to modernize the nation's electric delivery network. To accelerate progress, the Office of Electricity Delivery and Energy Reliability (OE) of the U.S. Department of Energy (DOE), has established the Smart Grid R&D program to provide research and financial assistance to certain projects related to distributed energy sources (DERs). The OE is currently supporting nine projects with a total value exceeding US$100 million. The goal of this program is to reduce the peak demand at the distribution feeder level by 15% using DERs and microgrids [2]. Most DERs use power electronics to process and interface energy to the grid. Furthermore, there is a constant growth in the demand of power electronic components in the current power system [2]. Uses of these components are important considering the evolution of smart grid and ac-dc microgrids and their interconnections. Advantages of DER based distribution systems were mentioned in [3]. R.H. Lasseter proposed the concept of microgrid in [4], where he defined a microgrid as a cluster of loads and microsources operated as a single controllable system. He presented a method of sharing power during microgrid islanding operation as well. Some of the technical challenges associated with the microgrid were discussed in [5]. Microgrid control strategies with single-master and multi-master operation were explained in [6]. A more detailed control algorithm was presented for grid-connected and islanded operation in [7]. The algorithms were implemented in a test bed and results were verified for different control architectures. Apart from these control strategies, different types of droop controllers have been used for power sharing during islanded operation of parallel inverters [8, 9, 10, 11]. A control strategy for different distribution line impedances was discussed in [12], and small-signal models were developed. Experimental results for different controller modes of operation were presented as well. An improved control method for an isolated single-phase inverter was shown in [13]. Active and reactive power sharing methods were explained with simulation results by T.L. Vandoorn *et al.* [14, 15].

Small-signal modeling and steady-state analysis of an autonomous microgrid was investigated in [9]. A mathematical model for the microgrid was developed. Small-signal results were verified with a time domain simulation. Howerver, the dynamics of the phase locked loop (PLL) were not discussed. A more detailed small-signal modeling was done by F. Katiraei *et al.* [16], in which the autonomous system was built with both conventional and electronically interfaced DERs to study the system's stability and dynamic behavior. Filter dynamics were ignored, though, which are an essential part of electronically interfaced DER systems. Although the filter components were included in [17] for modeling an inverter, line parameters, an important aspect of the network, were ignored for parallel inverter operation. A model including distribution line and filter dynamics was prepared in [18], but only for a single inductor based filter, which does not always guarantee stability. A method for modeling a microgrid with all network components was presented in [19], but the procedure for obtaining the small-signal model was rather complex. Also, the damping resistors of the LCL filters, which play an important role in ensuring stability of the system, were ignored. Additionally, the model was designed such that a load current transient was used as a perturbation input, while in practice a change in impedance was observed during the transient analysis. This improper perturbation technique resulted in a significant reactive power mismatch between the experimental results and the results obtained from the model. Another small-signal model was derived in [20]. Again, the model did not include the passive damping properties of the filter. Results from this model were not validated against those from a hardware experiment. The models from the last two papers did not include the dynamics of the PLL to verify system frequency during load perturbation. A small-signal model was developed in [21] which included the PLL dynamics and a damping resistor in the filter. Once again, the model was not validated against the experimental results. Also, the input matrix was defined in such a way that it did not reflect the load perturbation in the system.

As a solution to the issues associated with these prior models, a more accurate small-signal model is presented in this paper. The development and verification of this model is as follows. First, the proposed control structure is described using a block diagram. A set of nonlinear equations is then derived from the controller blocks and the plant. These equations are linearized around stable operating points. To simulate the effect of the load perturbation, a switched system arrangement is implemented. Finally, the transient response predicted by the mathematical model is verified against both the simulation and experimental results. The proposed model is intended to serve as a building block for control of more complex systems of modern distributed generation sources.

1.2. OVERVIEW OF THE SYSTEM

The islanded microgrid under consideration is presented in Fig. 1.1. Each inverter is connected to a respective bus through a filter. Variable passive loads connected to these buses are considered as local loads. Depending on the status of the system, either grid-connected or islanded, the switch at the point of common coupling (PCC) may connect the system to the main grid. A distribution line with impedance Z_L is used to couple the inverter buses. While the proposed system can operate in either grid-connected mode or as an autonomous system, only the autonomous operation will be considered in this paper.
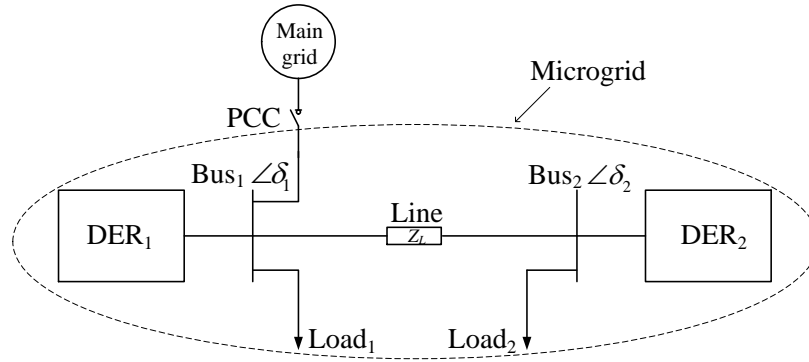
Figure 1.1. Proposed microgrid architecture

In autonomous operation, the inverter is controlled using the droop control method. An individual inverter control strategy is depicted in Fig. 1.2. The output of the inverter is passed through an LCL filter to reject the high frequency switching noise. The filtered voltage and current measurements are then converted to dq axis components using a reference frame transformation. The inverter's output power is calculated based on these measurements. The calculated power is passed through a low pass filter and sent to the droop controllers. Droop controllers set voltage and frequency references based on the current level of active and reactive power being generated. These voltage and frequency references are then compared with the measured voltage and frequency.

The 'error signal' obtained by comparing the reference values and measured values are passed through PI controllers to generate references for the current flowing through the output filter inductor. These reference current signals are then compared with the corresponding measured filter inductor currents, and are passed through another set of PI controllers to produce voltage commands. These voltage values appear across the input of the LCL filter. The coupling inductor of the filter is used to connect the inverter to the bus. A resistor in series with the filter capacitor ensures the proper damping of the resonant frequency associated with the output filter.

As mentioned before, a frequency measurement is needed for voltage controllers to operate. The frequency of the system is measured by forcing the d axis component of the voltage to zero in a dq based PLL. This PLL not only measures the frequency of the system but also calculates the phase angle of the voltage. This angle is used to make all the conversions between stationary and synchronous reference frames. All controllers and filters are modeled in the individual reference frame local to each inverter as determined by the phase angle from the PLL. The inverters' dynamics are influenced by the output filter, coupling inductor, average power calculation, PLL, droop controllers, and current controllers. The overall system dynamics include those of each individual inverter, load, and the distribution line between them.
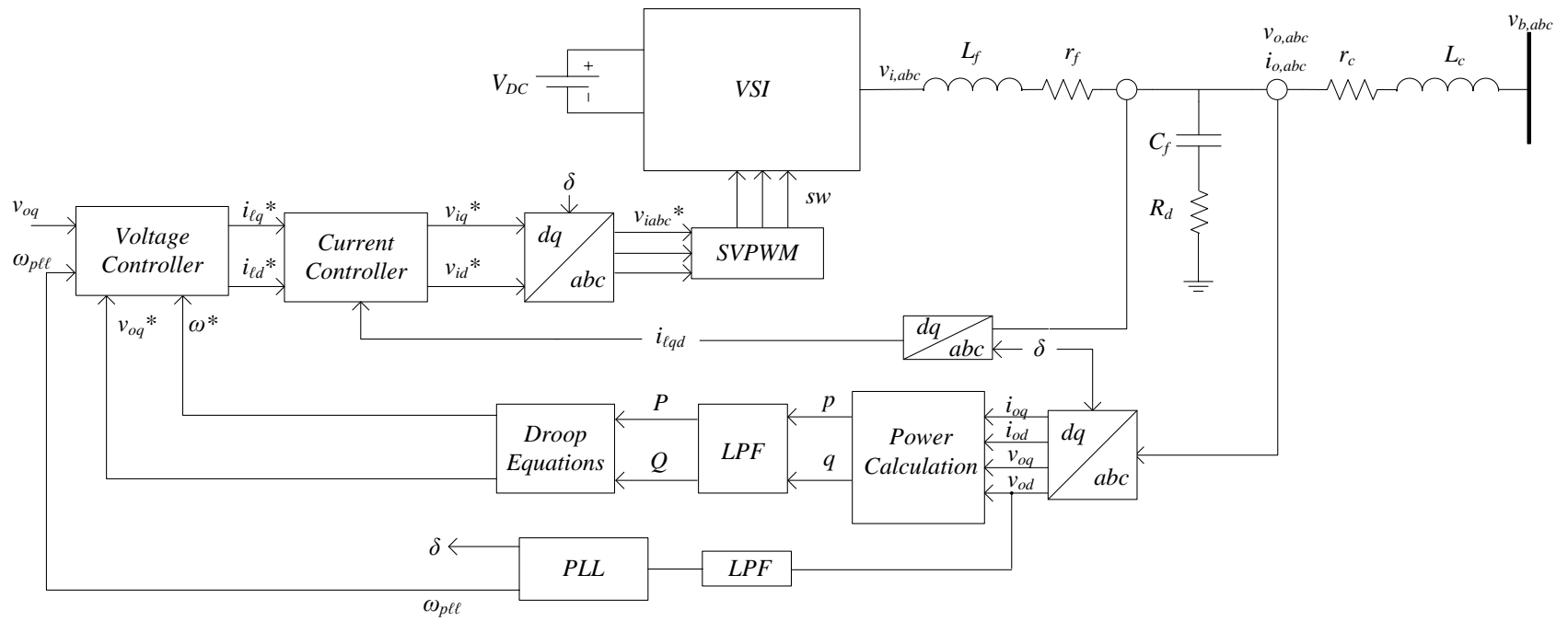
Figure 1.2. Control strategy of an individual DER

1.3. SYSTEM MODELING IN STATE-SPACE FORM

1.3.1. Nonlinear Equations of the Inverter Model. In this section, the controllers shown as blocks in Fig. 1.2 are analyzed and expressed in terms of mathematical equations. These equations are nonlinear and need to be linearized around an operating point to study the system dynamics.

Average Power Calculation. The dq axis output voltage and current measurements are used to calculate the instantaneous active power (p) and reactive power (q) generated by the inverter.

$$p = \frac{3}{2} \left(v_{od} i_{od} + v_{oq} i_{oq} \right) \tag{1.1}$$

$$q = \frac{3}{2} \left(v_{oq} i_{od} - v_{od} i_{oq} \right) \tag{1.2}$$

Instantaneous powers are then passed through low pass filters with the corner frequency ω_c to obtain the filtered output power.

$$P = \frac{\omega_c}{s + \omega_c} p \Rightarrow \dot{P} = -P\omega_c + 1.5\omega_c \left(v_{od} i_{od} + v_{oq} i_{oq} \right) \tag{1.3}$$

$$Q = \frac{\omega_c}{s + \omega_c} q \Rightarrow \dot{Q} = -Q\omega_c + 1.5\omega_c \left(v_{oq} i_{od} - v_{od} i_{oq} \right) \tag{1.4}$$

Droop Equations. In grid-connected mode, the inverter's output voltage is set by the grid voltage magnitude. The PLL ensures proper tracking of grid phase so that inverter output remains synchronized to the grid. During islanded operation, the inverter does not have these externally generated reference signals. As a result, the inverter must generate its own frequency and voltage magnitude references using the droop equations. The references are generated using conventional $P - \omega$ and $Q - V$ droop equations. Fig. 1.3 shows the characteristics of these droop curves.

$$\omega^* = \omega_n - mP \tag{1.5}$$
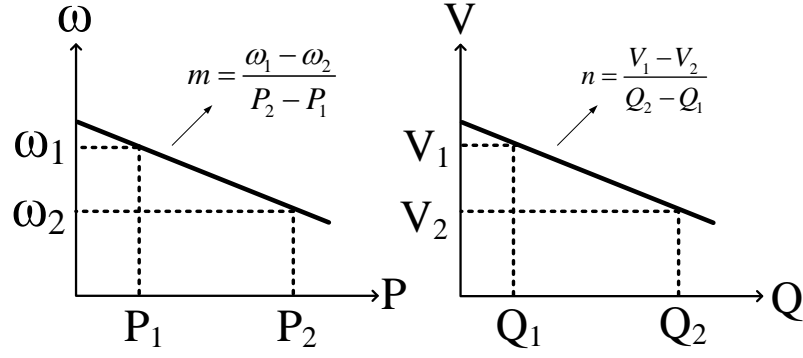
Figure 1.3. Droop characteristic curves

$$v_{oq}{}^* = V_{oq,n} - nQ \qquad (1.6)$$

Phase Locked Loop (PLL). A PLL is required to measure the actual frequency of the system. A *dq* based PLL was chosen [22, 23, 24]. The PLL input is the *d* axis component of the voltage measured across the filter capacitor. Therefore, the phase is locked such that $v_{od} = 0$ (Fig. 1.4). Some researchers instead set the PLL to lock such that v_{oq}, which would essentially swap d-axis quantities throughout the remainder of this work. There are three states associated with this PLL architecture.
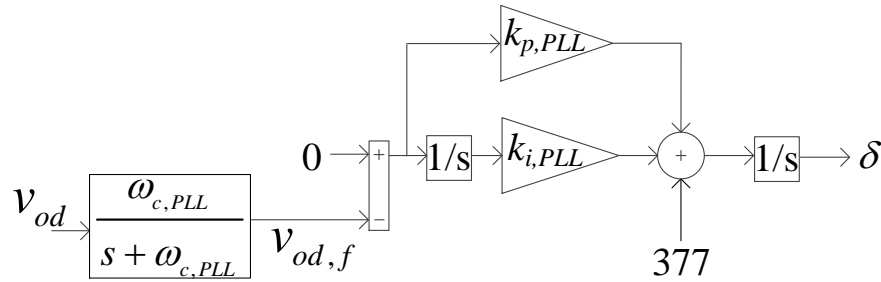
Figure 1.4. PLL used for the DER

$$\dot{v}_{od,f} = \omega_{c,PLL} v_{od} - \omega_{c,PLL} v_{od,f} \qquad (1.7)$$

$$\dot{\varphi}_{PLL} = -v_{od,f} \qquad (1.8)$$

$$\dot{\delta} = \omega_{PLL} \tag{1.9}$$

$$\omega_{PLL} = 377 - k_{p,PLL} v_{od,f} + k_{i,PLL} \varphi_{PLL} \tag{1.10}$$

Voltage Controllers. The reference frequency and voltage magnitude generated by the droop equations are used as set point values for the voltage controllers. Standard PI controllers are used for this purpose, shown in Fig. 1.5. The process variables are the angular frequency ω from the PLL and the measured q axis voltage (v_{oq}).
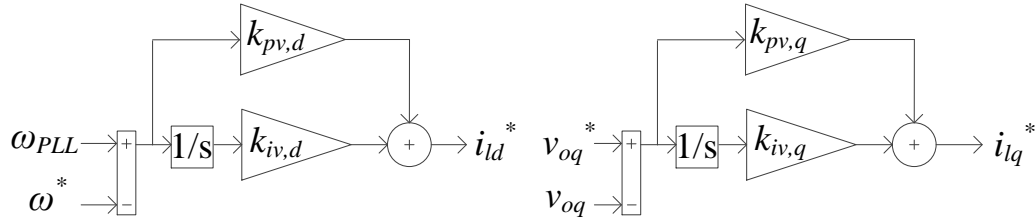
Figure 1.5. Voltage controllers

$$\dot{\varphi}_d = \omega_{PLL} - \omega^*; \quad i_{ld}^* = k_{iv,d} \varphi_d + k_{pv,d} \dot{\varphi}_d \tag{1.11}$$

$$\dot{\varphi}_q = v_{oq}^* - v_{oq}; \quad i_{lq}^* = k_{iv,q} \varphi_q + k_{pv,q} \dot{\varphi}_q \tag{1.12}$$

Current Controllers. Another set of PI controllers are used for the current controllers as shown in Fig. 1.6. These controllers take the difference between the commanded filter inductor currents (i_{ldq}^*), the measured filter inductor currents (i_{ldq}), and produce commanded voltage values (v_{idq}^*). The values of correspond to the inverter output voltages before the LCL filter. Cross coupling component terms are eliminated in these controllers as well.

$$\dot{\gamma}_d = i_{ld}^* - i_{ld}; \quad v_{id}^* = -\omega_n L_f i_{lq} + k_{ic,d} \gamma_d + k_{pc,d} \dot{\gamma}_d \tag{1.13}$$

$$\dot{\gamma}_q = i_{lq}^* - i_{lq}; \quad v_{iq}^* = \omega_n L_f i_{ld} + k_{ic,q} \gamma_q + k_{pc,q} \dot{\gamma}_q \tag{1.14}$$
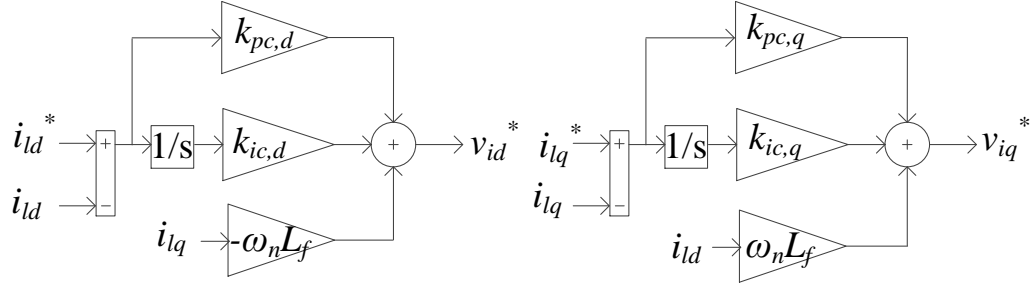
Figure 1.6. Current controllers

1.3.2. LCL Filter. The filter used for a DER is shown in Fig. 1.7. Without any major inaccuracies, we can assume that the commanded voltage (v^*_{idq}) appears at the input of the filter inductor i.e. $v^*_{idq} = v_{idq}$. This approach neglects only the losses in the IGBT and diodes. The resistors r_c and r_f are the parasitic resistances of the inductors. A damping resistor R_d is connected in series with the filter capacitor. The capacitor's ESR is not considered, as it can be lumped into R_d. The state equations governing the filter dynamics are presented below.
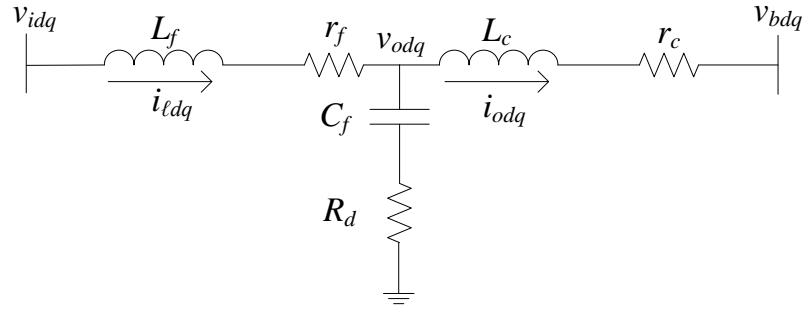
Figure 1.7. LCL filter for the DER

$$\dot{i}_{ld} = \frac{1}{L_f}\left(-r_f i_{ld} + v_{id} - v_{od}\right) + \omega_{PLL} i_{lq} \tag{1.15}$$

$$\dot{i}_{lq} = \frac{1}{L_f}\left(-r_f i_{lq} + v_{iq} - v_{oq}\right) - \omega_{PLL} i_{ld} \tag{1.16}$$

$$\dot{i}_{od} = \frac{1}{L_c}\left(-r_c i_{od} + v_{od} - v_{bd}\right) + \omega_{PLL} i_{oq} \tag{1.17}$$

$$\dot{i}_{oq} = \frac{1}{L_c}\left(-r_c i_{oq} + v_{oq} - v_{bq}\right) - \omega_{PLL} i_{od} \tag{1.18}$$

$$\dot{v}_{od} = \frac{1}{C_f}\left(i_{ld} - i_{od}\right) + \omega_{PLL} v_{oq} + R_d\left(\dot{i}_{ld} - \dot{i}_{od}\right) \tag{1.19}$$

$$\dot{v}_{oq} = \frac{1}{C_f}\left(i_{lq} - i_{oq}\right) - \omega_{PLL} v_{od} + R_d\left(\dot{i}_{lq} - \dot{i}_{oq}\right) \tag{1.20}$$

1.3.3. Equations for the Load. The loads for this system are chosen as combination of resistors and inductors (RL loads). A typical RL load connected to an inverter bus is shown in Fig. 1.8. Line 'a' connected to the bus represents the base load and line 'b' works as a variable load for that bus. In order to check the system's dynamic behavior, a load perturbation is done on 'b'. Line 'b' appears in parallel to 'a' when the breaker closes the contact. State equations describing the load dynamics are given below.
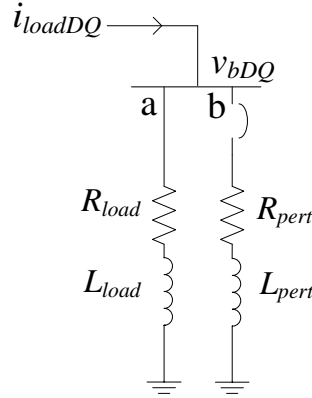
Figure 1.8. Load configuration

$$\dot{i}_{loadD} = \frac{1}{L_{load}}\left(-R_{load} i_{loadD} + v_{bD}\right) + \omega_{PLL} i_{loadQ} \tag{1.21}$$

$$\dot{i}_{loadQ} = \frac{1}{L_{load}}\left(-R_{load} i_{loadQ} + v_{bQ}\right) - \omega_{PLL} i_{loadD} \tag{1.22}$$

1.3.4. Equations for the Distribution Line. Similar to loads, the distribution line parameters consist of resistance and inductance. Resistor r_{line} represents the copper loss component of the line. Inductor L_{line} is considered as the lumped inductance resulting

from long line cables. Assuming that the line is connected between i-th and j-th bus of the system, the line dynamics are represented as follows.

$$\dot{i}_{lineDij} = \frac{1}{L_{line}} \left(-r_{line} i_{lineD} + v_{bD,i} - v_{bD,j} \right) + \omega_{PLL} i_{lineQ} \tag{1.23}$$

$$\dot{i}_{lineQij} = \frac{1}{L_{line}} \left(-r_{line} i_{lineQ} + v_{bQ,i} - v_{bQ,j} \right) - \omega_{PLL} i_{lineD} \tag{1.24}$$

The frequency is constant throughout the system, so the equations for the load and line dynamics can use the term derived from the ω_{PLL} of the first inverter. The variable subscript with upper case DQ denotes measurements from the global reference frame. Since the system does not have a fixed grid connected to it, the first inverter's phase angle can be arbitrarily set as the reference for the entire system. This results in a change in the reference angle calculation when small-signal model's matrices are derived. The new phase angle derivations for DER$_1$ and DER$_2$ are given in (1.25) and (1.26), where $\omega_{PLL,1}$ and $\omega_{PLL,2}$ come from DER$_1$ and DER$_2$ respectively.

$$\dot{\delta}_1 = \omega_{PLL,1} - \omega_{PLL,1} = 0 \tag{1.25}$$

$$\dot{\delta}_2 = \omega_{PLL,1} - \omega_{PLL,2} \tag{1.26}$$

1.3.5. Linearized Model of the System. Each inverter system contains 15 states, and each load and line model contain 2 states. A total of 36 states are contained in the full
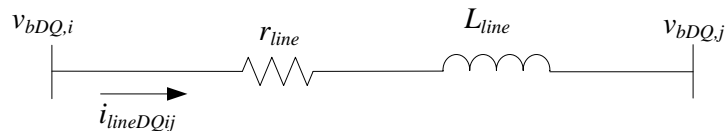
Figure 1.9. Line configuration

two inverter islanded microgrid system. The states are:

$$x_{inv1} = [\delta_1 \quad P_1 \quad Q_1 \quad \varphi_{d1} \quad \varphi_{q1} \quad \gamma_{d1} \quad \gamma_{q1} \quad i_{ld1} \quad i_{lq1} \quad v_{od1} \quad v_{oq1} \quad i_{od1} \quad i_{oq1} \quad \varphi_{PLL1}$$

$$v_{od1,f}] \tag{1.27}$$

$$x_{inv2} = [\delta_2 \quad P_2 \quad Q_2 \quad \varphi_{d2} \quad \varphi_{q2} \quad \gamma_{d2} \quad \gamma_{q2} \quad i_{ld2} \quad i_{lq2} \quad v_{od2} \quad v_{oq2} \quad i_{od2} \quad i_{oq2}$$

$$\varphi_{PLL2} \quad v_{od2,f}] \tag{1.28}$$

$$x_{load} = [i_{loadD1} \quad i_{loadQ1} \quad i_{loadD2} \quad i_{loadQ2}] \tag{1.29}$$

$$x_{line} = [i_{lineD21} \quad i_{lineQ21}] \tag{1.30}$$

The states of the system under consideration are then:

$$x = [x_{inv1} \quad x_{inv2} \quad x_{load} \quad x_{line}]^T \tag{1.31}$$

These nonlinear equations are linearized around stable operating points and a state-space equation of the form (1.32) is generated using Matlab's symbolic math toolbox.

$$\dot{\tilde{x}} = A\tilde{x} + B\tilde{u} \tag{1.32}$$

Where the inputs are defined as:

$$u = [v_{bD1} \quad v_{bQ1} \quad v_{bD2} \quad v_{bQ2}]^T \tag{1.33}$$

1.3.6. Virtual Resistor Method. When bus voltages were used as an input to the system, as in previous microgrid models, effects of load perturbation could not be accurately predicted. In practice, the only perturbation that occurs in the system comes from

the step change in load. A method is needed to include the terms relating to the bus voltages in the system 'A' matrix. This effectively translates the inputs defined in (1.33) to states. To do this, a virtual resistor with high resistance can be assumed connected at the inverter bus as shown in Fig. 1.10. This resistor (r_n) has a negligible impact on system dynamics. Using KVL, the equations describing the bus voltage in terms of the inverter, load currents and line currents can be expressed. This is shown in (1.34) and (1.35).
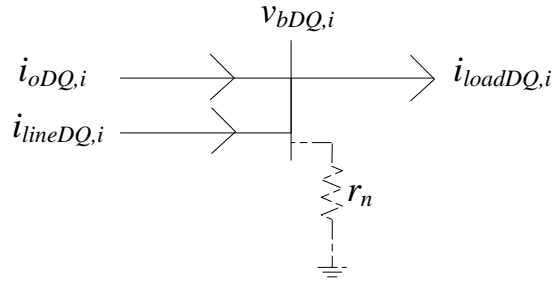
Figure 1.10. Virtual resistor at a DER bus

$$v_{bD,i} = r_n \left(i_{oD,i} + i_{lineD,i} - i_{loadD,i} \right) \tag{1.34}$$

$$v_{bQ,i} = r_n \left(i_{oQ,i} + i_{lindQ,i} - i_{loadQ,i} \right) \tag{1.35}$$

1.3.7. Reference Frame Transformation. As previously discussed, inverter bus 1 serves as the system's reference and consequently is labeled as the global reference frame. Each inverter operates in its own local reference frame. The individual inverter state equations are derived in terms of their individual local reference frame. A transformation is necessary to translate between values defined in the local reference frame to the global reference frame. An application of this transformation is shown graphically in Fig. 1.11. Again, the difference in subscript capitalization denotes whether the quantity is defined in the local or global reference frame.
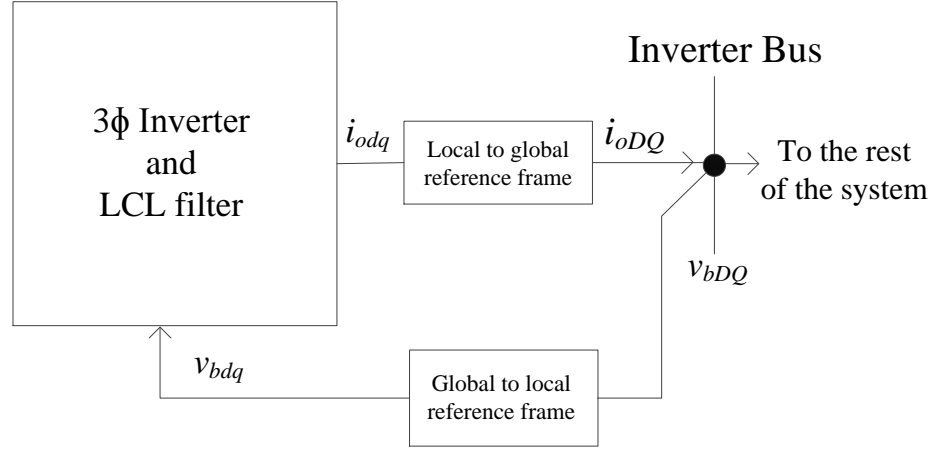
Figure 1.11. Reference frame transformation

$$
\begin{bmatrix} f_D \\ f_Q \end{bmatrix}_{global} = \begin{bmatrix} \cos\theta & \sin\theta \\ -\sin\theta & \cos\theta \end{bmatrix} \begin{bmatrix} f_d \\ f_q \end{bmatrix}_{local} \tag{1.36}
$$

$$
\begin{bmatrix} f_d \\ f_q \end{bmatrix}_{local} = \begin{bmatrix} \cos\theta & -\sin\theta \\ \sin\theta & \cos\theta \end{bmatrix} \begin{bmatrix} f_D \\ f_Q \end{bmatrix}_{global} \tag{1.37}
$$

Where θ is the difference between the global reference phase and the local reference phase as depicted in Fig. 1.12.

This transformation [25] is used to refer the virtual resistor equations that are defined in the global reference frame to the local reference frame. The equations (1.36), (1.37) and the reference frame transformations can then be linearized and included in the symbolic 'A' matrix. A new state matrix, 'A_{sys}', then describes the system in state space form. The states of this new system are the same as those given in (1.31):

$$
\dot{\tilde{x}} = A_{sys}\tilde{x} \tag{1.38}
$$
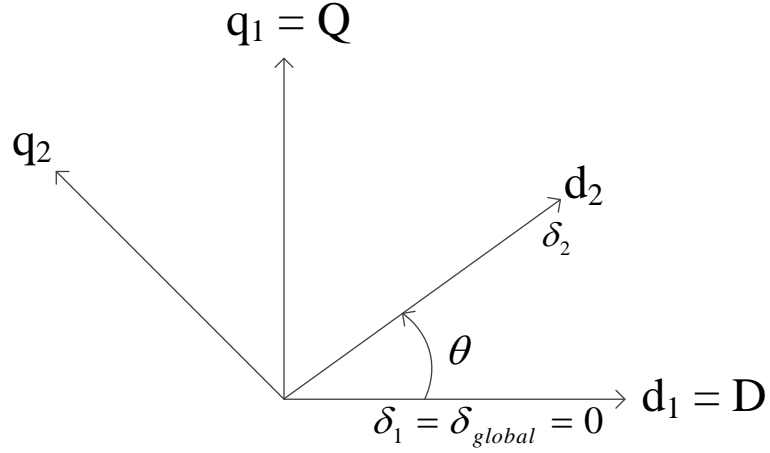
Figure 1.12. Transformation angle

1.4. EVALUATION OF THE MATHEMATICAL MODEL

The autonomous system described by the matrix 'A$_{sys}$' needs to be linearized around stable operating points. There are two ways of finding these operating points. One method is to set the nonlinear state equations to zero as ($\dot{x} = 0$). Another approach is to simulate the averaged model in PLECS to determine numerical solutions to the nonlinear system equations. Because both methods yielded same results, the simulation based method was used for convenience.

As mentioned previously, loads are connected to inverter buses as in Fig. 1.8. Initially load 'a' at bus 1 and bus 2 is switched on. A set of operating points is determined for this loading condition. These operating points are given in (1.39). A new set of operating points is determined after applying 'b' parallel to the initial load at bus 1 to simulate a load perturbation. R_{load1}, L_{load1} and R_{load2}, L_{load2} are the initial loads at bus 1 and bus 2, respectively. R_{pert1} and L_{pert1} are the new loads added to bus 1. New operating points for the equivalent load impedance seen at bus 1 are obtained. These operating points are given in (1.40). The dynamic response when changing between these two operating points yields

the mathematical model's prediction for a load step change transient [26]. The controller

gains and system parameters are listed in Table 1.1 and Table 1.2.

Fig. 1.13 shows the small-signal model evaluation arrangement in Simulink. Matrices 'A1' and 'A2' are obtained through linearization around stable operating points given in (1.39) and (1.40). Operating points are arranged in the order given in (1.31).
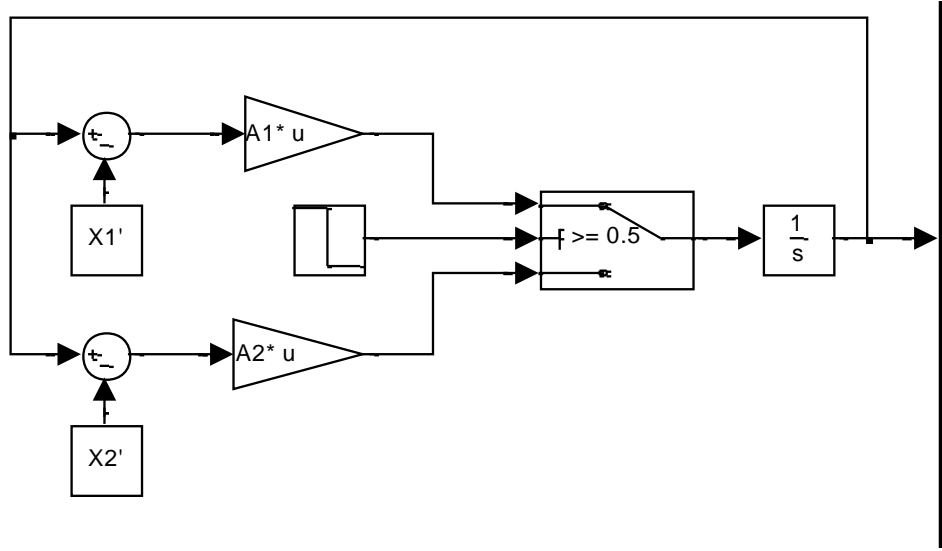
Figure 1.13. Small-signal simulation arrangement in Simulink

Table 1.1. Controller Gains

PI gains for	Parameter	Value
Voltage	$k_{pv,d}$, $k_{pv,q}$	0.50
controllers	$k_{iv,d}$, $k_{iv,q}$	25.0
Current	$k_{pc,d}$, $k_{pc,q}$	1.00
controllers	$k_{ic,d}$, $k_{ic,q}$	100
PLL	$k_{p,PLL}$	0.25
controller	$k_{i,PLL}$	2.00

Table 1.2. System Parameters and Initial Conditions

Parameter	Value	Parameter	Value
L_f	4.20 mH	r_f	0.50 Ω
L_c	0.50 mH	r_c	0.09 Ω
C_f	15 μf	R_d	2.025 Ω
ω_c	50.26 rad/s	ω_n	377 rad/s
$\omega_{c,PLL}$	7853.98 rad/s	ω_{PLL}	377 rad/s
m	1/1000 rad/Ws	n	1/1000 V/Var
r_n	1000 Ω	$V_{oq,n}$	85.0 V
R_{load1}	25 Ω	L_{load1}	15 mH
R_{load2}	25Ω	L_{load2}	7.50 mH
R_{pert1}	25 Ω	L_{pert1}	7.50 mH
r_{line}	0.15 Ω	L_{line}	0.40 mH
V_{bD1}	0.60585 V	V_{bQ1}	84.516 V
V_{bD2}	0.63937 V	V_{bQ2}	84.529 V

$$
\begin{aligned}
X1 =[&0; 418.18; 76.104; 0.0034259; 0.13152; 0.0014666; 0.86569; 0.1198; 3.2871; \\
&0.041403; 84.923; 0.59961; 3.2813; -0.20887; 0.042771; 0.00038; 415.95; 70.12; \\
&0.001539; 0.13084; 0.001221; 0.86564; 0.0719; 3.2716; 0.042439; 84.929; 0.55145; \\
&3.2659; -0.20868; 0.042; 0.74987; 3.2113; 0.40117; 3.3359; 0.15028; -0.0699]^T
\end{aligned}
$$

$$(1.39)$$

$$
\begin{aligned}
X2 =[&0; 627.15; 148.07; 0.027375; 0.19731; 0.0035517; 0.87317; 0.6842; 4.9328; \\
&-0.0037896; 84.835; 1.1644; 4.927; -0.3135; 0.00253; -0.0036217; 627.13; 53.113; \\
&-0.002506; 0.19709; -0.0001836; 0.87411; -0.06246; 4.9273; 0.0032628; 84.959; \\
&0.41577; 4.9216; -0.31357; -0.00298; 1.16; 6.518; 0.4117; 3.33; 0.0042; 1.5911]^T
\end{aligned}
$$

$$(1.40)$$

1.5. EXPERIMENT SETUP

In order to validate the results of the mathematical model, the dynamic response is compared against those of a simulation and experiment in hardware. An averaged model of the proposed system is simulated in PLECS. This average model is perturbed through a load change in bus 1 as discussed in the previous sections. In hardware implementation, a Texas Instruments TMS320F28335 digital signal processor was used to apply the control system to a 10 kW inverter designed around an Infineon BSM30GP60 IGBT module. A dc source was connected directly to the dc link and the three phase outputs were connected to the loads. Space vector modulation (SVPWM) was used as the switching scheme at a frequency of 10 kHz. The experimental results collected correspond to the actual values in the DSP, which were logged in real time. This was accomplished through transmission of the required values over serial connections to a host computer, as the internal storage capacity of the DSP was not sufficient to save the large volumes of data generated by the logs. In the same way as in the simulation, the system was perturbed by manually switching between load configurations and logging the dynamic response. A diagram of the experiemntal setup was provided in Fig. 1.1. Beacuse we are considering the islanded case, the switch shown as the PCC to the main grid in 1.1 was open for the entire experiment. Fig. 1.14 shows a partial photograph of the experimental setup, including sensors and circuit board, output filter, and load configuration. Although, only one DER is presented here, both the inverters had similar configuration. Each inverter had an individual DSP used for the controller implementation.

LCL filters with damping resistors are used at the IGBT output terminals. The impact of using an LCL filter in this kind of system is discussed in [27]. The filter was designed such that the resonant frequency was greater than 10 times the line frequency and less than half the switching frequency [27]. The resonant frequency of this wye-connected LCL filter, ignoring parasitic resistances, was found to be 1.94 kHz using (1.41). The ratio

(a)

(b)

(c)
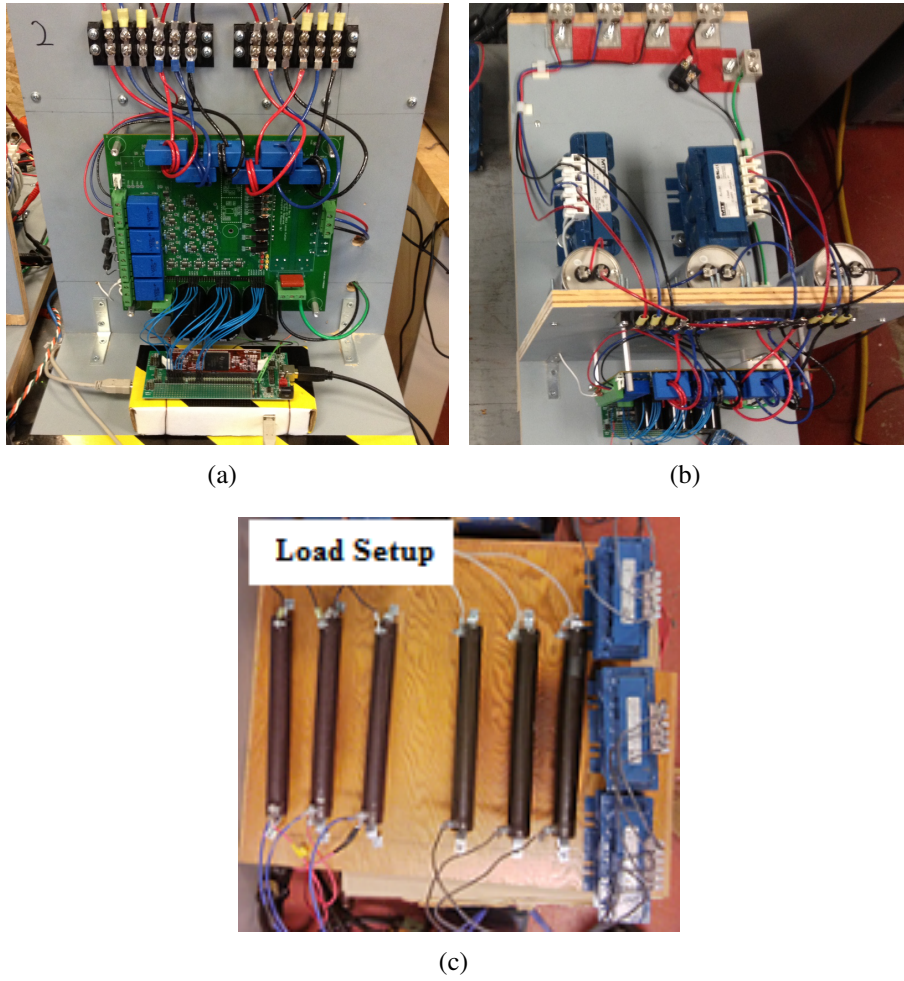
Figure 1.14. Partial photograph of the test bed

a. DER$_2$ b. LCL filter c. Loads at bus 1

of L_f to L_c was adequate for improving the total harmonic distortion (THD) and providing better bus voltage regulation.

$$f_{res} \cong \frac{1}{2\pi} \sqrt{\frac{L_f + L_c}{L_f L_c C_f}} \cong 1.944 \ kHz \qquad (1.41)$$

Passive damping using a damping resistor (R_d) in series with the filter capacitor was used to suppress the resonance frequency of the LCL filter. The value of R_d was found using [29]:

$$R_d = \frac{1}{3\omega_{res}C_f} = 1.8193 \ \Omega \qquad (1.42)$$

A resistor of this value was unavailable during the time the test bed was built. As a result, R_d with slightly higher value was used, as listed in the Table 1.2. Although the results were obtained with a grid voltage of 60 V_{LN}, the small-signal models are equally applicable to 120 V_{LN} voltage levels commonly used at the distribution side of a power system.

1.6. RESULTS AND DISCUSSIONS

A comparison of the small-signal model prediction, simulation results, and experimental results are shown below. Subscripts '*exp*' and '*models*' on y-axis labels denote whether the values were obtained from the experimental data or from the model data. The load perturbation takes place at $t = 1.885 \ s$. When plotted on the same graph, results from the averaged model simulation and from the mathematical model overlap, shown in Fig. 1.15 and Fig. 1.16. This indicates that the results from the models are consistent. The controller was designed such that v_{od} is maintained at zero. This is shown in the d axis voltage plot. From (1.1) and (1.2) it is clear that the dynamics of active and reactive power, P and Q, are dependent on the dynamics of i_{oq} and i_{od} respectively, provided that v_{oq} remains constant. This is shown graphically in Fig. 1.16 as well. In all of the graphs, the transient response decays in 1 s, which is acceptable for a power system application.

For all signals considered, the prediction of the mathematical model very closely resembles that found in the simulation and the hardware experiment, both in terms of transient and steady state response. In contrast to [19], the proposed small-signal model reaches a proper steady state value after a load perturbation in the system. The frequency of the system shows the actual variation during transient response, as opposed to the reference values generated by the $P - \omega$ droop controller. High frequency switching ripple cannot be completely avoided, and is visible in the experimental results for v_{od}, i_{od}, i_{ld}, i_{lq} and ω_{pll}. Also, overshoots and undershoots of slightly larger magnitude were present in the voltage graphs compared to that of the experimental results. Un-modeled breaker resistance in the mathematical model is the reason behind these behaviours. In practice, the values of the
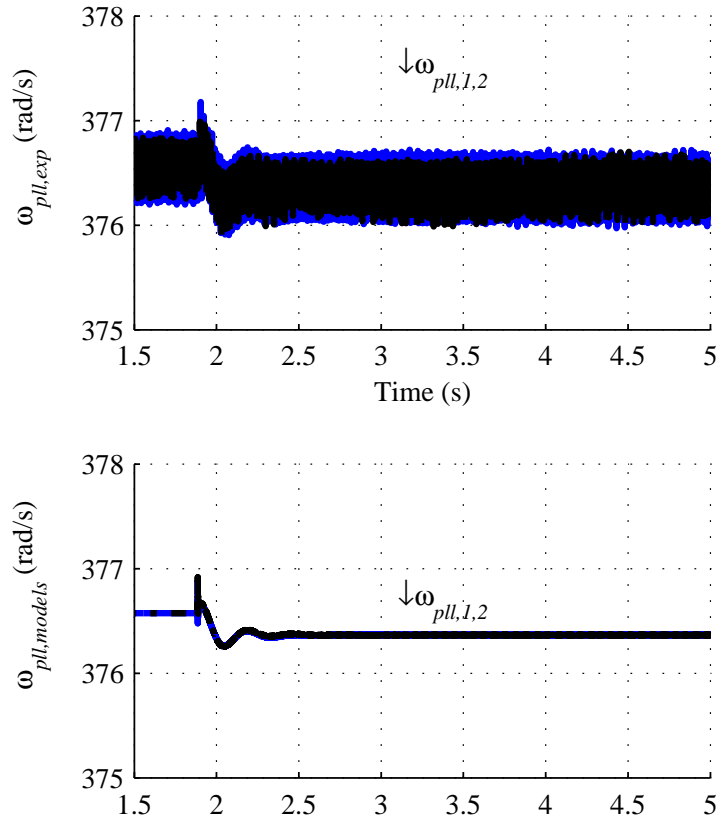
Figure 1.15. Frequency of the system
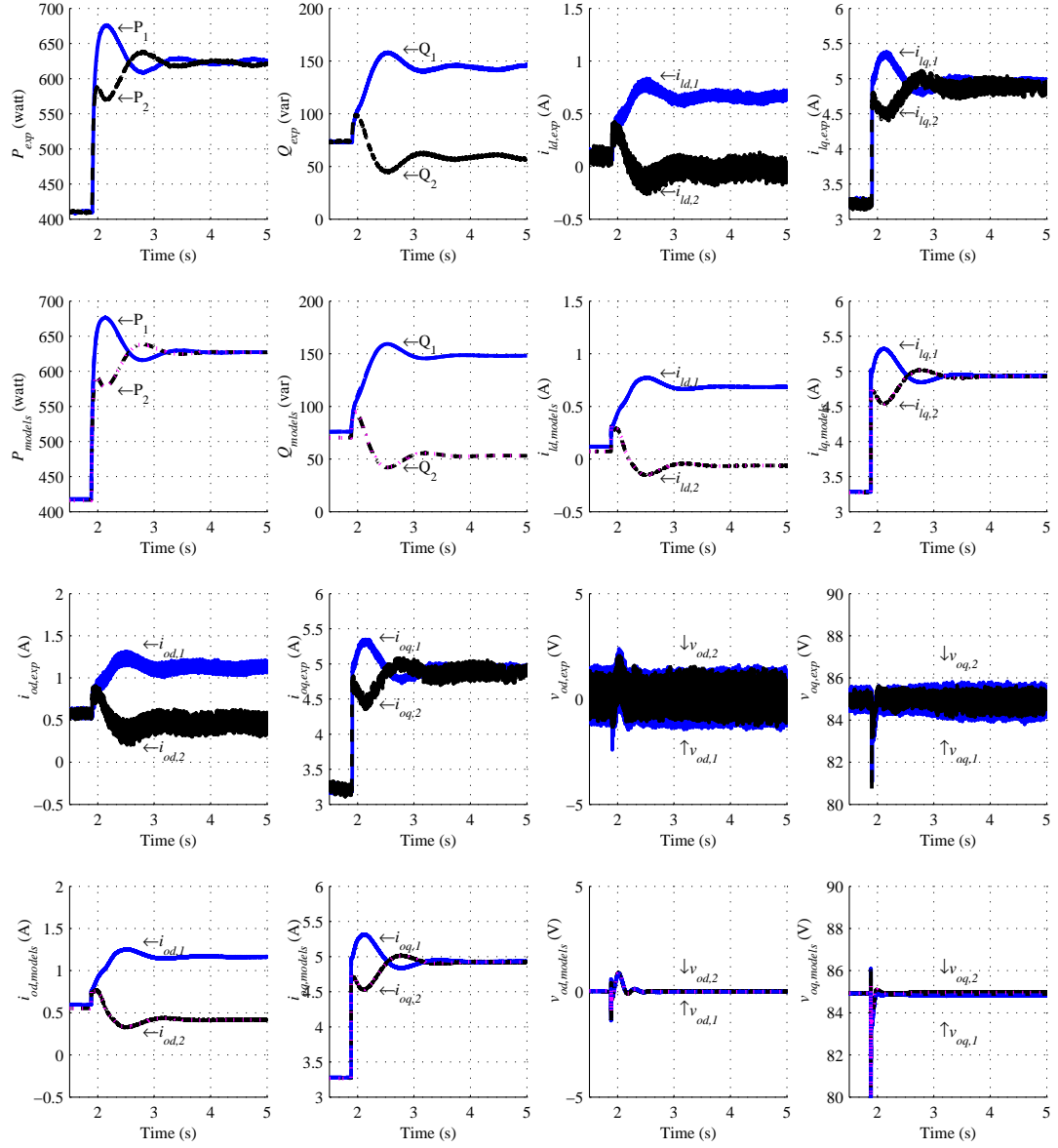
Figure 1.16. Varification of system dynamics with load perturbation

load resistors might vary slightly from the actual values, which could have some impact on the system damping.

The eigenvalues for 'A1' are determined and listed in Table 1.3. The first four eigenvalues' real parts are much more negative (on the order of 10^8) compared to the rest of the eigenvalues. These eigenvalues primarily correspond to the virtual resistor, r_n. They

are not considered when eigenvalues are plotted in Fig. 1.17. The negative real part of the eigenvalues obtained from 'A1' and 'A2' signifies the linearized system's local stability. According to Lyapunov's second method for stability analysis, the system is asymptotically stable in the small-signal sense. Although the sub-systems are exponentially stable, the stability of the overall system cannot be guaranteed [30, 31]. This is because the switched systems may have divergent trajectories for certain switch signals. However, these models may be used for a future study of the switched system.
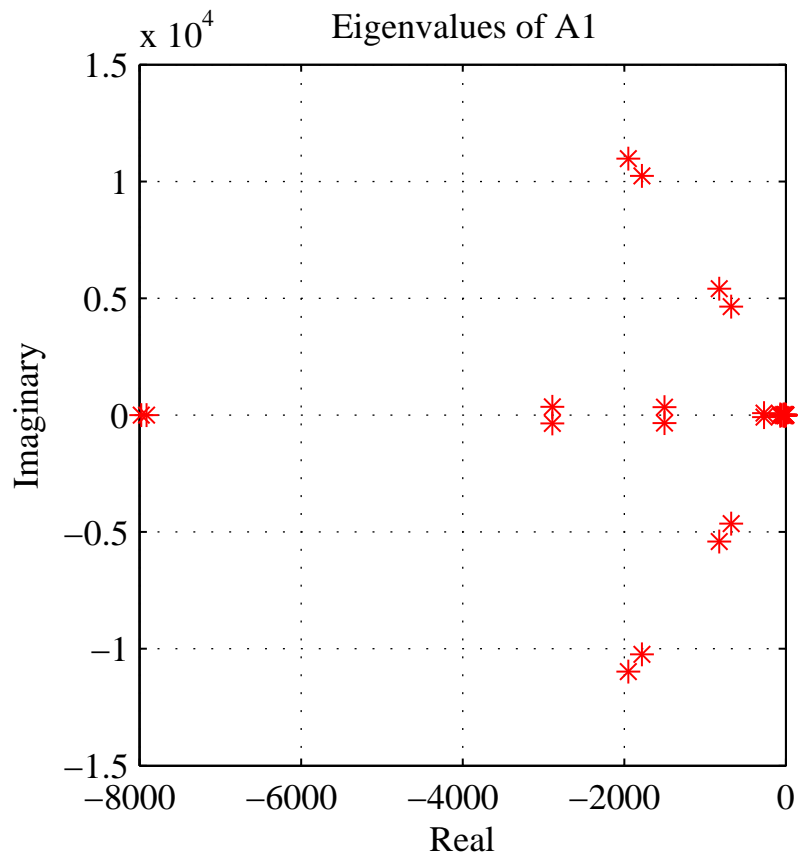
Figure 1.17. Partial eigenvalue plot of A1

An eigenvalue analysis investigates the dynamic behavior of a power system under different characteristic frequencies or 'modes'. In a power system it is required that all modes are properly damped to nullify the effect of oscillation due to perturbation in states. A well damped system provides good stability. Eigenvalues presented in Table 1.3 show

that there are 15 distinct oscillatory modes in the system. A participation factor analysis was done to identify the states which are major participants in those modes. Participation factors can be positive, zero, or negative. A positive participation factor associated with a particular state means that state is contributing to the oscillation of the system. A negative participation factor indicates a state that is dampening the system oscillation.

Table 1.3. Eigenvalues of A1

Index	Real (1/s)	Im (rad/s)	ξ^1 (%)	$\omega_o{}^2$ (Hz)	Mode	Major participants
1,2	-7.10×10^8	±376.57	100	1.13×10^8	1	i_{lineDQ}
3,4	-2.09×10^8	±376.58	100	3.34×10^8	2	i_{odq1}, i_{odq2}
5,6	-1951.65	±10980.03	17.50	1774.92	3	v_{oq1}, v_{oq2}
7,8	-1781.19	±10234.93	17.15	1653.42	4	v_{od1}, v_{od2}
9	-7981.28	0	100	1270.26		
10	-7915.62	0	100	1259.81		
11,12	-822.46	±5415.18	15.02	871.74	5	v_{oq1}, v_{oq2}
13,14	-674.16	±4643.15	14.37	746.73	6	v_{od1}, v_{od2}
15,16	-2889.85	±351.71	99.27	463.33	7	$i_{loadDQ1}, i_{loadDQ2}$
17,18	-1500.35	±336.76	97.57	244.73	8	$i_{loadDQ1}, i_{loadDQ2}$
19,20	-267.94	±82.01	95.62	44.60	9	i_{ldq1}, i_{ldq2}
21,22	-69.76	±21.47	95.58	11.62	10	$\gamma_{dq1}, \gamma_{dq2}$
27,28	-25.38	±31.18	63.12	6.40	11	$\varphi_{q1}, \gamma_{q1}, \varphi_{q2}, \gamma_{q2}$
29,30	-6.16	±22.90	25.97	3.77	12	$\varphi_{d1}, \gamma_{d1}, \varphi_{d2}, \gamma_{d2}$
34,35	-2.24	±4.68	43.21	0.83	13	$\varphi_{dq1}, \varphi_{dq2}$
31,32	-10.65	±8.14	79.45	2.13	14	$\delta_2, \varphi_{PLL1}, \varphi_{PLL2}$
33	-7.53	0	100	1.20		
23,24	-50.25	±0.02	100	8	15	P_1, Q_1, P_2, Q_2
25	-50.27	0	100	8		
26	-50.27	0	100	8		
36	0	0	∞	0		

---

[1] Damping ratio
[2] Natural frequency

The participation factor analysis shows that mode 1 and mode 2 are properly damped in the system. However, modes $3, 4, 5,$ and 6 are lightly damped. The states in these modes are more likely to make the system unstable during disturbances. Modes $10, 11, 12,$ and 13 are low frequency oscillatory and are largely influenced by the states related to the voltage and current controllers. Among them, mode 12 is not well damped. This mode can be designated as the 'problem mode' for this system. Mode 14 is heavily participated in by the phase angle of the second inverter. This is another low frequency oscillatory mode. This mode is also influenced by the dynamics of the PLL, which help dampen the oscillation generated by the phase angle. The states relating to the inverter output powers participate in mode 15. The natural frequency of oscillation of this mode is 8 *Hz* or 50.26 *rad/s*. This also happens to be the cut-off frequency of the low pass filter used during controller design.

From this analysis, modes $3, 4, 5,$ and 6 are at higher oscillatory frequencies and they have lower damping ratios. The *dq* axis output voltages participate heavily in those modes. Equations (1.19) and (1.20) show that the v_{odq} dynamics are governed by the damping resistor, R_d, along with some other state variables. As a result, any change in R_d will result a change in the output voltage dynamics as well. The initial value of the damping resistor was chosen based on its ability to suppress the resonant frequency of the filter. A higher damping resistor may be selected, but will contribute additional loss to the system. The advantage of using a higher damping resistance is explained using Table 1.4, which shows the system eigenvalues when a damping resistor of $R_d = 10$ Ω is used. Another method to increase damping in the system is to include active damping techniques in controller design. This method does not contribute loss to the system. Such controllers are beyond the scope of this paper but discussed more elaborately in [32].

Table 1.4 shows that the higher damping resistance R_d increases the damping ratio of modes $3, 4, 5,$ and 6. This improves the stability margin for the system. The low frequency oscillatory modes are now the dominant dynamics of the system. A good controller design for this system would achieve higher damping ratios for these modes such that they

decay as quickly as possible after a disturbance. This analysis is important to identify the states related to the low frequency oscillatory modes with lower damping ratios. During model reduction procedures these modes must be retained.

Table 1.4. Eigenvalues of A1 With $R_d = 10\ \Omega$

Index	Real $(1/s)$	Im (rad/s)	ξ $(\%)$	ω_o (Hz)	Mode
$1,2$	-7.1×10^8	± 376.60	100	1.1×10^8	1
$3,4$	-2.1×10^8	± 376.63	100	3.4×10^8	2
$5,6$	-9270.13	± 6519.71	81.80	1803.74	3
$7,8$	-8366.74	± 6038.22	81.09	1642.17	4
9	-7767.72	0	100	1236.27	
10	-7783.94	0	100	1238.85	
$11,12$	-2617.87	± 4785.71	48	868.18	5
$13,14$	-2070.05	± 4221.23	44.03	748.26	6
$15,16$	-2926.93	± 365.68	99.23	469.46	7
$17,18$	-1502.25	± 338.92	97.55	245.10	8
$19,20$	-267.94	± 82.04	95.62	44.60	9
$21,22$	-69.76	± 21.48	95.57	11.62	10
$27,28$	-25.38	± 31.18	63.12	6.40	11
$29,30$	-6.16	± 22.90	25.97	3.77	12
$34,35$	-2.24	± 4.68	43.21	0.83	13
$31,32$	-10.65	± 8.14	79.45	2.13	14
33	-7.53	0	100	1.20	
$23,24$	-50.25	± 0.02	100	8	15
25	-50.27	0	100	8	
26	-50.27	0	100	8	
36	0	0	∞	0	

A sparsity pattern of 'A1' is depicted in Fig. 1.18. The pattern shows that there are six regions in the matrix where the non-zero elements are distributed. Regions 1 and 3 are formed by DER_1 and regions and 2, 4, and 5 are formed by DER_2. Regions 3 and 4 are generated by the inclusion of the virtual resistor, r_n, in the respective inverter buses. These regions also include r_n's interaction with the damping resistors and the coupling inductors. Region 5 is formed based on (1.26), where the first inverter's phase angle was set as the reference angle for the second inverter. Region 6 is formed by the loads and the distribution line. If another inverter is added to this system then the new sparsity matrix will have additional patterns identical to those in regions 2, 4, and 5. These regions will be located on the diagonal of the matrix following the second inverter's sparsity pattern.
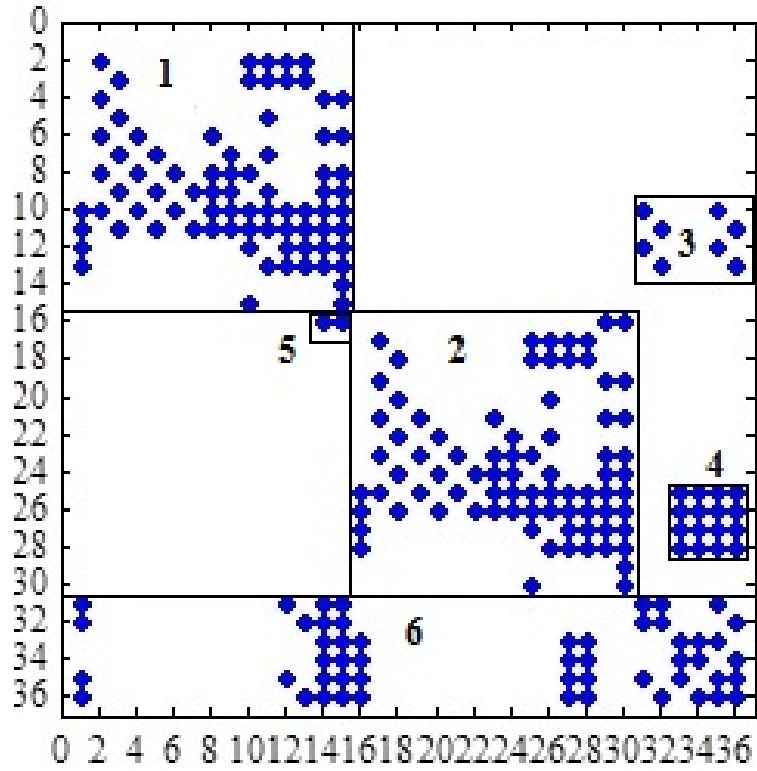
Figure 1.18. Sparsity pattern of A1

1.7. CONCLUSION

This work presents an accurate small-signal model of a multiple inverter microgrid system operating in islanded mode. The model is based on the nonlinear equations that describe system dynamics. These nonlinear equations is then linearized around stable operating points to develop the small-signal model. Load perturbation is done to study the system dynamics. The accuracy of the model is assessed through comparison to simulation and experimental results. An eigenvalue analysis is done using the small-signal model to determine the stability of the system. Low and high frequency oscillatory modes are identified from the eigenvalue analysis. A participation factor analysis is included to identify the states contributing to the different oscillatory modes. It is found that some of these oscillatory modes can be controlled using proper damping resistors. A sparsity pattern of the system is investigated. The most important contribution of this paper is the proposed model of an islanded microgrid and its ability to accurately predict the dynamic response of the system. It is possible that similar power system networks could be accurately developed as switched autonomous systems. Future work for this project will include determination and application of a proper model reduction technique to reduce the fast decaying states. Also, system modeling with capacitive and nonlinar load are considered as separate research objectives.

1.8. REFERENCES

[1] M. Smith and D. Ton, "Key connections: The U.S. department of energy's microgrid initiative," *IEEE Power and Energy Magazine*, vol. 11, no. 4, pp. 22–27, Jul. 2013.

[2] D. Boroyevich, I. Cvetkovic, R. Burgos, and D. Dong, "Intergrid: A future electronic energy network?" *IEEE J. Emerg. Sel. Top. Power Electron.*, vol. 1, no. 3, pp. 127–138, Sep. 2013.

[3] R. H. Lasseter, "Smart distribution: Coupled microgrids," *Proc. IEEE*, vol. 99, no. 6, pp. 1074–1082, Jun. 2011.

[4] R. H. Lasseter, "Microgrids," in *Power Engineering Society Winter Meeting, 2002. IEEE*, vol. 1, 2002, p. 305–308.

[5] I. Grau, L. M. Cipcigan, N. Jenkins, and P. Papadopoulos, "Microgrid intentional islanding for network emergencies," in *Universities Power Engineering Conference (UPEC), 2009 Proceedings of the 44th International*, 2009, p. 1–5.

[6] J. Peas Lopes, C. Moreira, and A. Madureira, "Defining control strategies for Mi-croGrids islanded operation," *IEEE Trans. Power Syst.*, vol. 21, no. 2, pp. 916–924, 2006.

[7] T. Green and M. Prodanović, "Control of inverter-based micro-grids," *Electric Power Systems Research*, vol. 77, no. 9, pp. 1204–1213, Jul. 2007.

[8] H.-K. Kang, S.-J. Ahn, and S.-I. Moon, "A new method to determine the droop of inverter-based DGs," in *Power & Energy Society General Meeting, 2009. PES'09. IEEE*, 2009, p. 1–6.

[9] S. Tabatabaee, H. R. Karshenas, A. Bakhshai, and P. Jain, "Investigation of droop characteristics and X/R ratio on small-signal stability of autonomous microgrid," in *Power Electronics, Drive Systems and Tech. Conf. (PEDSTC), 2011 2nd*, 2011, p. 223–228.

[10] W. Yao, M. Chen, J. Matas, J. M. Guerrero, and Z.-M. Qian, "Design and analysis of the droop control method for parallel inverters considering the impact of the complex impedance on the power sharing," *IEEE Trans. Ind. Electron.*, vol. 58, no. 2, pp. 576–588, Feb. 2011.

[11] C.-T. Lee, C.-C. Chu, and P.-T. Cheng, "A new droop control method for the au-tonomous operation of distributed energy resource interface converters," *IEEE Trans. Power Electron.*, vol. 28, no. 4, pp. 1980–1993, Apr. 2013.

[12] Y. Guan, Y. Wang, Z. Yang, R. Cao, and H. Xu, "Control strategy for autonomous op-eration of three-phase inverters dominated microgrid under different line impedance," in *Electrical Machines and Systems (ICEMS), 2011 Int. Conf. on*, 2011, p. 1–5.

[13] T. L. Vandoorn, B. Meersman, L. Degroote, B. Renders, and L. Vandevelde, "A con-trol strategy for islanded microgrids with DC-Link voltage control," *IEEE Trans. Power Deliv.*, vol. 26, no. 2, pp. 703–713, Apr. 2011.

[14] T. L. Vandoorn, B. Renders, B. Meersman, L. Degroote, and L. Vandevelde, "Reactive power sharing in an islanded microgrid," in *Universities Power Engineering Conf. (UPEC), 2010 45th Int.*, 2010, p. 1–6.

[15] T. L. Vandoorn, B. Renders, L. Degroote, B. Meersman, and L. Vandevelde, "Active load control in islanded microgrids based on the grid voltage," *IEEE Trans. Smart Grid*, vol. 2, no. 1, pp. 139–151, Mar. 2011.

[16] F. Katiraei, M. Iravani, and P. Lehn, "Small-signal dynamic model of a micro-grid including conventional and electronically interfaced distributed resources," *IET Generation, Transmission & Distribution*, vol. 1, no. 3, p. 369, 2007.

[17] Y. Zhang, Z. Jiang, and X. Yu, "Small-signal modeling and analysis of parallel-connected voltage source inverters," in *Power Electronics and Motion Control Conf., 2009. IPEMC'09. IEEE 6th Int.*, 2009, p. 377–383.

[18] E. A. A. Coelho, P. C. Cortizo, and P. F. D. Garcia, "Small-signal stability for parallel-connected inverters in stand-alone AC supply systems," *IEEE Trans. Ind. App.*, vol. 38, no. 2, p. 533–542, 2002.

[19] N. Pogaku, M. Prodanovic, and T. C. Green, "Modeling, analysis and testing of autonomous operation of an inverter-based microgrid," *IEEE Trans. Power Electron.*, vol. 22, no. 2, pp. 613–625, Mar. 2007.

[20] Y. Mohamed and E. El-Saadany, "Adaptive decentralized droop controller to preserve power sharing stability of paralleled inverters in distributed generation microgrids," *IEEE Trans. Power Electron.*, vol. 23, no. 6, pp. 2806–2816, Nov. 2008.

[21] M. A. Hassan and M. A. Abido, "Optimal design of microgrids in autonomous and grid-connected modes using particle swarm optimization," *IEEE Trans. Power Electron.*, vol. 26, no. 3, pp. 755–769, Mar. 2011.

[22] R. M. dos Santos Filho, P. F. Seixas, and P. C. Cortizo, "A comparative study of three-phase and single-phase PLL algorithms for grid-connected systems," in *Proc. INDUSCON Conf. Rec*, 2006.

[23] V. Kaura and V. Blasko, "Operation of a phase locked loop system under distorted utility conditions," *Industry Applications, IEEE Transactions on*, vol. 33, no. 1, p. 58–63, 1997.

[24] J. Ögren, "PLL design for inverter grid connection: Simulations for ideal and non-ideal grid conditions," Master's thesis, Uppsala University, 2010.

[25] P. Krause, "The method of symmetrical components derived by reference frame theory," *IEEE Trans. Power Appar. Syst.*, vol. PAS-104, no. 6, pp. 1492–1499, 1985.

[26] M. Rasheduzzaman, J. Mueller, and J. W. Kimball, "Small-signal modeling of a three-phase isolated inverter with both voltage and frequency droop control," in *Proc. of the IEEE Applied Power Electronics Conf. (APEC) 2014*.

[27] J. Dannehl, M. Liserre, and F. W. Fuchs, "Filter-based active damping of voltage source converters with LCL filter," *IEEE Trans. Ind. Electron.*, vol. 58, no. 8, pp. 3623–3633, Aug. 2011.

[28] M. Liserre, F. Blaabjerg, and S. Hansen, "Design and control of an LCL-Filter-Based three-phase active rectifier," *IEEE Trans. Ind. App.*, vol. 41, no. 5, pp. 1281–1291, Sep. 2005.

[29] H. Cha and T.-K. Vu, "Comparative analysis of low-pass output filter for single-phase grid-connected photovoltaic inverter," in *Applied Power Electronics Conference and Exposition (APEC), 2010 Twenty-Fifth Annual IEEE.* IEEE, 2010, p. 1659–1665.

[30] D. Liberzon, *Switching in Systems and Control.* Boston, MA: Birkhauser Boston : Imprint: Birkhauser, 2003.

[31] M. Rasheduzzaman, T. Paul, and J. W. Kimball, "Markov jump linear system analysis of microgrid," in *Proc. of American Control Conf. (ACC) 2014.*

[32] C. Bao, X. Ruan, X. Wang, W. Li, D. Pan, and K. Weng, "Step-by-step controller design for LCL-Type grid-connected inverter with capacitor-current-feedback active-damping," *IEEE Trans. Power Electron.*, vol. 29, no. 3, pp. 1239–1253, Mar. 2014.

II. REDUCED ORDER SMALL-SIGNAL MODEL OF MICROGRID SYSTEMS-PART I

Md. Rasheduzzaman, Jacob A. Mueller, and Jonathan W. Kimball

Department of Electrical and Computer Engineering

Missouri University of Science & Technology, Rolla, MO 65409

ABSTRACT— The integration of renewable energy sources as a means of power generation will result in an increase in the number of grid-tied inverters. Linear, small-signal models of these inverters and their controllers are required in order to perform power system stability and eigenvalue analyses. State-space models of such sources, when aggregated in multi-bus systems tend to be of prohibitively high order, thus need to be reduced for faster calculation of the dominant eigenvalues and simplified determination of the important dynamics. The objective of this study was to develop a reduced order small-signal model of a microgrid system capable of operating both in the grid-tied and islanded conditions. Part-I of the paper discussed the grid-tied microgrid, and part-II of the paper discussed the islanded operation of the microgrid system. The nonlinear equations of the proposed system were derived in the dq reference frame and then linearized around stable operating points to construct a small-signal model. The large order state matrix was then reduced using the singular perturbation technique. The first part of the paper presents the modeling and reduction of the grid-tied inverters in a microgrid. Step responses of the model were compared to the experimental results from a hardware test to assess their accuracy and similarity to the full order system. The proposed reduced order model was applied to a modified IEEE-37 bus grid-tied microgrid system.

Index Terms— Microgrid modeling, singular perturbation, grid-tied inverter, voltage source inverter.

2.1. INTRODUCTION

Integration of the renewable energy sources to the distribution grid has increased over the years. Unlike the conventional synchronous generators, these distributed energy resources (DERs) are inertia-less. From a power systems point of view, use of these inertia-less sources makes the time domain simulations of the distribution system very interesting during both transient response and fault analysis. The DER converter uses the modern control algorithm and controller design approach [1] for stable operation in grid-tied mode as well as in islanded mode of operation. The concept of a microgrid is now well-established as a step towards modernizing the nation's electric delivery network to smart-grid using DERs [2]. Microgrids supply power to local loads with or without the grid support to ensure energy security [3], [4]. As the concept of the microgrid system is getting popular among the researchers, the reduced order modeling of such systems is still emerging.

In this study, operation of a grid-connected DER and its controllers are discussed. The power processing unit is a voltage source inverter (VSI). The controllers for the VSI are developed in the synchronous reference frame [5]. The 15th order mathematical model of the VSI, consisting of the controllers and the LCL filter, are developed to facilitate the dynamics analysis and the eigenvalue studies. The IGBT's dynamic response was approximated using a controlled voltage source, which eliminated the need of including the parasitic elements in the state equations. However, the time domain analysis of a microgrid system with such numerous DERs, each having 15 states, is still time-consuming and a computational burden. As a result, the necessity of the reduced order modeling of these grid-tied inverters has never been more obvious.

The use of the reduced order grid-tied inverter model is suggested for dynamic response analysis during the black-start of the decentralized islanded microgrid. During the black-start procedure, the microgrid is first energized using a synchronous generator or a master DER which sets the voltage and frequency reference for the system. After that,

slave DERs are connected to the system one-by-one using the grid-connected controllers before they switch to droop controlled mode [6, 7, 8, 9]. The proposed reduced order model is useful not only for the stability analysis of inverter based generator emulator in test-bed for power systems [10] but also for transient stability analysis in a microgrid system [11]. Similarly, the wind turbine's grid side converter could be modeled using the reduced order models to simulate the impact of wind farm's installations in utility grid [12]. In addition, development of common quadratic Lyapunov function becomes easier by using the reduced order state matrices linearized around different operating points.

Another important use of this reduced order model includes the study of the system stability using Markov Jump Linear System (MJLS) [20] analysis. The microgrid's transition from grid-tied to islanded mode results in a change in the controller operation mode. Stability of such system could be characterized using the switched system analyses, where the system jumps from one state space model to another. An example of such system is presented in the second part of this work.

Model order reduction techniques based on the behavior of coherent groups of generators were used to study system dynamics in large-disturbance stability analyses [14, 15, 16, 17]. Another type of model order reduction method based on the state variable grouping and eigenvalue grouping was introduced in [18]. This technique ignored states with large time constants associated with the inertia of the synchronous generators and did not consider the input-output dynamics of the full model [19].

Often equations with larger time constants were ignored in the transient analysis as the information they carry can be neglected. These techniques are not applicable for the proposed inertia-less inverter system. Moreover, the plant model is nothing but the LCL filter at the inverter output. This study shows that the LCL filter contributed to the less important dynamics compared to the other states such as the voltage and the current controllers. This is opposite to [20] where the output filter consists of only an inductor and the controller dynamics are ignored while reducing the order of the model. However, a

more realistic model of the microgrid inverter includes an LCL filter instead of using only an L (inductor type) filter.

Construction of a reduced order model of the proposed system by ignoring the states from the LCL filter would result in erroneous output when simulated. As a result, a full order model is developed considering all the states present in the grid-tied inverter system and then the model is reduced using well-known singular perturbation technique. The proposed reduced order grid-tied inverter model is verified using the experimental results obtained from the laboratory test bed. Once verified, the proposed model becomes useful for application in a larger system such as in IEEE-37 node distribution test feeder.

The rest of this paper, which is Part-I, is ordered as follows: section II presents a brief background on the singular perturbation technique, section III contains a derivation of a linearized small-signal model of a grid-tied inverter, and section IV demonstrates the model order reduction technique. Section V presents the experimental test-bed and section VI contains the results obtained from the reduced order model of the grid-tied inverter and the experimental test bed. Part-II of the paper contains reduced order modeling of the islanded microgrid system. Verification of the microgrid dynamics during islanded mode of operation and during grid-tied to islanded mode transition are presented in the second part of the paper.

2.2. PRELIMINARIES

In a grid-tied microgrid network, all the bus voltages and the system frequency are maintained by the stiff main grid. As a result, the same model that is developed for a particular grid-tied inverter could be applied to the rest of the inverters in a microgrid system. The system under consideration is depicted in Fig. 2.1.

The DER in question consists of a three-phase VSI and its controllers. In a practical system, this DER could be replaced with the renewable energy inverters such as the DC-AC

side of the wind firm's power converter or the photo-voltaic energy converter. In a typical microgrid system numerous DERs could be found that supply power to the local loads in coordination with the main grid. To study the dynamics of a microgrid, such large scale systems are needed to be modeled and analyzed.

Large scale systems are a computational burden because of the storage capacity and computational speed they require, as well as accuracy complications resulting from the likelihood of an ill-conditioned matrix [21]. According to the parsimony principle, the best model of a system is defined as "the one that accurately represents a transfer function with a minimum number of parameters" [22]. A model order reduction (MOR) algorithm provides a tool to replace the original system with one of a smaller dimension. The guidelines for model order reduction are discussed in [21, 23, 24].

The non-linear equations that capture the system dynamics are expressed in terms of the slow dynamic variables (x) and the fast dynamic variables (z). With the presence of the system input variable vector u, and the small model parameter ε, where $\varepsilon =$
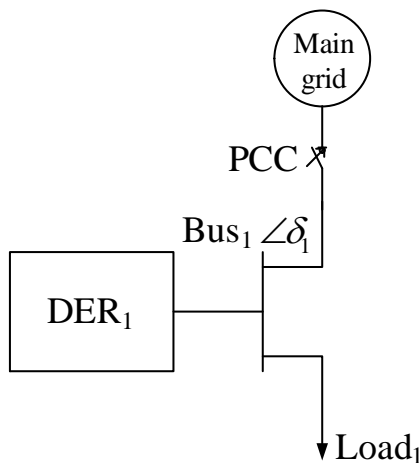
Figure 2.1. A grid connected DER in a microgrid system

$diag\{\varepsilon_1, \varepsilon_2, ..., \varepsilon_m\}$, the slow subsystem and the fast subsystem are presented as:

$$\dot{x}(t) = f(x, z, u, t, \varepsilon) \qquad (2.1a)$$

$$\varepsilon\dot{z}(t) = g(x, z, u, t, \varepsilon) \qquad (2.1b)$$

The small–signal model of the system is then:

$$\dot{x} = A_{11}x + A_{12}z + B_1 u \qquad (2.2a)$$

$$\varepsilon\dot{z} = A_{21}x + A_{22}z + B_2 u \qquad (2.2b)$$

$$y = [C_1 \quad C_2][x \quad z]^T + Du \qquad (2.2c)$$

Here, the system state matrix is $A = \begin{bmatrix} A_{11} & A_{12} \\ A_{21} & A_{22} \end{bmatrix} \in \mathfrak{R}^{n\times n}$, the input matrix is $B = \begin{bmatrix} B_1 \\ B_2 \end{bmatrix}$

$\in \mathfrak{R}^{n\times m}$ and the output matrix is $C = \begin{bmatrix} C_1 & C_2 \end{bmatrix} \in \mathfrak{R}^{p\times n}$. The feed-through matrix is $D \in$

$\mathfrak{R}^{p\times m}$. The transfer function of the original system is:

$$G(s) = C(sI - A)^{-1}B + D = \begin{pmatrix} A & B \\ C & D \end{pmatrix} \qquad (2.3)$$

The expected r^{th} order reduced order system $(r < n)$ is then:

$$G_r(s) = C_r(sI - A_r)^{-1}B_r + D_r = \begin{pmatrix} A_r & B_r \\ C_r & D_r \end{pmatrix} \qquad (2.4)$$

The interaction of fast and slow phenomena in high-order systems results in 'stiff' numerical problems which require expensive integration routines. The singular perturbation approach alleviates both dimensionality and stiffness difficulties [25]. It lowers the

model order by first neglecting the 'fast' phenomena. It then improves the approximation by reducing their effect as 'boundary layer' corrections calculated in separate time scales.

Singular perturbation technique provides a means for justifying the elimination of fast dynamic states without losing the physical nature of the states. A very small perturbation parameter ε, $(0 < \varepsilon << 1)$, is associated with the fast states, signifying the fact that their elimination has little effect on the dynamics.

In the singular perturbation technique, instead of discarding the less important states entirely in the reduced model, residues from the less important states are substituted in the important states. This substitution results in a better approximation at steady-state, meaning the dc gain of the reduced order model is approximately the same as that of the full order system.

As $\varepsilon \to 0$ the quasy-steady-state (QSS) solution obatined from (2.2b) is:

$$z = -A_{22}^{-1}A_{21}x - A_{22}^{-1}B_2u \tag{2.5}$$

Substituting z in (2.2a) provides us with the reduced order model:

$$A_r = A_{11} - A_{12}A_{22}^{-1}A_{21}; \quad B_r = B_1 - A_{12}A_{22}^{-1}B_2 \tag{2.6a}$$

$$C_r = C_1 - C_2A_{22}^{-1}A_{21}; \quad D_r = D - C_2A_{22}^{-1}B_2 \tag{2.6b}$$

Thus, the new reduced order system is given by (2.4). The modification of the feed-through matrix to D_r ensures that the gain of the reduced system matches the gain of the high order system at low frequency [26].

2.3. SMALL-SIGNAL MODEL OF THE GRID-TIED INVERTER

The DER in Fig. 2.2 consists of a synchronous reference frame based three-phase inverter with LCL filter connected to the distribution grid at the inverter bus. The inputs to

the system are the commanded active and reactive power, P^* and Q^*. The control architecture has an outer power control loop and an inner current control loop. A phase-locked loop (PLL) ensures tracking of the grid voltages' phase. The power control loop compares the commanded active and reactive power to the calculated active and reactive power, P and Q. The error signals derived from this comparison are used as an input to proportional-integral (PI) controllers whose outputs are current references i_{ld}^* and i_{lq}^*. The current controller compares the measured filter inductor currents i_{ld} and i_{lq} to the commanded currents and provides commanded output voltages v_{id}^* and v_{iq}^* using another set of PI controller. This loop removes the cross-coupling terms caused by the reference frame transformation. Commanded voltages are passed through a *qd0* to *abc* transformation block and then through the space vector modulation (SVPWM) to generate the appropriate switching sequence. The reference frame transformations use a reference phase angle δ calculated by the PLL. The PLL used in the system is a conventional synchronous reference frame PLL, which drives the *d*-axis voltage component to 0 [27]. By adding a low-pass filter to the PI controller of the PLL, much of the high-frequency ripple in the *d*-axis voltage is eliminated.

2.3.1. Nonlinear Equations of the Inverter Model. In this section, controllers shown as blocks in Fig. 2.2 are analyzed and their dynamics are expressed using equations. Although similar controllers were used by different authors in [28], [29] and [30], the controller dynamic equations are presented here for better clarity and understanding of the two time-scale property of the system.

Average Power Calculation. The *dq* axis output voltage and current measurements are used to calculate the instantaneous active and reactive power generated by the inverter:

$$p = \frac{3}{2}\left(v_{od}i_{od} + v_{oq}i_{oq}\right); \quad q = \frac{3}{2}\left(v_{oq}i_{od} - v_{od}i_{oq}\right) \tag{2.7}$$
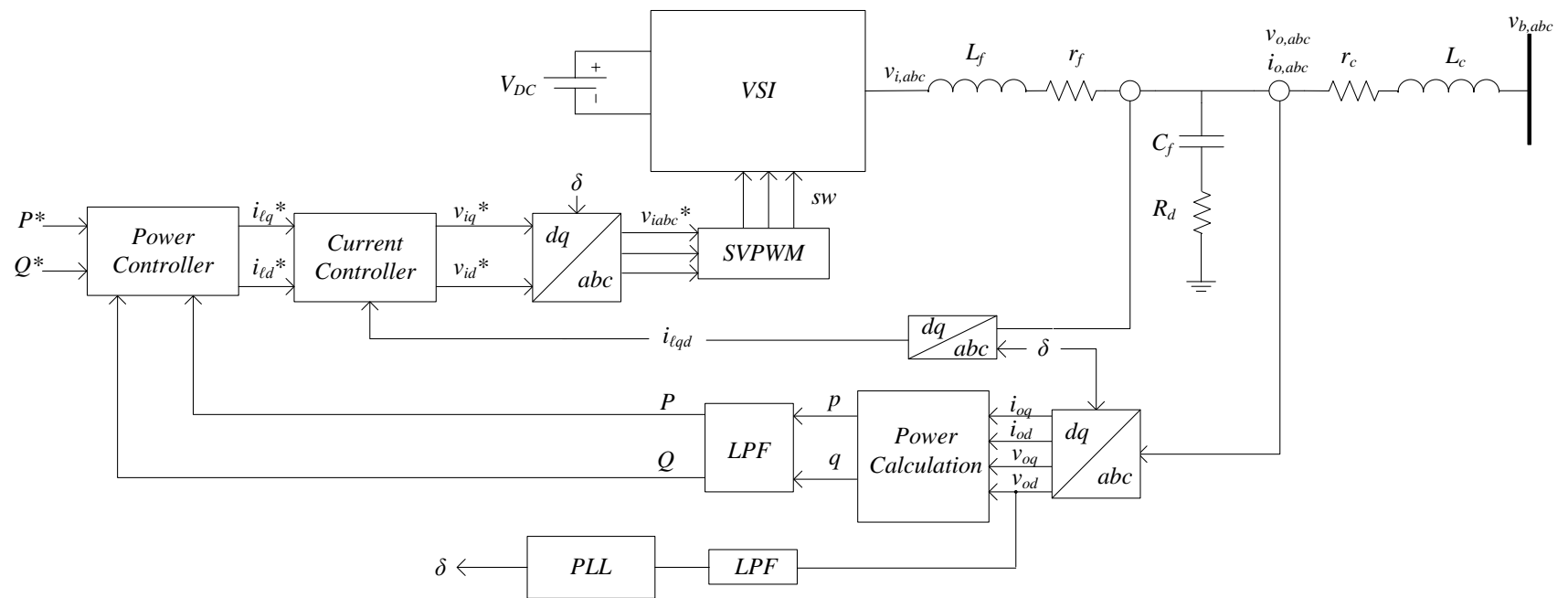
Figure 2.2. Proposed DER and the controller block diagram

Instantaneous powers are then passed through low pass filters with corner frequency ω_c to obtain the average output power.

$$P = \frac{\omega_c}{\omega_c + s} p \Rightarrow \dot{P} = -P\omega_c + 1.5\omega_c \left(v_{od}i_{od} + v_{oq}i_{oq} \right) \tag{2.8}$$

$$Q = \frac{\omega_c}{\omega_c + s} q \Rightarrow \dot{Q} = -Q\omega_c + 1.5\omega_c \left(v_{oq}i_{od} - v_{od}i_{oq} \right) \tag{2.9}$$

Phase Locked Loop (PLL). The PLL presented in this paper is the same as that one presented in [31]. There are three states governing PLL dynamics.

$$\dot{v}_{od,f} = \omega_{c,PLL}v_{od} - \omega_{c,PLL}v_{od,f} \tag{2.10}$$

$$\dot{\varphi}_{PLL} = -v_{od,f} \tag{2.11}$$

$$\dot{\delta} = \omega_{PLL} \tag{2.12}$$

$$\omega_{PLL} = 377 - k_{p,PLL}v_{od,f} + k_{i,PLL}\varphi_{PLL} \tag{2.13}$$

Power Controller. Two PI controllers (Fig. 2.3) are used in the power controller block. The set-points are the commanded active and reactive powers.

Figure 2.3. Power controllers

$$\dot{\varphi}_P = P^* - P; \quad i_{lq}{}^* = k_{i,pq}\varphi_p + k_{p,pq}\dot{\varphi}_P \tag{2.14}$$

$$\dot{\varphi}_Q = Q^* - Q; \quad i_{ld}{}^* = k_{i,pq}\varphi_Q + k_{p,pq}\dot{\varphi}_Q \tag{2.15}$$

Current Controllers. The current controllers consist of another set of PI controllers [31].

$$\dot{\gamma}_d = i_{ld}{}^* - i_{ld}; \quad v_{id}{}^* = -\omega_n L_f i_{lq} + k_{ic}\gamma_d + k_{pc}\dot{\gamma}_d \tag{2.16}$$

$$\dot{\gamma}_q = i_{lq}{}^* - i_{lq}; \quad v_{iq}{}^* = \omega_n L_f i_{ld} + k_{ic}\gamma_q + k_{pc}\dot{\gamma}_q \tag{2.17}$$

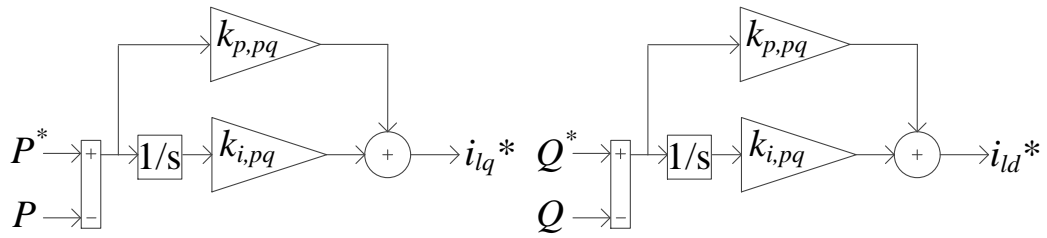**LC Filter and Coupling Inductor.** The state equations governing the filter dynamics presented in [31] are:

$$\dot{i}_{ld} = \frac{1}{L_f}\left(-r_f i_{ld} + v_{id} - v_{od}\right) + \omega_n i_{lq} \tag{2.18}$$

$$\dot{i}_{lq} = \frac{1}{L_f}\left(-r_f i_{lq} + v_{iq} - v_{oq}\right) - \omega_n i_{ld} \tag{2.19}$$

$$\dot{i}_{od} = \frac{1}{L_c}\left(-r_c i_{od} + v_{od} - v_{bd}\right) + \omega_n i_{oq} \tag{2.20}$$

$$\dot{i}_{oq} = \frac{1}{L_c}\left(-r_c i_{oq} + v_{oq} - v_{bq}\right) - \omega_n i_{od} \tag{2.21}$$

$$\dot{v}_{od} = \frac{1}{C_f}\left(i_{ld} - i_{od}\right) + \omega_n v_{oq} + R_d(\dot{i}_{ld} - \dot{i}_{od}) \tag{2.22}$$

$$\dot{v}_{oq} = \frac{1}{C_f}\left(i_{lq} - i_{oq}\right) - \omega_n v_{od} + R_d(\dot{i}_{lq} - \dot{i}_{oq}) \tag{2.23}$$

Reference Frame Transformation. The DER state equations are derived in terms of the local reference frame. The main grid is assumed to be in the global reference frame. A transformation is necessary to translate into values defined in the local reference frame to the global reference frame. An application of this transformation is shown graphically in Fig. 2.4. The difference in subscript capitalization denotes whether the quantity is defined in the local or global reference frame.

$$\begin{bmatrix} f_D \\ f_Q \end{bmatrix}_{global} = \begin{bmatrix} \cos\theta & \sin\theta \\ -\sin\theta & \cos\theta \end{bmatrix} \begin{bmatrix} f_d \\ f_q \end{bmatrix}_{local} \qquad (2.24)$$

$$\begin{bmatrix} f_d \\ f_q \end{bmatrix}_{local} = \begin{bmatrix} \cos\theta & -\sin\theta \\ \sin\theta & \cos\theta \end{bmatrix} \begin{bmatrix} f_D \\ f_Q \end{bmatrix}_{global} \qquad (2.25)$$

Where θ is the difference between the global reference phase and the local reference phase as depicted in Fig. 2.5.
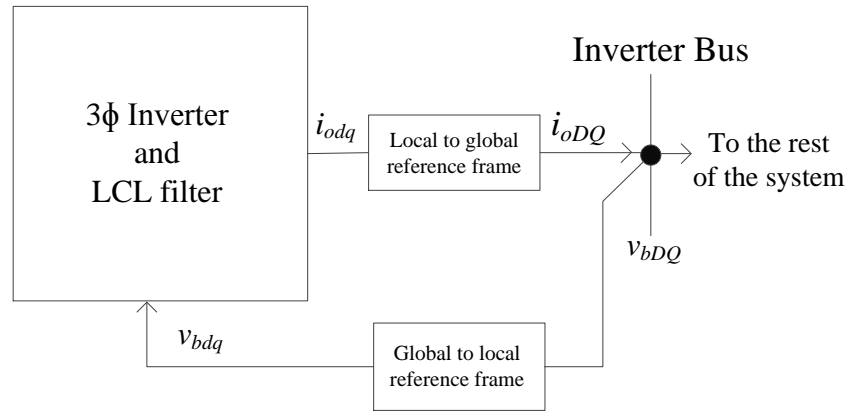
Figure 2.4. Reference frame transformation
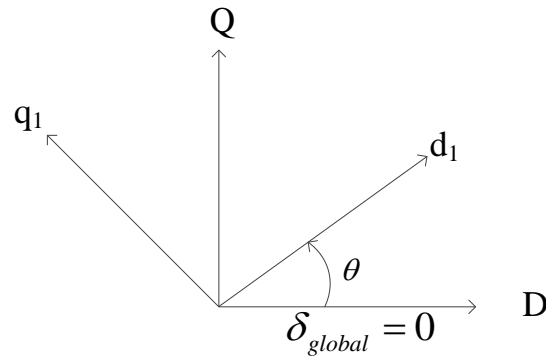
Figure 2.5. Transformation angle

2.3.2. Linearized Model . The proposed system has 15 states that describe the system dynamics:

$$x_{sys} = [P \quad Q \quad v_{od,f} \quad \varphi_{PLL} \quad \delta \quad \varphi_P \quad \varphi_Q \quad \gamma_d \quad \gamma_q$$
$$i_{ld} \quad i_{lq} \quad i_{od} \quad i_{oq} \quad v_{od} \quad v_{oq}]^T$$

(2.26)

Table 2.1 shows the controller gains used, and Table 2.2 shows the other parameters needed to linearize the system. The linearized LTI system of the form (2.27) is generated using Matlab's symbolic math toolbox.

$$\dot{\tilde{x}}_{sys} = A\tilde{x}_{sys} + B\tilde{u}; \quad \tilde{y} = C\tilde{x}_{sys} + D\tilde{u}$$

(2.27)

Where the inputs and outputs are defined as:

$$u = [P^* \quad Q^*]^T$$

(2.28)

$$y = [P \quad Q \quad i_{od} \quad i_{oq} \quad i_{ld} \quad i_{lq} \quad v_{od} \quad v_{oq} \quad \omega_{PLL}]^T$$

(2.29)

Table 2.1. Controller Gains

PI gains for	Parameter	Value
Power	$k_{p,pq}$	0.01
controllers	$k_{i,pq}$	0.10
Current	k_{pc}	1.00
controllers	k_{ic}	100
PLL	$k_{p,PLL}$	0.25
controller	$k_{i,PLL}$	2.00

Table 2.2. System Parameters

Parameter	Value	Parameter	Value
L_f	4.20 mH	r_f	0.5 Ω
L_c	0.60 mH	r_c	0.425 Ω
C_f	15 μf	R_d	2.025 Ω
ω_c	50.26 rad/s	ω_n	377 rad/s
$\omega_{c,PLL}$	7853.98 rad/s		

2.4. MODEL ORDER REDUCTION

In the singular perturbation approach, the fast states are characterized by the small model parameters used as their coefficients. To identify the small model parameters, the dynamic equations are normalized as:

$$[\frac{1}{\omega_c}\dot{P} \quad \frac{1}{\omega_c}\dot{Q} \quad \frac{1}{\omega_{c,PLL}}\dot{v}_{od,f} \quad \dot{\varphi}_{PLL} \quad \dot{\delta} \quad \frac{k_{p,pq}}{k_{i,pq}}\dot{\varphi}_{PQ} \frac{k_{pc}}{k_{ic}}\dot{\gamma}_{dq} \quad \frac{L_f}{r_f}\dot{i}_{ldq} \quad \frac{L_c}{r_c}\dot{i}_{odq} \quad \frac{C_f}{R_d}\dot{v}_{odq}]^T.$$

$$(2.30)$$

The values of the small model parameters are obtained using Table 2.1 and Table 2.2. Using these values the dynamic equations become:

$$diag\{0.02, 0.02, 1.27 \times 10^{-4}, 1, 1, 0.1, 0.01, 8.4 \times 10^{-3}, 1.4 \times 10^{-3}, 7.4 \times 10^{-6}\} \times \dot{\tilde{x}}_{sys}$$

$$(2.31)$$

The small-model parameters in (2.31) suggest that, the co-efficients of $[\dot{v}_{od,f}, \dot{i}_{ldq}, \dot{i}_{odq}, \dot{v}_{odq}]$ are much lower in magnitude compared to the coefficients of the rest of the states. This is an evidence of the two-time scale nature of this model. States with these lower order co-efficients are the fast states of the proposed system. The slow and the fast states are then

divided as:

$$\tilde{x}_{sys} = \begin{bmatrix} x \\ z \end{bmatrix} \tag{2.32}$$

Where,

$x = [P \quad Q \quad \varphi_{PLL} \quad \delta \quad \varphi_P \quad \varphi_Q \quad \gamma_d \quad \gamma_q]$, and

$z = [v_{od,f} \quad i_{ld} \quad i_{lq} \quad i_{od} \quad i_{oq} \quad v_{od} \quad v_{oq}]$.

Once the states are determined, the elements of matrices in (2.28) are reordered as in (2.2a) and (2.2b). After that, the reduced order system is obtained by following (2.6a) and (2.6b). The reduced model has a lower order (8th) compared to the original 15th order model. The states associated with the voltage and current measurements in the LCL filter and the state from the PLL filter contributed to the less important dynamics in the system.

2.5. EXPERIMENTAL SETUP AND MODEL EVALUATION PARAMETERS

A set of linearization points is obtained with $u = [0 \quad 0]^T$ to evaluate the initial higher order matrices A, B, C, D in (2.27):

$$\begin{aligned} &[P \quad Q \quad v_{od,f} \quad v_{od} \quad v_{oq} \quad i_{ld} \quad i_{lq} \quad i_{od} \quad i_{oq} \quad \varphi_{PLL} \quad \delta \quad v_{bD} \quad v_{bQ} \quad \theta] \\ =&[0 \quad 0 \quad 0 \quad 0 \quad 83.3 \quad -0.4709 \quad 0.005 \quad 0 \quad 0 \quad -0.0044 \quad 0 \quad 0 \quad 83.3 \quad 0] \end{aligned} \tag{2.33}$$

To justify our assumption that the system is stable for any set points (within the inverter ratings), different linearization points are considered and used for building the system matrices. The state-space model is found stable in all cases.

In order to validate the small-signal model, the dynamic response is compared against those of a simulation and experiment in hardware. An average model of the proposed system is simulated in PLECS. This average model is perturbed using a step change in the input. In hardware implementation, a Texas Instruments TMS320F28335 digital signal processor is used to apply the control system to a 10 kW inverter built around an

Infineon BSM30GP60 IGBT module. A dc source is connected directly to the DC link and the three phase outputs are connected to the inverter bus. The switching scheme is at a frequency of 10 kHz. The experimental results collected correspond to the actual values in the DSP, which are logged in real time. Fig. 2.6 shows the experimental setup including sensors, circuit board and the output filter.

The LCL filter design and the selection of the passive damping resistor are described in [31].

2.6. RESULTS AND DISCUSSIONS

The accuracy of the reduced order model is verified using the results obtained from the full order model and the hardware testbed. The full order model of the proposed DER has a 15×15 state matrix. The singular perturbation method resulted in a 8th order reduced model. The full order model's eigenvalues are: $-2323.3 \pm j11393, -2198.7 \pm j10686, -7834.4, -305.23 \pm j67.56, -66.89 \pm j54.25, -71.53 \pm j33.91, -10.88 \pm j7.56, -5.99 \pm j0.01$. The reduced order model's eigenvalues are: $-63.07 \pm j31.41, -61.74 \pm$

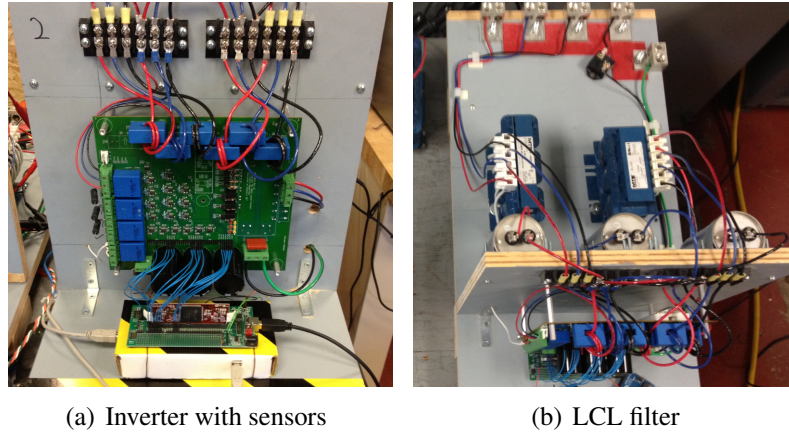(a) Inverter with sensors   (b) LCL filter

Figure 2.6. Partial photograph of the test bed

$j42.2, -10.87 \pm j7.56, -5.99 \pm j0.008$. Latter eigenvalue's are close to that of the slow eigenvalues of the full order system.

Some of the results of interest are presented in Fig. 2.7. Experimental results are gathered from the DSP as *dq* axis quantities. Since the small-signal model is based on the averaged model of the system, high-frequency switching noise is absent from the results obtained using the models. The dynamics obtained from the small-signal model match with that of the experimental results. In this case, the initial steady state condition corresponds to both active and reactive power commands of zero i.e. the inverter is synchronized to the grid and delivering no power. A step change in the power commands, 1000 *W* and 500 *Var*, shifts the system to a new set of steady-state operating points following a brief transient period. The results obtained from the full-order model and the reduced order model overlap in all the graphs. Although the results are obtained with a grid voltage of 60 V_{LN}, the small-signal models are equally applicable to 120 V_{LN} voltage levels commonly used at the distribution side of a power system.

Results acquired from the experimental testbed and the simulation model indicate that the reduced order model approximates the original model well. However, the fast states show some error in predicting the overshoots and the undershoots. This error is caused as the fast dynamics are overlooked in the reduced model. Although the singular perturbation method reduced the full model's order by 46.67%, the reduced model still provided a good approximation for transient analysis. Different linearization points are used for evaluating the system matrices and similar results are obtained from the reduced order models. The model reduction techniques are independent of the choice of operating points for the example system.

Once the accuracy of the model is verified, the model is now ready to be used in a larger microgrid system. An IEEE-37 node distribution test feeder is selected as a sample microgrid system. The standard IEEE-37 bus is modified by adding seven inverters in seven different nodes. Details of the modified system including the load and line parameters are
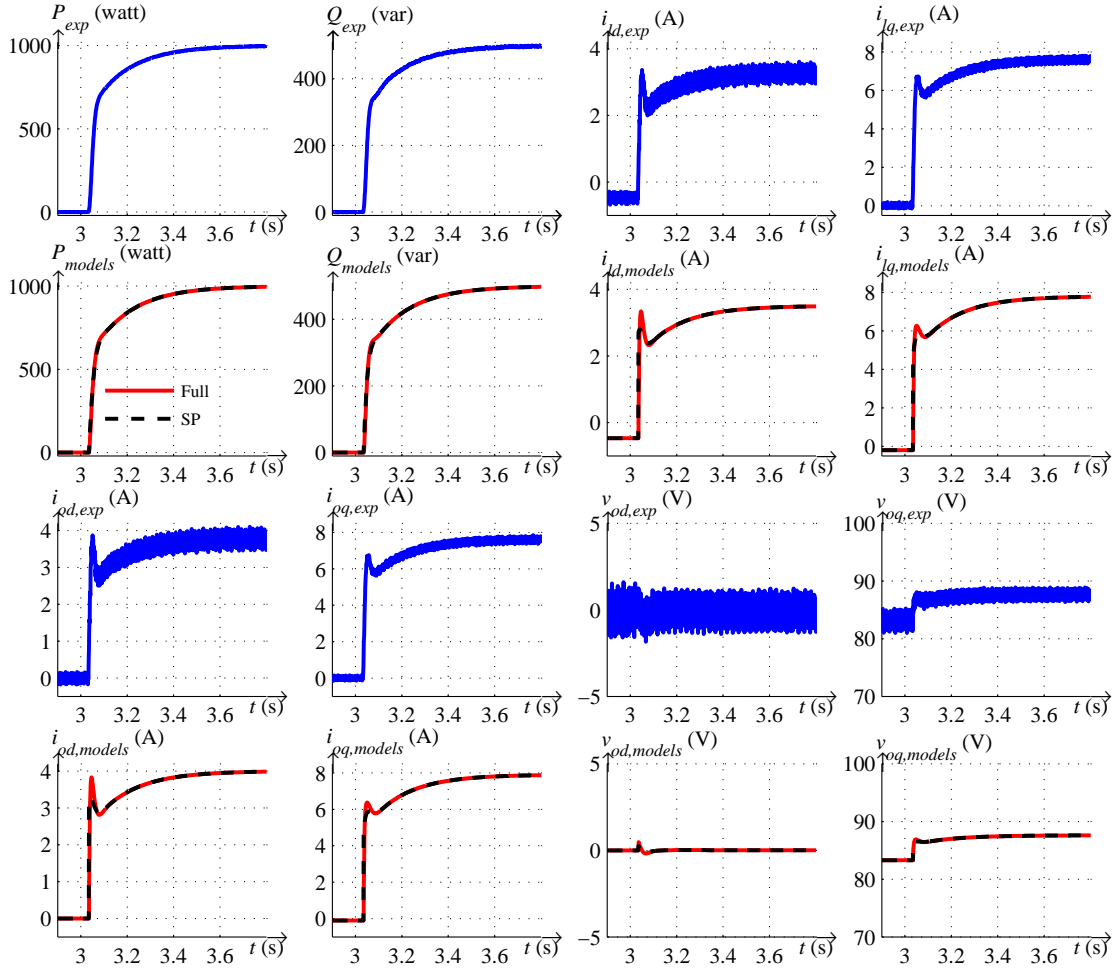
Figure 2.7. Verification of the system dynamics of interests

given in [20]. The modified system's one-line diagram is shown in Fig. 2.8. The inverters connected to bus 15, 18, 22, 24, 29, 33 and 34 are indicated by the larger circles.

The mathematical model describing the overall system's dynamics is of 225 order. Whereas the reduced order model is of 56th order. The full order system includes the distribution lines and the loads. The equations for those are found from [31]. The loads and the distribution lines are also the fast states of the system. As a result, a large number of states are treated as fast states in this system.
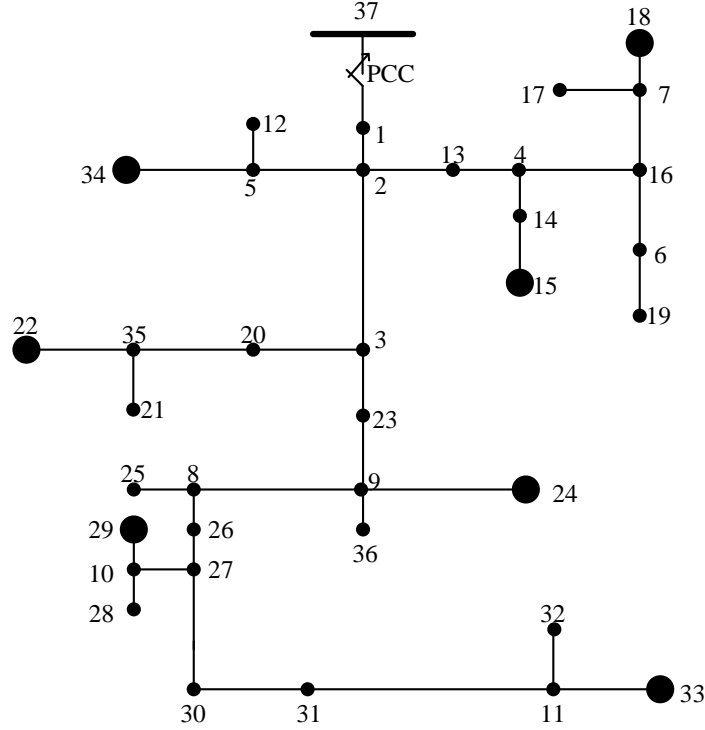
Figure 2.8. One-line diagram of the IEEE-37 node distribution test feeder

For the proposed IEEE-37 bus system, the simulation time required by the reduced model (9.91 *s*) is much less compared to that of the full order system. The full order model takes in excess of 48 *hrs* to simulate. The time measurements are done using ode45 solver with both maximum step size and relative tolerance of 1×10^{-3}. The Simulink profiler's time measurement's precision was 30 *ns* using a CPU clock speed of 3 *GHz*.

Results plotted in Fig. 2.9 verify the accuracy of the reduced model. A step change in the active and reactive power commands in all seven DERs are observed at 0.5 *s* and 1 *s*. Output power dynamics of the inverters are preserved accurately in the reduced order model. As before, the reduced order dynamics suffer from the loss of fast states, as a result the overshoots and undershoots seem more damped compared to that of the full order model.
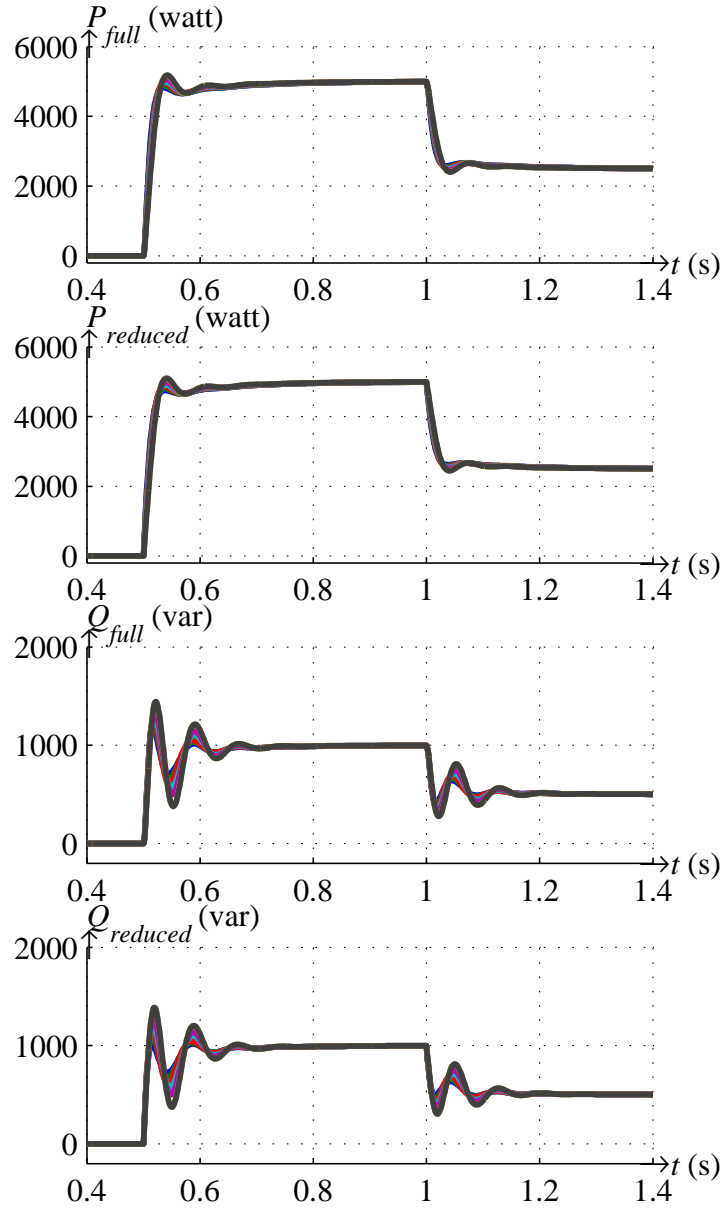
Figure 2.9. Active and reactive power dynamics obtained from seven inverters

2.7. CONCLUSION

A small-signal model of the proposed single bus grid-tied inverter is derived. The full order system consists of 15 states. This system is then reduced applying the singular perturbation algorithm. The reduced order model is compared and its accuracy is assessed

using experimental results. The model is then applied to a multibus bus microgrid system. A modified IEEE-37 node distribution test feeder is used for this purpose. Seven inverters are placed at seven different nodes in that system. A linearized mathematical model of the system is developed using the reduced order model. A step change in the active and reactive power is simulated for all seven inverters. A graph is presented to compare the results obtained using the full order model and the reduced model of this multi-bus system. It is observed that the reduced model can predict the power injection at different buses. A slight difference in predicting the overshoots and undershoots are because of the loss of the fast states from the model. The reduced order model eliminates the issue with the 'stiff' solver type and runs much faster than the full order model when simulated. As an added advantage this model could be used to study the system stability when microgrid jumps from grid-tied mode to islanded mode. Part-II of the paper includes the reduced order model of the islanded microgrid system. The grid-tied microgrid model and the islanded microgrid model are integrated to predict the grid-tied to islanded transition dynamics in the second part of the paper.

2.8. REFERENCES

[1] M. Cespedes and J. Sun, "Adaptive control of grid-connected inverters based on online grid impedance measurements," *IEEE Transactions on Sustainable Energy*, vol. 5, no. 2, pp. 516–523, Apr. 2014.

[2] M. Smith and D. Ton, "Key connections: The u.s. department of energy's microgrid initiative," *IEEE Power Energy Mag.*, vol. 11, no. 4, pp. 22–27, Jul. 2013.

[3] B. Zhao, X. Zhang, and J. Chen, "Integrated microgrid laboratory system," *Power Systems, IEEE Transactions on*, vol. 27, no. 4, pp. 2175–2185, 2012.

[4] A. Kahrobaeian and Y. A.-R. I. Mohamed, "Interactive distributed generation interface for flexible micro-grid operation in smart distribution systems," *IEEE Transactions on Sustainable Energy*, vol. 3, no. 2, pp. 295–305, Apr. 2012.

[5] M. Prodanovic and T. Green, "Control and filter design of three-phase inverters for high power quality grid connection," *IEEE Transactions on Power Electronics*, vol. 18, no. 1, pp. 373–380, Jan. 2003.

[6] M. S. El Moursi, H. H. Zeineldin, J. L. Kirtley, and K. Alobeidli, "A dynamic master/slave reactive power-management scheme for smart grids with distributed generation," *IEEE Transactions on Power Delivery*, pp. 1–11, 2014.

[7] R. A. Ferreira, H. A. Braga, A. A. Ferreira, and P. G. Barbosa, "Analysis of voltage droop control method for dc microgrids with simulink: Modelling and simulation," in *Industry Applications (INDUSCON), 2012 10th IEEE/IAS International Conference on*. IEEE, 2012, pp. 1–6.

[8] J.-Y. Kim, J.-H. Jeon, S.-K. Kim, C. Cho, J. H. Park, H.-M. Kim, and K.-Y. Nam, "Cooperative control strategy of energy storage system and microsources for stabilizing the microgrid during islanded operation," *IEEE Transactions on Power Electronics*, vol. 25, no. 12, pp. 3037–3048, Dec. 2010.

[9] P. Tenti, T. Caldognetto, A. Costabeber, and P. Mattavelli, "Microgrids operation based on master-slave cooperative control," in *Industrial Electronics Society, IECON 2013-39th Annual Conference of the IEEE*. IEEE, 2013, pp. 7623–7628.

[10] L. Yang, X. Zhang, Y. Ma, J. Wang, L. Hang, K. Lin, L. M. Tolbert, F. Wang, and K. Tomsovic, "Stability analysis of inverter based generator emulator in test-bed for power systems," in *Energy Conversion Congress and Exposition (ECCE), 2013 IEEE*. IEEE, 2013, pp. 5410–5417.

[11] F. Andrade, J. Cusido, and L. Romeral, "Transient stability analysis of inverter-interfaced distributed generators in a microgrid system," in *Proceedings of the 2011-14th European Conference on Power Electronics and Applications (EPE 2011)*, Aug. 2011, pp. 1–10.

[12] R. M. Castro and J. M. Ferreira de Jesus, "A wind park reduced-order model using singular perturbations theory," *Energy Conversion, IEEE Transactions on*, vol. 11, no. 4, pp. 735–741, 1996.

[13] M. Rasheduzzaman, T. Paul, and J. W. Kimball, "Markov jump linear system analysis of microgrid stability," in *American Control Conference (ACC), 2014*. IEEE, 2014, pp. 5062–5066.

[14] R. Podmore, "Identification of coherent generators for dynamic equivalents," *Power Appar. Syst., IEEE Trans.*, no. 4, pp. 1344–1354, 1978.

[15] G. Troullions and J. Dorsey, "Coherency and model reduction," *IEEE Trans. Power Syst.*, pp. 988–995, 1989.

[16] S.-K. Joo, C.-C. Liu, L. Jones, and J.-W. Choe, "Coherency and aggregation techniques incorporating rotor and voltage dynamics," *IEEE Trans. Power Syst.*, vol. 19, no. 2, pp. 1068–1075, May 2004.

[17] J. H. Chow, R. Galarza, P. Accari, and W. W. Price, "Inertial and slow coherency aggregation algorithms for power system dynamic model reduction," *Power Syst., IEEE Trans.*, vol. 10, no. 2, pp. 680–685, 1995.

[18] A. Kuppurajulu and S. Elangovan, "Simplified power system models for dynamic stability studies," *Power Appa. Syst., IEEE Trans.*, no. 1, pp. 11–23, 1971.

[19] J. R. Winkelman, J. H. Chow, B. C. Bowler, B. Avramovic, and P. V. Kokotovic, "An analysis of interarea dynamics of multi-machine systems," *Power Appar. Syst., IEEE Trans.*, no. 2, pp. 754–763, 1981.

[20] L. Luo and S. V. Dhople, "Spatiotemporal model reduction of inverter-based islanded microgrids," *IEEE Transactions on Energy Conversion*, pp. 1–10, 2014.

[21] A. C. Antoulas and D. C. Sorensen, "Approximation of large-scale dynamical systems: An overview," *App. Math. Comp. Science*, vol. 11, no. 5, pp. 1093–1122, 2001.

[22] D. I. Trudnowski, "Order reduction of large-scale linear oscillatory system models," *Power Syst, IEEE Trans.*, vol. 9, no. 1, pp. 451–458, 1994.

[23] A. Feliachi, X. Zhang, and C. S. Sims, "Power system stabilizers design using optimal reduced order models. i. model reduction," *Power Syst., IEEE Trans.*, vol. 3, no. 4, pp. 1670–1675, 1988.

[24] D. Chaniotis and M. Pai, "Model reduction in power systems using krylov subspace methods," *IEEE Trans. Power Syst.*, vol. 20, no. 2, pp. 888–894, May 2005.

[25] P. V. Kokotovic, R. E. O'Malley, and P. Sannuti, "Singular perturbations and order reduction in control theory—an overview," *Automatica*, vol. 12, no. 2, pp. 123–132, 1976.

[26] Y. Liu and B. Anderson, "Singular perturbation approximation of balanced systems," Tampa, FL, Dec. 1989, pp. 1355 – 1360.

[27] M. Liserre, F. Blaabjerg, and S. Hansen, "Design and control of an LCL-filter-based three-phase active rectifier," *IEEE Trans. Ind. App.*, vol. 41, no. 5, pp. 1281–1291, Sep. 2005.

[28] N. Bottrell, M. Prodanovic, and T. C. Green, "Analysed small signal state-space model of an active rectifier," in *Universities Power Engineering Conference (UPEC), 2010 45th International*.   IEEE, 2010, pp. 1–6.

[29] N. Kroutikova, C. Hernandez-Aramburo, and T. Green, "State-space model of grid-connected inverters under current control mode," *IET Electric Power Applications*, vol. 1, no. 3, p. 329, 2007.

[30] E. Twining and D. Holmes, "Grid current regulation of a three-phase voltage source inverter with an LCL input filter," *IEEE Transactions on Power Electronics*, vol. 18, no. 3, pp. 888–895, May 2003.

[31] M. Rasheduzzaman, J. A. Mueller, and J. W. Kimball, "An accurate small-signal model of inverter-dominated islanded microgrids using dq reference frame," *IEEE Journal on Emerging and Selected Topics in Power Electronics*, 2014.

III. REDUCED ORDER SMALL-SIGNAL MODEL OF MICROGRID SYSTEMS-PART II

Md. Rasheduzzaman, Jonathan W. Kimball, and Jacob A. Mueller

Department of Electrical and Computer Engineering

Missouri University of Science & Technology, Rolla, MO 65409

ABSTRACT— This work develops an algorithm that can obtain the reduced order model of an islanded microgrid system. This system consists of two inverters that are connected to their respective buses with some local loads. A set of non-linear first order differential equations was developed to describe the system dynamics. The dynamic equations were divided into two groups based on the small-signal model parameters, ε. This process indicated the system's two-time scale nature. State variables that fell into these groups were listed and re-ordered. State matrices were divided into slow and fast subsystems to demonstrate the two-time scale property. The 'slow' states which dominated the system's dynamics were preserved while the 'fast' states were eliminated by the singular perturbation method as discussed in part-I of this work. An algorithm was developed for the model order reduction of the proposed switched autonomous system. The dynamics from the reduced order model were compared with both the experimental results and the full order simulation results. A comparison of simulation time was made using both full order and reduced order models for a multibus islanded microgrid. Once verified the model was used in an IEEE-37 bus microgrid system to evaluate system's dynamic response in an islanded condition, and also when the system switches from grid-tied to islanded mode.

Index Terms— Islanded microgrid, singular perturbation, model order reduction.

3.1. INTRODUCTION

A practical power system network is comprised of numerous generating units and loads. Ordinary differential equations have been used to develop mathematical models of these power system components that can investigate the physical system's dynamics. These equations are often non-linear and need to be linearized around some steady-state operating points to simplify calculations that can provide a better understanding of the system's dynamic response. These equations represent the rate of change of states that are evaluated with an integration algorithm at incremental time steps. The presence of both the 'fast' and 'slow' states in a model produces a two-time scale property in the system, making real-time simulation difficult. A fast decaying state will require a small-time-step during integration to capture the system's fast dynamics. Thus, small-time-constant states increase the time required for dynamic power system simulations [1]. In most cases, these fast states originate from the moment of inertia, inductance, capacitance, and some similar parasitic parameters. These parameters (when included) make the order of the model unacceptably higher than required for optimal design [2]. Simplifications of these models are often made by neglecting these components. However, neglecting the effect of small parameters does not always guarantee system stability and accurate DC gain. The singular perturbation method overcomes these issues by not only treating the fast transients as boundary layers but also including them in the slow states [3].

The most well-known application of singular perturbation method includes the model order reduction of synchronous machines [4]. S. Pekarek *et al.* discussed neglecting the dynamic saliency in a synchronous machine by using the singular perturbation approach for faster transient analysis [5]. An iterative approach that uses singular perturbation was adopted to obtain the reduced order model of synchronous machines in [6]. In many cases, the singular perturbation method was used to develop induction machine models [7] to predict the dynamic response under variable system frequency and voltage magnitude.

Additional applications include the design of feedback stabilization systems based on the reduced order model [8], application to PFC converters [9], long-term stability analysis due to system frequency variation [10], and the estimation of the stability region of power systems with saturation nonlinearity [11]. Utility distribution grid-tied systems with wind power based renewable energy sources were previously modeled using the singular perturbation method [12]. The application of singular perturbation method for developing the reduced order model of a diode interfaced wind farm with DC power system was discussed in [13].

However, islanded microgrid systems are relatively new trends in power system analysis. Thus, the small-signal models developed for such systems require attention before they can be simulated in real-time for dynamic studies. Related to this work, singular perturbation method was applied in [14]. The inverter model used in that paper excluded the filter capacitors. These filter capacitors are needed to meet the industry standards in terms of the harmonics rejection especially when the inverters are used for system's voltage and frequency regulation. The stability assessment of the reduced order islanded microgrid using singular perturbation approach was discussed in [15]. The inverter model was overly simplistic and the effect of the filter dynamics were ignored in that paper. This paper overcomes these issues by including all the necessary elements of an industry standard inverter.

Reduced-order dynamic modeling of power electronic components using singular perturbation method was discussed in [16]. In that paper, a full order model of the system was developed with all the parasitic components, then the model was reduced based on the input-output behavior of the system to preserve the model accuracy and to get the computational efficiency. Because the proposed system is autonomous, reduction algorithms including the input/output knowledge of the system are not applicable. Singular perturbation technique allows for the elimination of states based on small-signal model parameters. Similar to the approach mentioned above, in this paper, an accurate full order model of

the microgrid is developed using all the parasitic components in the system, and then the system's fast and slow states are identified using the small-signal model parameters. Part-I of this paper discusses the method to separate the fast and the slow states. The singular perturbation method is used to eliminate the fast states using the boundary layer correction to obtain a reduced order model of the proposed system. This new model converts the stiff system into a non-stiff system that accelerates the simulation time. The reduced model is applied to a modified IEEE-37 bus system to verify the dynamic response. The reduced order model would be useful to assess the system's stability [17], [18], [19]. The reduced order models are also important for evaluating the feasible bounds on state jumps when the microgrid switches from grid tied to islanded mode, the load perturbation events in an islanded system [20] or to study the Markov chain models [21].

3.2. SYSTEM UNDER CONSIDERATION

A two bus islanded microgrid system is considered. A single line diagram of the system is presented in Fig. 3.1. In that system, two voltage source inverters with their local loads are connected to the respective buses. Each bus has at least one fixed load and either one or more additional loads that can switch on or off arbitrarily. Each combination of loads has a different nominal operating point and, therefore, a different small-signal model. Static loads comprised of resistance and inductances are considered. These buses are coupled with a distribution line that has line impedance Z_{line}. A small-signal model was developed in [22] to describe the system's dynamic response. The proposed mathematical model was verified against the experimental results using a hardware test-bed. For accurate dynamic analysis, the model was developed as a switched linear autonomous system, where switching from one state matrix to another state matrix was dependent on load perturbation. Mathematical analysis determined the presence of both slow decaying and fast decaying eigenvalues in the system. These slow and fast modes made the system 'stiff'.
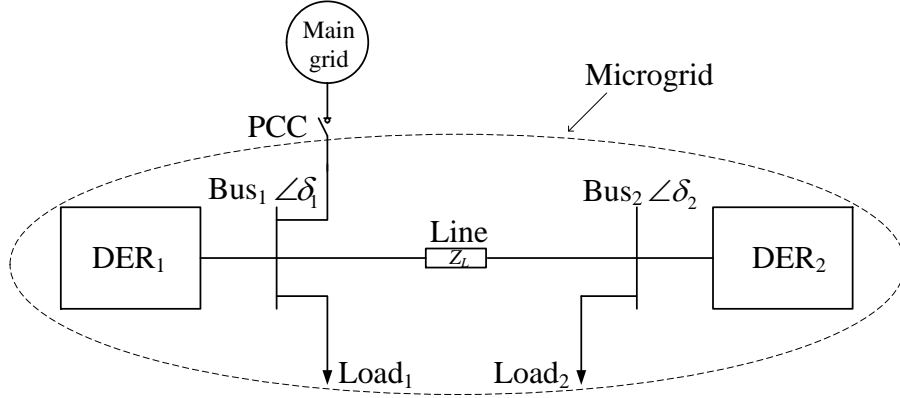
Figure 3.1. Proposed microgrid setup

In this work, a reduced order model of the proposed islanded microgrid system is considered. Each inverter includes the power hardware and control system depicted in Fig. 3.2. This is a standard benchmark that is analyzed more thoroughly using block diagrams in [22]. Details of these blocks are not discussed here to avoid repetitions. The output stage uses space vector pulse width modulation (SVPWM) and an LCL filter to achieve high performance and low ripple. All three-phase variables (denoted *abc*) are converted to a rotating reference frame (denoted *dq*). The rotating reference frame frequency and phase are determined with a phase-locked loop (PLL). The active (P) power, and the reactive (Q) power are computed and filtered. The filtered powers are passed through the droop controllers to determine the output frequency from P and the output voltage from Q. Finally, the voltage and current control loops are used to determine the voltage vector commands for the SVPWM block. The states that are generated from the controller blocks, the LCL filter, the distribution line and the loads are given in Table 3.1.

A set of nonlinear equations is derived in the synchronous reference frame to describe the system's dynamics. The variables used in those equations are given in Fig. 3.2 and in [22]. These equations are:
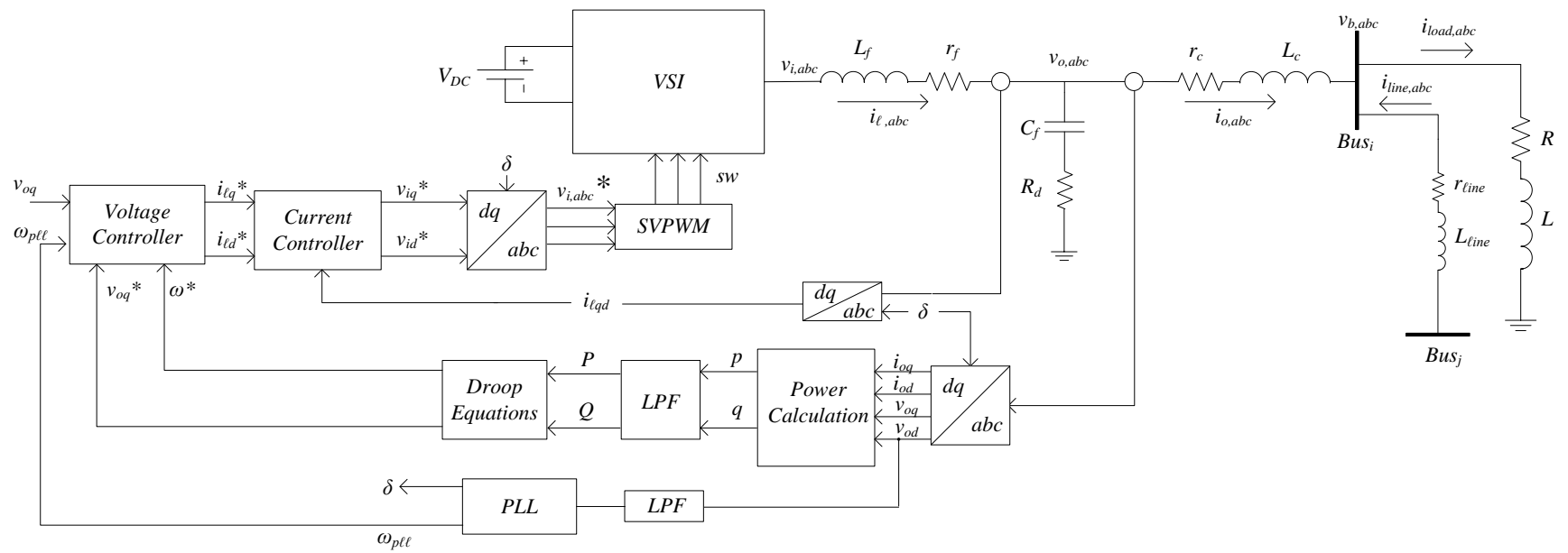
Figure 3.2. Voltage source inverter, inverter controllers, loads and distribution line

$$P = \frac{\omega_c}{s + \omega_c} p \Rightarrow \dot{P} = -P\omega_c + 1.5\omega_c \left(v_{od} i_{od} + v_{oq} i_{oq} \right) \tag{3.1}$$

$$Q = \frac{\omega_c}{s + \omega_c} q \Rightarrow \dot{Q} = -Q\omega_c + 1.5\omega_c \left(v_{oq} i_{od} - v_{od} i_{oq} \right) \tag{3.2}$$

$$\omega^* = \omega_n - mP \tag{3.3}$$

$$v_{oq}{}^* = V_{oq,n} - nQ \tag{3.4}$$

$$\dot{v}_{od,f} = \omega_{c,PLL} v_{od} - \omega_{c,PLL} v_{od,f} \tag{3.5}$$

$$\dot{\varphi}_{PLL} = -v_{od,f} \tag{3.6}$$

$$\dot{\delta} = \omega_{PLL} \tag{3.7}$$

$$\omega_{PLL} = 377 - k_{p,PLL} v_{od,f} + k_{i,PLL} \varphi_{PLL} \tag{3.8}$$

$$\dot{\varphi}_d = \omega_{PLL} - \omega^*; \quad i_{ld}{}^* = k_{iv,d} \varphi_d + k_{pv,d} \dot{\varphi}_d \tag{3.9}$$

$$\dot{\varphi}_q = v_{oq}{}^* - v_{oq}; \quad i_{lq}{}^* = k_{iv,q} \varphi_q + k_{pv,q} \dot{\varphi}_q \tag{3.10}$$

$$\dot{\gamma}_d = i_{ld}{}^* - i_{ld}; \quad v_{id}{}^* = -\omega_n L_f i_{lq} + k_{ic,d} \gamma_d + k_{pc,d} \dot{\gamma}_d \tag{3.11}$$

Table 3.1. States of the Proposed System

Block	States
Power+LPF	P, Q
Voltage Controller	φ_{dq}
Current Controller	γ_{dq}
LPF+PLL	$v_{od,f}, \delta, \varphi_{PLL}$
LCL Filter	$i_{ldq}, v_{odq}, i_{odq}$
Load	i_{loadDQ}
Line	i_{lineDQ}

$$\dot{\gamma}_q = i_{lq}{}^* - i_{lq}; \quad v_{iq}{}^* = \omega_n L_f i_{ld} + k_{ic,q}\gamma_q + k_{pc,q}\dot{\gamma}_q \tag{3.12}$$

$$\dot{i}_{ld} = \frac{1}{L_f}\left(-r_f i_{ld} + v_{id} - v_{od}\right) + \omega_{PLL}i_{lq} \tag{3.13}$$

$$\dot{i}_{lq} = \frac{1}{L_f}\left(-r_f i_{lq} + v_{iq} - v_{oq}\right) - \omega_{PLL}i_{ld} \tag{3.14}$$

$$\dot{i}_{od} = \frac{1}{L_c}\left(-r_c i_{od} + v_{od} - v_{bd}\right) + \omega_{PLL}i_{oq} \tag{3.15}$$

$$\dot{i}_{oq} = \frac{1}{L_c}\left(-r_c i_{oq} + v_{oq} - v_{bq}\right) - \omega_{PLL}i_{od} \tag{3.16}$$

$$\dot{v}_{od} = \frac{1}{C_f}\left(i_{ld} - i_{od}\right) + \omega_{PLL}v_{oq} + R_d(\dot{i}_{ld} - \dot{i}_{od}) \tag{3.17}$$

$$\dot{v}_{oq} = \frac{1}{C_f}\left(i_{lq} - i_{oq}\right) - \omega_{PLL}v_{od} + R_d(\dot{i}_{lq} - \dot{i}_{oq}) \tag{3.18}$$

$$\dot{i}_{loadD} = \frac{1}{L_{load}}\left(-R_{load}i_{loadD} + v_{bD}\right) + \omega_{PLL}i_{loadQ} \tag{3.19}$$

$$\dot{i}_{loadQ} = \frac{1}{L_{load}}\left(-R_{load}i_{loadQ} + v_{bQ}\right) - \omega_{PLL}i_{loadD} \tag{3.20}$$

$$\dot{i}_{lineDij} = \frac{1}{L_{line}}\left(-r_{line}i_{lineD} + v_{bD,i} - v_{bD,j}\right) + \omega_{PLL}i_{lineQ} \tag{3.21}$$

$$\dot{i}_{lineQij} = \frac{1}{L_{line}}\left(-r_{line}i_{lineQ} + v_{bQ,i} - v_{bQ,j}\right) - \omega_{PLL}i_{lineD} \tag{3.22}$$

The inverter reference angle at bus 1 is set as the reference for the rest of the system using:

$$\dot{\delta}_1 = \omega_{PLL,1} - \omega_{PLL,1} = 0 \tag{3.23}$$

$$\dot{\delta}_2 = \omega_{PLL,1} - \omega_{PLL,2} \tag{3.24}$$

Finally using the virtual resistor method and the reference frame transformation theory (as in Fig. 3.3) the input bus voltages are replaced using the states as follows:

$$v_{bD,i} = r_n\left(i_{oD,i} + i_{lineD,i} - i_{loadD,i}\right) \tag{3.25}$$

$$v_{bQ,i} = r_n \left(i_{oQ,i} + i_{lindQ,i} - i_{loadQ,i} \right) \tag{3.26}$$

Nonlinear equations are linearized around stable operating points to generate a set of linear ordinary differential equations. The complete system in Fig. 3.1 has 36 state variables, including both physical variables and internal control variables. These states are:

$$\begin{aligned}
x_{sys} = [& \delta_1 \quad P_1 \quad Q_1 \quad \varphi_{d1} \quad \varphi_{q1} \quad \gamma_{d1} \quad \gamma_{q1} \quad i_{ld1} \quad i_{lq1} \quad v_{od1} \quad v_{oq1} \quad i_{od1} \quad i_{oq1} \quad \varphi_{PLL1} \\
& v_{od1,f} \quad \delta_2 \quad P_2 \quad Q_2 \quad \varphi_{d2} \quad \varphi_{q2} \quad \gamma_{d2} \quad \gamma_{q2} \quad i_{ld2} \quad i_{lq2} \quad v_{od2} \quad v_{oq2} \quad i_{od2} \quad i_{oq2} \\
& \varphi_{PLL2} \quad v_{od2,f} \quad i_{loadD1} \quad i_{loadQ1} \quad i_{loadD2} \quad i_{loadQ2} \quad i_{lineD} \quad i_{lineQ}]^T
\end{aligned}$$

$$\tag{3.27}$$

The dynamics of the system are verified using a hardware setup by treating it as a switched autonomous system where switching of the state matrices is dependent on the load perturbation. The mathematical model of the overall system is:
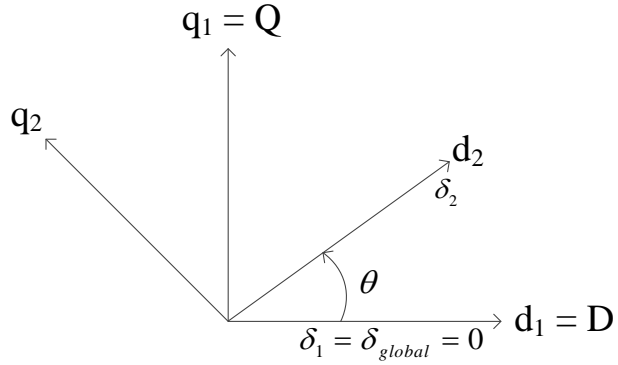
$$\dot{x} = A_p x; \quad p = 1, 2 \tag{3.28}$$

Figure 3.3. Reference frame transformation

3.3. MODEL ORDER REDUCTION OF ISLANDED MICROGRID

This section focuses on reduced order modeling of islanded microgrid systems using singular perturbation technique. The fundamentals of the singular perturbation method are broadly covered by P. Kokotovic *et al.* in [23] and D.S. Naidu in [24]. Hence, the details of this method are not discussed here. The system's eigenvalues (listed in Table 3.2) are evaluated before the load perturbation event. This is a 'stiff' system where the dynamics of the states are influenced by both slow decaying and fast decaying eigenvalues. This system thus possesses a two time-scale property. The objective is to identify and separate the fast and slow subsystems using small-model parameters, ε.

A discussion on the model order reduction of this microgrid using singular perturbation technique is presented in the Part - I of this work. Following that work, the fast states of the system are characterized by the small model parameters, ε. It is necessary to normalize the system dynamic equations using these small model parameters. The normalized dynamic equations become:

$$
\begin{aligned}
[\frac{1}{\omega_c}\dot{P} \quad \frac{1}{\omega_c}\dot{Q} \quad \frac{1}{\omega_{c,PLL}}\dot{v}_{od,f} \quad \dot{\varphi}_{PLL} \quad \dot{\delta} \quad \frac{k_{p,pq}}{k_{i,pq}}\dot{\varphi}_{dq} \quad \frac{k_{pc}}{k_{ic}}\dot{\gamma}_{dq} \quad \frac{L_f}{r_f}\dot{i}_{ldq} \quad \frac{L_c}{r_c}\dot{i}_{odq} \\
\frac{C_f}{R_d}\dot{v}_{odq} \frac{L_{load}}{R_{load}}\dot{i}_{loadDQ} \quad \frac{L_{line}}{r_{line}}\dot{i}_{lineDQ}]^T
\end{aligned}
\tag{3.29}
$$

Based on the values of the controller gains and the system parameters, given in [22], the fast states are obtained with lower order co-efficients. States associated with the voltage controllers, current controllers, active-reactive power filters, phase-locked loops and their reference angles contributed to the system's slow dynamics. Remaining states, starting from index 1 through 20, contributed to the fast dynamics. To confirm the identification of the slow and fast states, system's modes are evaluated and major participant states in those modes are found using participation factor analysis.

Table 3.2. Eigenvalues of A_1

Index	Eigenvalues	Major participants
1,2	$-7.10 \times 10^8 \pm j376.57$	i_{lineDQ}
3,4	$-2.09 \times 10^8 \pm j376.58$	i_{odq1}, i_{odq2}
5,6	$-1951.65 \pm j10980.03$	v_{oq1}, v_{oq2}
7,8	$-1781.19 \pm j10234.93$	v_{od1}, v_{od2}
9	-7981.28	$v_{od1,f}, v_{od2,f}$
10	-7915.62	$v_{od1,f}, v_{od2,f}$
11,12	$-822.46 \pm j5415.18$	v_{oq1}, v_{oq2}
13,14	$-674.16 \pm j4643.15$	v_{od1}, v_{od2}
15,16	$-2889.85 \pm j351.71$	$i_{loadDQ1}, i_{loadDQ2}$
17,18	$-1500.35 \pm j336.76$	$i_{loadDQ1}, i_{loadDQ2}$
19,20	$-267.94 \pm j82.01$	i_{ldq1}, i_{ldq2}
21,22	$-69.76 \pm j21.47$	$\gamma_{dq1}, \gamma_{dq2}$
27,28	$-25.38 \pm j31.18$	$\varphi_{q1}, \gamma_{q1}, \varphi_{q2}, \gamma_{q2}$
29,30	$-6.16 \pm j22.90$	$\varphi_{d1}, \gamma_{d1}, \varphi_{d2}, \gamma_{d2}$
34,35	$-2.24 \pm j4.68$	$\varphi_{dq1}, \varphi_{dq2}$
31,32	$-10.65 \pm j8.14$	$\delta_2, \varphi_{PLL1}, \varphi_{PLL2}$
33	-7.53	$\delta_2, \varphi_{PLL1}, \varphi_{PLL2}$
23,24	$-50.25 \pm j0.02$	P_1, Q_1, P_2, Q_2
25	-50.27	P_1, Q_1, P_2, Q_2
26	-50.27	P_1, Q_1, P_2, Q_2
36	0	δ_1

Although the reference angle of the system (δ_1) is recorded as a slow state, its small-signal response during both the transient and the steady-state is zero. This state is thus ignored in calculations when the reduced order system is being developed. In the singular perturbation method, the rate of change of the fast states is set to zero. The fast states are solved in terms of the slow states and then added to the slow dynamics to provide a zero steady-state error.

The steps needed to develop the reduced order model are discussed below.

1. Discard $\dot{\delta}_1$ (corresponding to the reference angle) by removing the corresponding row and column.

2. Rearrange the states of the original state vector x_{sys} such that the slow states (x) are placed in the upper rows and fast states (z) are placed at the lower rows. Use a transformation matrix T_r for re-ordering. For example, $[x_1 \; x_2 \; x_3]^T$ needs to be re-ordered as $[x_1 \; x_3 \; x_2]^T$. Use the transformation matrix T_r to multiply the original vector. The new state vector and steady-state operating point vectors become: $x_{new} = T_r x_{sys}$ and $X_{new} = T_r X_{sys}$ respectively.

$$
T_r = \begin{bmatrix} 1 & 0 & 0 \\ 0 & 0 & 1 \\ 0 & 1 & 0 \end{bmatrix}
$$

3. Find the new state matrix A_{new} using T_r: $A_{new} = T_r A_{sys} T_r^{-1}$

4. Separate the new state matrix and the new states as follows:

$$
\begin{bmatrix} \dot{x} \\ \dot{z} \end{bmatrix} = \begin{bmatrix} A_{11} & A_{12} \\ A_{21} & A_{22} \end{bmatrix} \begin{bmatrix} x \\ z \end{bmatrix} ; \; x_{new} = \begin{bmatrix} x \\ z \end{bmatrix} ; \; X_{new} = \begin{bmatrix} X \\ Z \end{bmatrix}
$$

Where $A_{11} \in \mathfrak{R}^{r \times r}$, $A_{12} \in \mathfrak{R}^{r \times (n-r)}$, $A_{21} \in \mathfrak{R}^{(n-r) \times r}$, $A_{22} \in \mathfrak{R}^{(n-r) \times (n-r)}$. Also, x is representative of the slow states and z is representative of the fast states.

5. Perform the following iteration to find the value of L for a linear system composed of two subsystems [25]:

$$L_{i+1} = A_{22}^{-1}(A_{21} + L_i A_{11} - L_i A_{12} L_i); \; i = 1, 2, \cdots$$

Start with the initial value $L_0 = A_{22}^{-1} A_{21}$ and iterate 100 times. This will ensure that the reduced order system's eigenvalues are as close as possible to that of the full order system's slow eigenvalues. For this system, 100 iterations achieved excellent accuracy with minimal computation time.

6. Transform the system into following using the slow manifold condition $z_f = z + Lx$:

$$\begin{bmatrix} \dot{x} \\ \dot{z}_f \end{bmatrix} = \begin{bmatrix} A_s & A_{12} \\ 0 & A_f \end{bmatrix} \begin{bmatrix} x \\ z_f \end{bmatrix}$$

Where $A_s = A_{11} - A_{12}L$; $A_f = A_{22} + LA_{12}$

7. Perform the following iteration to find the value of M:

$$M_{i+1} = [(A_{11} - A_{12}L)M_i - M_i LA_{12}]A_{22}^{-1} + A_{12}A_{22}^{-1}$$

Start with the initial value $M_0 = A_{12}A_{22}^{-1}$ and iterate 100 times as before for L.

8. Decouple the system into slow and fast time-scale using the fast manifold condition $x_s = x - Mz_f$

$$\begin{bmatrix} \dot{x}_s \\ \dot{z}_f \end{bmatrix} = \begin{bmatrix} A_s & 0 \\ 0 & A_f \end{bmatrix} \begin{bmatrix} x_s \\ z_f \end{bmatrix}$$
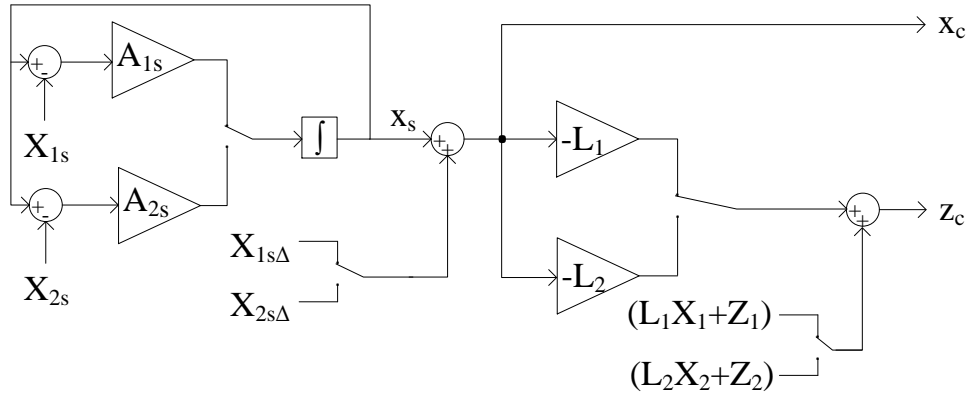
Figure 3.4. Corrected response from the reduced order model

9. The operating points corresponding to the slow states become:

$$X_s = (I - ML)X - MZ$$

10. In order to get the corrected response x_c, add $X_{s\Delta}$ to the output of X_s, where $X_{s\Delta} = MLX + MZ$. New outputs are similar to that of the dynamics obtained from the slow states of the original system.

11. Predict the fast states using algebraic solutions:

$$z_f = Lx_c + z_c$$

$$\Rightarrow z_c = -Lx_c + z_f = -Lx_c + (LX + Z)$$

12. The reduced order system is now ready for simulation. Fig. 3.4 shows the final arrangement for obtaining the dynamic response considering both the slow and the fast states.

   The eigenvalue sensitivity of the reduced model with respect to the neglected parasitics is determined using (3.30), where u_i and v_i are the eigenvectors of A_s and of its

transpose A_s' respectively [26]. The small positive scalar ε is the ratio of speeds of slow and fast modes.

$$\frac{\partial \lambda_{si}}{\partial \varepsilon} = -\lambda_{si} v_i' A_{12} A_{22}^{-2} A_{21} u_i \tag{3.30}$$

Equation (3.30) gives the actual sensitivity of the eigenvalues of the full order matrix which remain finite as $\varepsilon \to 0$. This also represents the change of eigenvalues when, instead of 0, ε takes a small positive value.

3.4. RESULTS AND DISCUSSIONS

The model order reduction algorithm is applied to the proposed two bus islanded microgrid system. The reduced order system has only 15 differential equations as compared to 36 differential equations for its full order counterpart. This is a reduction of 58.33% of the original state equations. The dynamics of the reduced order system are verified against the dynamics of the full order system. This is done by switching between two state matrices that correspond to two different load setups within the system. The eigenvalues of the reduced order state matrix, 'A_{1s}' and the eigenvalue sensitivities of the slow system with respect to ε are evaluated. These are presented in Table 3.3. A large condition number measures the absolute sensitivity of an eigenvalue with respect to absolute normwise perturbation of the matrix. Condition numbers listed in Table 3.3 are obtained from 'A_{1s}'. The inverter output powers and the states from the current controllers are more sensitive to perturbation than other slow states in the system. This shows that the method developed in [14] is not generic and can not be applied to a system such as the one proposed in this paper.

A stability analysis on the reduced order matrices, 'A_{1s}' and 'A_{2s}' proves the proposed system's quadratically stable nature. There exists a common quadratic Lyapunov function for this system with a quadratic decay rate of -4.4731.

Table 3.3. Eigenvalues, Eigenvalue Sensitivity and Condition Number

Index	Eigenvalues	Sensitivity	Condition Number
1,2	$-69.76 \pm j21.47$	$9.15\text{e-}04 \pm j2.77\text{e-}05$	17923
3,4	$-25.38 \pm j31.18$	$-1.99\text{e-}03 \pm j2.8\text{e-}03$	588.5
5,6	$-6.16 \pm j22.90$	$-1.5635 \pm j0.085$	5.136
7,8	$-2.24 \pm j4.68$	$-2.29\text{e-}03 \pm j1.21\text{e-}03$	4856.3
9,10	$-10.65 \pm j8.14$	$-7.93\text{e-}04 \pm j1.75\text{e-}03$	3451.7
11	-7.53	-0.89858	4.201
12,13	$-50.25 \pm j0.02$	$8.87\text{e-}07 \pm j1.58\text{e-}07$	20349
14	-50.27	$3.224\text{e-}07$	1424.9
15	-50.27	$3.153\text{e-}07$	2477.6

The transient response plots in Fig. 3.5 compare the accuracy of the reduced order model and the full order model with the experimental results. Both the active and reactive power variation plots are generated from the slow states. In contrast, plots for the LCL filter's voltage and current dynamics are generated by the fast states. the system is perturbed at 1.885 s by adding an RL load parallel to the initial load, at bus$_1$. Dynamic responses obtained from the full-scale model overlapped with those obtained from the reduced order model. As depicted in Fig. 3.6, the fast dynamics in both the v_{od} and the v_{oq} creates a spike during the transient period. The effects of the fast states disappear in the reduced order model. As a result, these fast decaying spikes are absent from the graphs once the reduced order model is simulated.

Three different solvers (in Matlab/Simulink) are used to conduct a simulation time comparison between the full order model and the reduced order model. The results from the comparison verify that the reduced system accelerates the simulation speed. The ode45 solver option offers 4th order medium accuracy using Runge-Kutta method for solving a set of differential equations numerically [27], [28]. This algorithm uses variable step size i.e. algorithm increases the step size when the solution varies less. This method is intended
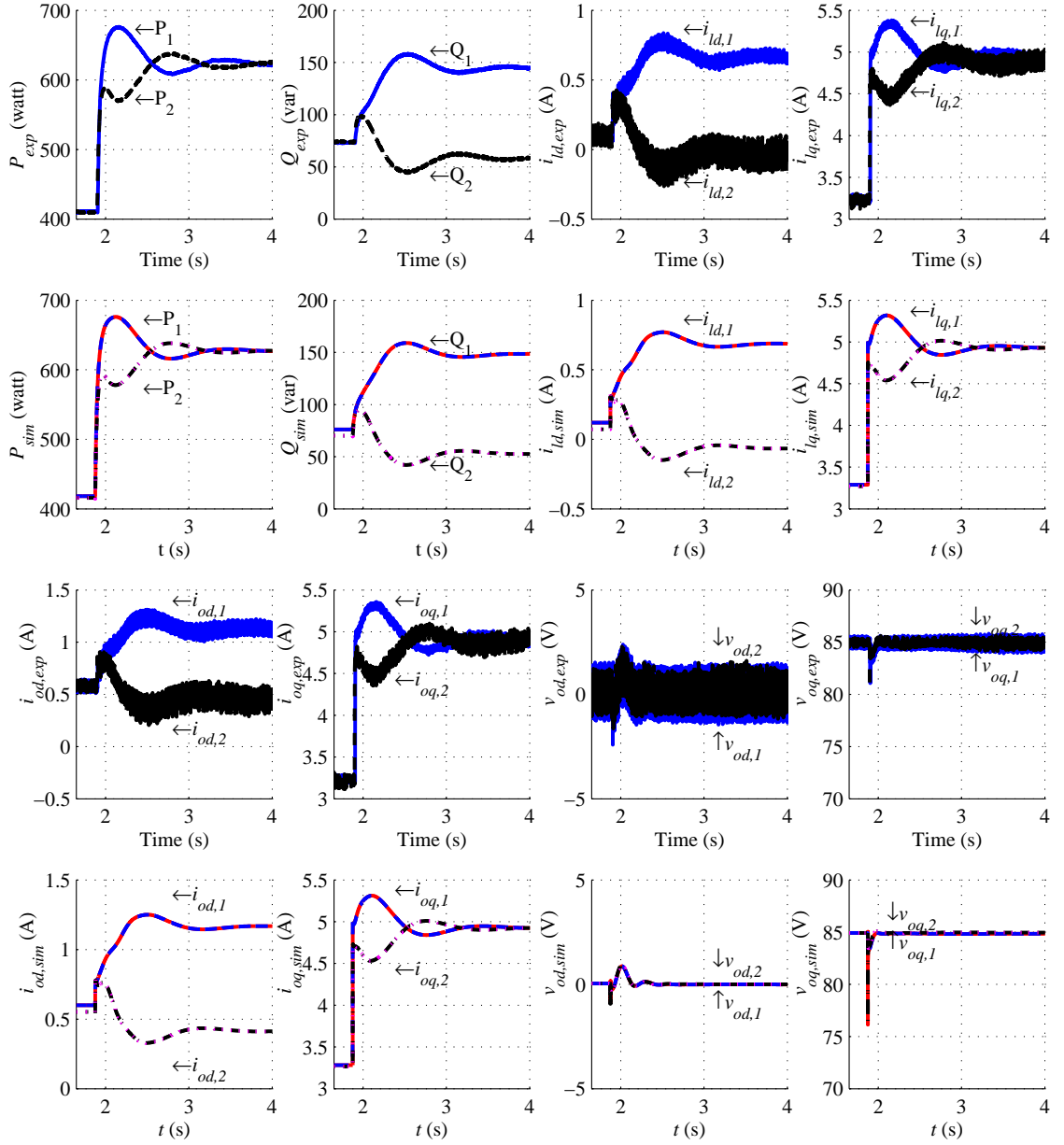
Figure 3.5. Verification of system dynamics using results from experiment, full order model simulation and reduced order model simulation

to be used for non-stiff differential equations and works better than other methods for such (non-stiff) systems. However, both ode15s and ode23s provide better simulation speed for stiff systems, the latter being less accurate than the former. These methods are useful once ode45 fails to provide a reasonable computational time during integration. These solvers
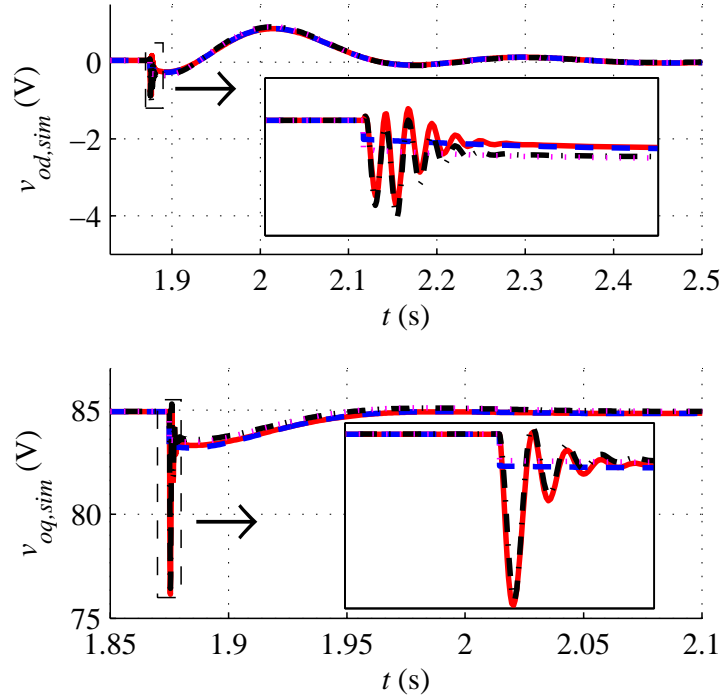
Figure 3.6. Fast states marked with rectangles, are oscillatory in the full order model but disappear in the reduced order model and become straight lines

are applied with both maximum step size and relative tolerance of 1×10^{-3}. In all cases, the Simulink profiler's time measurement's precision is 30 *ns* using a CPU clock speed of 3 *GHz*. The two bus simulation is extended for multibus systems. Full order state matrices are derived for these systems. Reduced order state matrices are generated using the algorithm provided in section III. The plots in Fig. 3.7 are obtained for 2, 3, 4, 5, 7 and 10 buses within the system. In all cases, load perturbation occurs at bus_1 with the same values of RL load. Similar controller gains, loads, and line parameters are used during system simulation and mathematical model building procedure.

Application of the model reduction algorithm converts the system from a stiff type to a non-stiff type. This conversion allows the use of ode45 solver for solving the slow state equations. the simulation time needed by ode45 to solve the reduced order model is
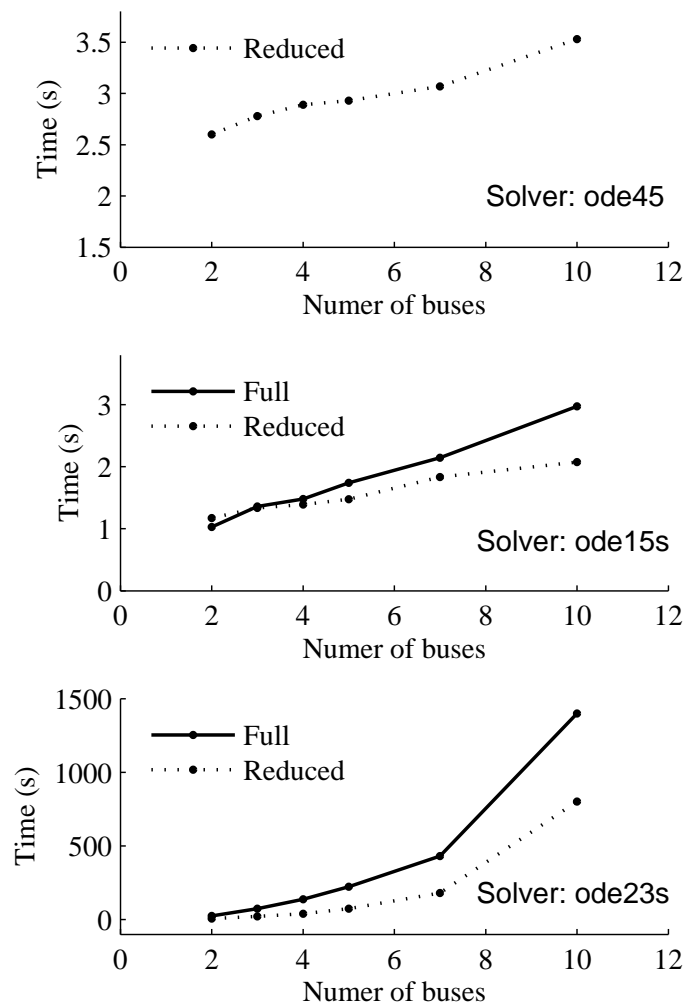
Figure 3.7. Comparison of simulation time using different Matlab solvers

comparable to the time needed by other solvers. When ode15s is used, the simulation time difference between the full order model and the reduced order model increased as more buses are added to the system. However, when the ode23s is used, the simulation time needed by both the full order models and the reduced order models is much higher than that needed by the ode15s.

The reduced models are then used in a multi-bus system. An example of such multibus system is IEEE-37 node distribution test feeder. The IEEE-37 bus is modified

for islanded microgrid application. The system load and line parameters are given in [14]. There are seven inverter at seven different buses as shown in Part - I of the paper. The overall system dynamics (in the small signal sense) is obtained using the model reduction algorithm developed in this paper. The plot of the active and reactive power change due to a step change in the load at 3 *s* is depicted in the Fig. 3.8.

The reduced order models (both grid-tied and islanded) obtained for the modified IEEE-37 bus test microgrid system are useful to predict the dynamics during microgrid's transition from the grid connected mode to the islanded mode. During this transition the inverter controllers switch from one operating mode to another. To simulate the effect of this transition, the small-signal models are arranged similar to the switched autonomous system in (28). The dynamics during microgrid transition are plotted in Fig. 3.9. Before the transition occurs, the inverters were supplying 5 *kW* and 1 *kVar* to the system. As soon the as the transition takes place the DER controllers switch to the droop mode and the inverters share the loads of the islanded system. In future, the stability of such switched linear autonomous system will be analyzed using the Markov jump linear system analysis as discussed in authors previous work [20].

3.5. CONCLUSION

This study examines the small-signal model of an inverter dominated islanded microgrid system. The full order model of the example 2 bus system had 36 states governing the overall system dynamics. Small-signal model of the proposed system possesses a two-time scale property. From the small model parameters a total of 15 slow dominating states are identified. The full scale system is reduced by applying the singular perturbation technique. An algorithm is developed for the model order reduction of islanded microgrid systems. This proposed algorithm is applied to the example system, thereby reducing the order of the system by 58.33%. The reduced system's accuracy is verified against not only
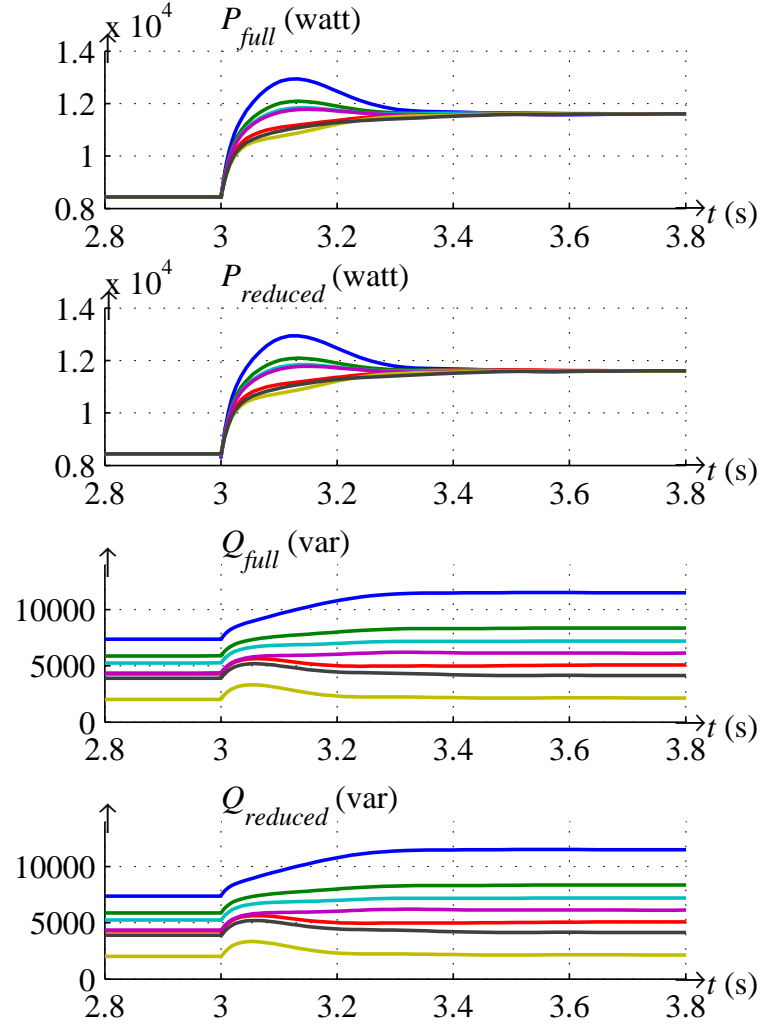
Figure 3.8. Inverter output powers - step change in the islanded microgrid load

the experimental results but also the full order model simulation results. The proposed two-bus system is extended for multi-bus systems. For each of these systems, a comparison of simulation times, taken by different solvers in Matlab/Simulink, are presented. The reduced order systems becomes non-stiff meaning that they are ideal for simulation using ode45 solver type, which has better accuracy compared ode15s or ode23s. Finally, the reduced order model is applied to a modified IEEE-37 bus system. The islanded system's dynamics are verified against the full order model. The reduced order grid-tied model (obtained from Part-I of this work), and the reduced order islanded system's model (discussed
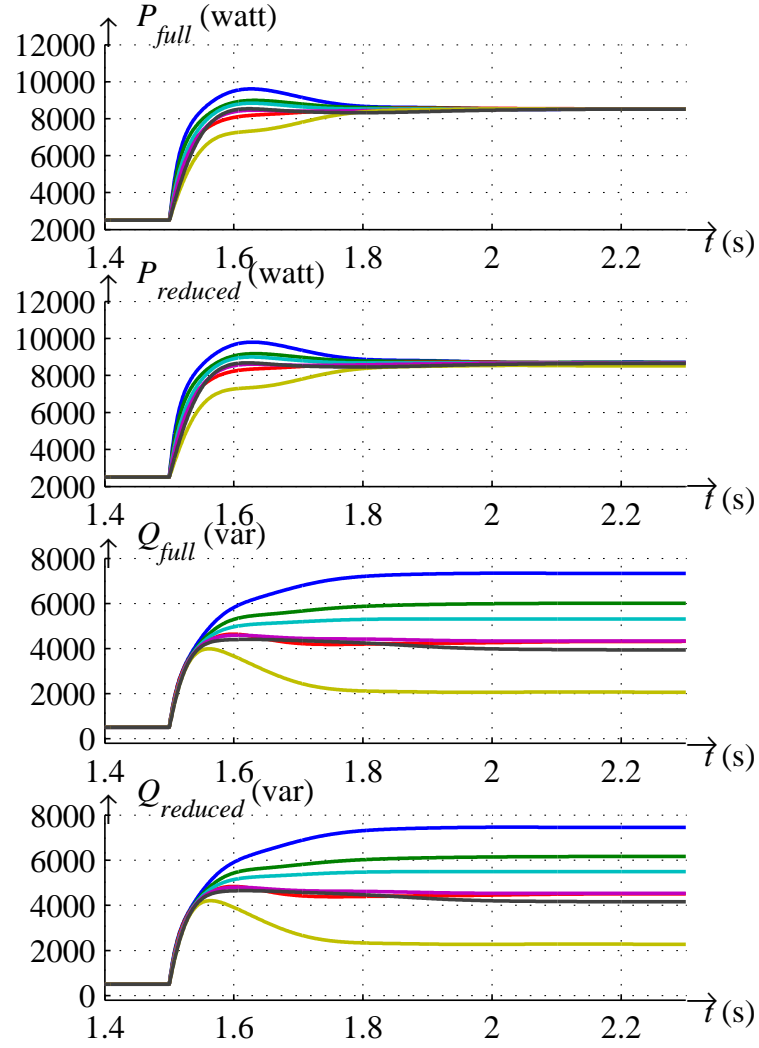
Figure 3.9. Inverter output powers during microgrid's transition

in this paper) are used to predict the microgrid's dynamic response during the grid-tied to islanded transition event.

3.6. REFERENCES

[1] X. Xu, R. M. Mathur, J. Jiang, G. J. Rogers, and P. Kundur, "Modeling of generators and their controls in power system simulations using singular perturbations," *Power Syst., IEEE Trans.*, vol. 13, no. 1, pp. 109–114, 1998.

[2] P. V. Kokotovic and P. Sannuti, "Singular perturbation method for reducing the model order in optimal control design," *Automatic Control, IEEE Transactions on*, vol. 13, no. 4, pp. 377–384, 1968.

[3] P. V. Kokotovic, R. E. O'Malley, and P. Sannuti, "Singular perturbations and order reduction in control theory—an overview," *Automatica*, vol. 12, no. 2, pp. 123–132, 1976.

[4] S. Ahmed-Zaid, P. W. Sauer, M. A. Pai, and M. Sarioglu, "Reduced order modeling of synchronous machines using singular perturbation," *Circuits and Systems, IEEE Transactions on*, vol. 29, no. 11, pp. 782–786, 1982.

[5] S. Pekarek, M. Lemanski, and E. Walters, "On the use of singular perturbations to neglect the dynamic saliency of synchronous machines," *IEEE Transactions on Energy Conversion*, vol. 17, no. 3, pp. 385–391, Sep. 2002.

[6] N. P. Singh, Y. P. Singh, and S. I. Ahson, "An iterative approach to reduced-order modeling of synchronous machines using singular perturbation," *Proc. of IEEE*, vol. 74, no. 6, pp. 892–893, Jun. 1986.

[7] X. Xu, R. M. Mathur, J. Jiang, G. J. Rogers, and P. Kundur, "Modeling effects of system frequency variations in induction motor dynamics using singular perturbations," *Power Systems, IEEE Transactions on*, vol. 15, no. 2, pp. 764–770, 2000.

[8] L. Cao and H. M. Schwartz, "Reduced-order models for feedback stabilization of linear systems with a singular perturbation model," *Asian Journal of Control*, vol. 7, no. 3, pp. 326–336, 2005.

[9] J. W. Kimball and P. T. Krein, "Singular perturbation theory for dc-dc converters and application to PFC converters," *IEEE Transactions on Power Electronics*, vol. 23, pp. 2970–2981, Nov. 2008.

[10] R. K. Varma, R. M. Mathur, G. J. Rogers, and P. Kundur, "Modeling effects of system frequency variation in long-term stability studies," *Power Systems, IEEE Transactions on*, vol. 11, no. 2, pp. 827–832, 1996.

[11] M. Huang, H. Xin, K. Wang, and D. Gan, "Estimating the stability region of singular perturbation power systems with saturation nonlinearities: an linear matrix inequality-based method," *IET Control Theory & Applications*, vol. 4, no. 3, pp. 351–361, Mar. 2010.

[12] R. M. Castro and J. M. Ferreira de Jesus, "A wind park reduced-order model using singular perturbations theory," *Energy Conversion, IEEE Transactions on*, vol. 11, no. 4, pp. 735–741, 1996.

[13] S. Chuangpishit and A. Tabesh, "Reduced model and control of diode-interfaced offshore wind farms with DC power systems," in *Electrical Power & Energy Conference (EPEC), 2013 IEEE*. IEEE, 2013, pp. 1–5.

[14] L. Luo and S. V. Dhople, "Spatiotemporal model reduction of inverter-based islanded microgrids," *IEEE Transactions on Energy Conversion*, pp. 1–10, 2014.

[15] V. Mariani, J. M. Guerrero, and F. Vasca, "Analysis of droop controlled parallel inverters in islanded microgrids."

[16] A. Davoudi, P. L. Chapman, J. Jatskevich, and H. Behjati, "Reduced-order dynamic modeling of multiple-winding power electronic magnetic components," *IEEE Transactions on Power Electronics*, vol. 27, no. 5, pp. 2220–2226, May 2012.

[17] I. Malloci, J. Daafouz, and C. Iung, "Stabilization of continuous-time singularly perturbed switched systems," in *Joint 48th IEEE Conference on Decision and Control and 28th Chinese Control Conference*, Shanghai, P.R. China, Dec. 2009.

[18] F. El Hachemi, M. Sigalotti, and J. Daafouz, "Stability analysis of singularly perturbed switched linear systems," *IEEE Transactions on Automatic Control*, vol. 57, no. 8, pp. 2116–2121, Aug. 2012.

[19] Y. Zhang, Y. Chen, and L. Xie, "Multi-scale integration and aggregation of power system modules for dynamic security assessment," in *Power and Energy Society General Meeting (PES), 2013 IEEE*. IEEE, 2013, pp. 1–5.

[20] M. Rasheduzzaman, T. Paul, and J. W. Kimball, "Markov jump linear system analysis of microgrid stability," in *American Control Conference (ACC), 2014*. IEEE, 2014, pp. 5062–5066.

[21] R. Phillips and P. V. Kokotovic, "A singular perturbation approach to modeling and control of markov chains," *Automatic Control, IEEE Transactions on*, vol. 26, no. 5, pp. 1087–1094, 1981.

[22] M. Rasheduzzaman, J. A. Mueller, and J. W. Kimball, "An accurate small-signal model of inverter-dominated islanded microgrids using dq reference frame," *IEEE Journal on Emerging and Selected Topics in Power Electronics*, 2014.

[23] P. V. Kokotovic, H. K. Khali, and J. O'Reilly, *Singular Perturbation Methods in Control: Analysis and Design*, ser. TJ213.K3924, 1999.

[24] D. Naidu, *Singular Perturbation Methodology in Control Systems*, Dec. 1987.

[25] P. V. Kokotovic, "A riccati equation for block-diagonalization of ill-conditioned systems," *Automatic Control, IEEE Transactions on*, vol. 20, no. 6, pp. 812 – 814, Dec. 1975.

[26] J. J. Allemong and P. V. Kokotovic, "Eigensensitivities in reduced order modeling," *IEEE Trans. Autom. Control*, vol. 25, no. 4, pp. 821–822, Aug. 1980.

[27] "Choose a solver - MATLAB and simulink," *Available: http://www.mathworks.com/help/simulink/ug/choosing-a-solver.html*.

[28] L. F. Shampine and M. W. Reichelt, "The MATLAB ODE suite," *SIAM J. Scientific Computing*, vol. 18, pp. 1–22, Jan. 1997.

IV. MARKOV JUMP LINEAR SYSTEM ANALYSIS OF MICROGRID STABILITY

Md. Rasheduzzaman, Tamal Paul, and Jonathan W. Kimball

Department of Electrical and Computer Engineering

Missouri University of Science & Technology, Rolla, MO 65409

ABSTRACT— In a typical microgrid, the power generation capacity is similar to the maximum total load. The low inertia of the system provides little margin for error in the power balance, both active and reactive, and requires rapid control response to load changes. In the present work, a microgrid is modeled as a Markov jump linear system (MJLS). An MJLS is a dynamic system with continuous states governed by one of a set of linear systems, and a continuous-time Markov process that determines which linear system is active. When the discrete state of the Markov process changes, there is a "jump" in the dynamics of the continuous states. In addition, the jump may be impulsive.

The present work first explores impulsive MJLS stability. Conservative bounds on the expected value of the state are determined from a combination of the Markov process parameters, the dynamics of each linear system, and the magnitude of the impulses. Then the microgrid model is cast into the MJLS framework and stability analysis is performed. The conclusions are verified with detailed simulations.

Index Terms— Markov jump linear system, almost sure stability, microgrid

4.1. INTRODUCTION

Microgrids have gained significant attention in recent years in several application scenarios. Here, a microgrid is defined as a relatively small, closed, finite-inertia power system with generation capacity similar to the maximum load. Often, but not always, energy storage is included. At the larger end of the scale, a microgrid is a portion of the existing power distribution network that includes sufficient generation capacity to operate islanded. This type of microgrid is seen as a means to increase renewable energy market penetration, such as in the FREEDM system [1]. Similarly, military forward operating bases (FOBs) may be operated as microgrids, connecting to the local power grid when available or remaining islanded otherwise [2]. Microgrids may also be found on "vehicles," meaning any structure that is not fixed in location: naval ships [3], locomotives, hybrid electric vehicles, and more electric aircraft [4]. A microgrid may rely on either ac or dc power distribution. The present work will focus on ac systems, but many of the methods discussed apply equally to dc systems.

One challenge in a microgrid is that there is less of a buffer in power generation to accommodate changes in load, along with a tighter coupling among the various elements in the system. A variety of analysis techniques have been proposed to address the stability of small power systems, such as [5, 6, 7, 8].

The stability of microgrids may be studied by framing them as Markov jump linear systems (MJLSs). An MJLS is composed of two coupled systems. First is a continuous-time Markov process, which has some number of discrete states, N. For each discrete state i, there is a transition rate λ_i that corresponds to an exponential random variable (the dwell time, τ_i, spent in state i) and a set of transition probabilities $\pi_{i,j}$ that determine the relative probabilities of transitioning to one of the other discrete states. Here, the Markov process identifies which loads are switched "on" in the microgrid, and a particular discrete state corresponds to a particular combination of active loads.

To complete the MJLS, each discrete state of the Markov process is mapped to a linear system with continuous states, either discrete-time or continuous-time. Here, the linear systems are all continuous-time small-signal models of the microgrid, each linearized around a different nominal operating point. Conceptually, an MJLS lies somewhere between a hybrid automaton [9] and a switched system [10]. The switching has some structure, like a hybrid automaton, but the timing is stochastic. Therefore, concepts like *almost sure stability* [11, 12, 13] are relevant.

To extend the MJLS framework, each discrete state transition may also include a change in the value of the continuous states, that is, an impulse. Impulsive MJLSs have received little study. In [14], some useful stability bounds are determined, but only for the case where a strict subset of the possible discrete state transitions result in an impulse and the impulses are separated by some minimum dwell time. For the generic case, where every transition may be impulsive and dwell times are exponentially distributed (and therefore may be arbitrarily small), no stability results are available in the literature. The present work therefore derives bounds for an impulsive MJLS, where the impulses correspond to the changes in steady-state operating point when transitioning between small-signal models.

This paper is structured as follows. First, impulsive MJLS stability is studied, resulting in a bound on the expected value of the state for a restricted class of systems. The bound is conservative for the fully generic case, but is useful for typical microgrids. Next, a model (abstracted from [15]) for a microgrid composed primarily of renewable energy sources, and therefore using switching power converters, is presented. The microgrid model is cast into the impulsive MJLS framework and its stability is studied. Simulations verify the analysis.

4.2. IMPULSIVE MJLS STABILITY ANALYSIS

4.2.1. Preliminaries. Consider a switched linear system of the form

$$\dot{\tilde{x}} = A_{\sigma_j}\tilde{x} \tag{4.1}$$

$$\tilde{x}(t_j^+) = \tilde{x}(t_j) + \beta_j \tag{4.2}$$

The various system models are indexed by $\sigma \in \mathscr{S} = \{0,1,2,...\}$, the output of a Markov process. In general, $\mathscr{S}$ may be finite or countably infinite. These are all small-signal models, where the real (large-signal) state is

$$x(t) = \tilde{x}(t) + X_{\sigma_j} \tag{4.3}$$

including the nominal operating point X_{σ_j}. The jth transition in the Markov process occurs at time $t = t_j$. The dwell time after the jth transition then is $\tau_j = t_{j+1} - t_j$, so that

$$t_j = \sum_{i=0}^{j-1} \tau_i \tag{4.4}$$

The corresponding transition from σ_{j-1} to σ_j requires an impulsive change in $\tilde{x}$ because the real state, x, is continuous. Therefore,

$$\beta_j = X_{\sigma_{j-1}} - X_{\sigma_j} \tag{4.5}$$

The evolution of x and $\tilde{x}$ for a one-dimensional system is shown conceptually in Fig. 4.1. Whether $\mathscr{S}$ is finite or infinite, we assume that the impulsive changes are bounded, so that

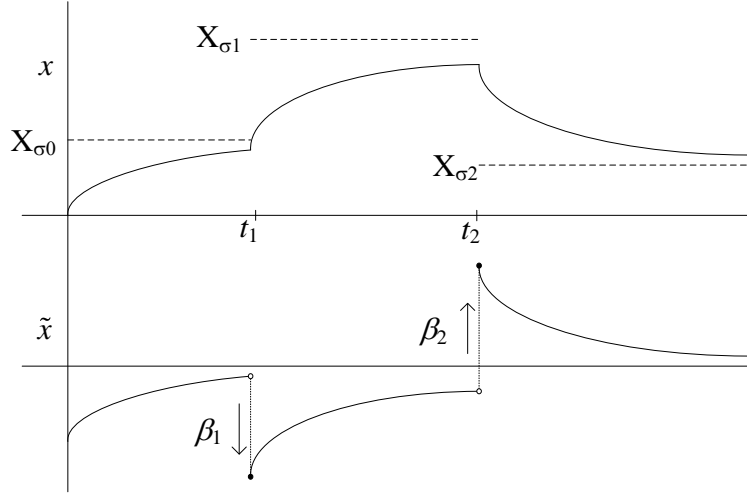$$||\beta_j|| \leq \beta_{max} \, \forall j \tag{4.6}$$

Figure 4.1. Example evolution of a one-dimensional dynamical system with two impulsive transitions

for some β_{max}. We also assume that each system model is stable, that is, A_σ is Hurwitz $\forall \sigma$. Therefore, the state transition matrices Φ_σ given by

$$\Phi_\sigma(t,0) = e^{A_\sigma t} \tag{4.7}$$

may all be dominated by exponentials of the form

$$||\Phi_\sigma(t,0)|| \leq e^{a_\sigma + b_\sigma t}, \ b_\sigma < 0 \tag{4.8}$$

Just as the impulsive changes are bounded, a_σ and b_σ are bounded by a_{max} and b_{max} respectively (remembering that $b_{max} < 0$).

The value of the discrete state σ is determined by a time-homogeneous, continuous-time Markov process. The transition rate directly between two different states x, y is defined as $\lambda(x,y)$. The total transition rate *out of* state x is

$$\lambda(x) = \sum_{y \neq x} \lambda(x,y) \tag{4.9}$$

The transition rates correspond to exponentially-distributed random variables. Therefore,

$$E\left[\tau_j\right] = \frac{1}{\lambda(\sigma_j)} \tag{4.10}$$

4.2.2. Bounds on the State. Given the generic impulsive MJLS framework described above, hard bounds on the state are not possible. In any finite, non-zero time, there is a non-zero probability of an arbitrarily large number of switching events. However, one may determine bounds on the expected value of the state. The usefulness of the bounds depends on the transition rates, the continuous state dynamics, and the maximum possible impulse.

Because each continuous system model is linear time-invariant, the solution of the switched system may be found for a given switching sequence. For an initial state of x_0, the state after the jth transition is

$$x(t_j^+) = \left(\prod_{i=j-1}^{0} e^{A_{\sigma_i}\tau_i}\right) x_0 + \sum_{k=1}^{j-1}\left(\prod_{i=j-1}^{k} e^{A_{\sigma_i}\tau_i}\right)\beta_k + \beta_j \tag{4.11}$$

The order of multiplication is important at this stage because all elements are matrices or vectors. However, from (4.8), the magnitudes of the matrix exponentials may be bounded with scalar exponentials. Furthermore, because the dwell times are exponentially distributed, the bounds on the expected values of the matrix exponentials may be found explicitly,

$$E\left[\left\|e^{A_{\sigma_i}\tau_i}\right\|\right] \leq \frac{e^{a_{\sigma_i}}\lambda(\sigma_i)}{\lambda(\sigma_i) - b_{\sigma_i}} \triangleq \gamma_{\sigma_i} \tag{4.12}$$

By construction, $\gamma_\sigma > 0$, and because each term in (4.12) is bounded, $\gamma_\sigma \leq \gamma_{max} \forall \sigma$. Now the expected value of the first product of (4.11) may be bounded,

$$E\left[\left\|\left(\prod_{i=j-1}^{0} e^{A_{\sigma_i}\tau_i}\right)\right\|\right] \leq \prod_{i=j-1}^{0} \gamma_{\sigma_i} \leq \gamma_{max}^j \tag{4.13}$$

Clearly, if $\gamma_{max} < 1$, then this product will converge to zero as $j \to \infty$. Therefore, the contribution to $x(t_j^+)$ due to initial conditions will decay with a rate that depends on both the transition rates of the Markov process and the dynamics of the continuous systems.

There will also be a significant contribution, though, due to the impulses. Using similar reasoning,

$$E\left[\left\|\sum_{k=1}^{j-1}\left(\prod_{i=j-1}^{k} e^{A_{\sigma_i}\tau_i}\right)\beta_k\right\|\right] \leq \beta_{max}\gamma_{max}\frac{1-\gamma_{max}^{j-1}}{1-\gamma_{max}} \tag{4.14}$$

Again, convergence requires $\gamma_{max} < 1$, but in practice requires a significant margin. For example, if $\gamma_{max} = 0.9$, then the asymptote for (4.14) is $9\beta_{max}$—possibly significant growth, depending on the magnitudes of the impulses. Combining all of the terms in (4.11-4.14),

$$E\left[\left\|x(t_j^+)\right\|\right] \leq \gamma_{max}^j\|x_0\| + \beta_{max}\frac{1-\gamma_{max}^j}{1-\gamma_{max}} \tag{4.15}$$

and in the limit,

$$\lim_{j\to\infty} E[\|x(t_j^+)\|] \leq \beta_{max}\frac{1}{1-\gamma_{max}} \tag{4.16}$$

Unfortunately, this bound can be quite large for certain systems, particularly those with lightly-damped eigenvalues or systems that have a wide range in eigenvalues. Then the lightly-damped modes dictate the $e^{a_{\sigma_i}}$ factor and the slow eigenvalues determine b_{σ_i}. In these situations, another approach is needed.

One way to compute a matrix exponential is to transform the matrix using eigen-vectors. A solution is found to $A_\sigma V_\sigma = V_\sigma D_\sigma$, where D_σ is a diagonal matrix of the eigen-values. Then

$$e^{A_\sigma t} = V_\sigma e^{D_\sigma t}V_\sigma^{-1} \tag{4.17}$$

Although this approach is not numerically stable in general, it is useful in the present case. The product in (4.14) will contain factors like $V_{\sigma+1}^{-1}V_\sigma$, which is generally small. Define

$$W_{max} = \max_\sigma ||V_{\sigma+1}^{-1}V_\sigma|| \tag{4.18}$$

$$M_{max} = \max_\sigma ||V_\sigma|| \tag{4.19}$$

Then the exponential in (4.17) may be dominated by a scalar exponential, now with no growth term (just $e^{b_\sigma t}$). Each term in the summation in (4.14) is dominated by

$$exp\left(\sum_{i=k}^{j-1} b_{\sigma_i}\tau_i\right) V_{\sigma_{j-1}} W_{max}^{j-1} V_{\sigma_k}^{-1}\beta_k \tag{4.20}$$

The final two-factor product in (4.20) may be bounded by

$$||V_{\sigma_k}^{-1}\beta_k|| \le \delta_{max} \tag{4.21}$$

Defining

$$\hat{\gamma}_\sigma = \frac{\lambda(\sigma)}{\lambda(\sigma) - b_\sigma} \tag{4.22}$$

and following the same logic as above, we may find a new bound,

$$\lim_{j\to\infty} E[||x(t_j^+)||] \le \frac{M_{max}\delta_{max}}{1 - W_{max}\hat{\gamma}_{max}} \tag{4.23}$$

as long as $W_{max}\hat{\gamma}_{max} < 1$.

In summary, the initial assumption that each switching state corresponds to a stable system and an additional assumption regarding the transition rates ensures that there is a net decrease, on average, between switching events. The amount of decrease and the size of the impulses determine the long-term bound on the expected value of the magnitude of the state according to (4.15-4.16) or (4.23).

4.3. MICROGRID MODEL

Consider the simple microgrid shown in Fig. 4.2. A typical microgrid is composed of one or more power converters that interface between a renewable energy source or energy storage device and the grid, at least one fixed load, and one or more additional loads that may switch on or off arbitrarily. Conventional (rotating) generators may also be included, but are not considered here. For each combination of loads, there is a different nominal operating point, and therefore a different small-signal model. For simplicity, only one switching load (on bus 1) and two inverters (labeled INV in Fig. 4.2) will be considered here. The loads on the two buses are shown in Fig. 4.3.
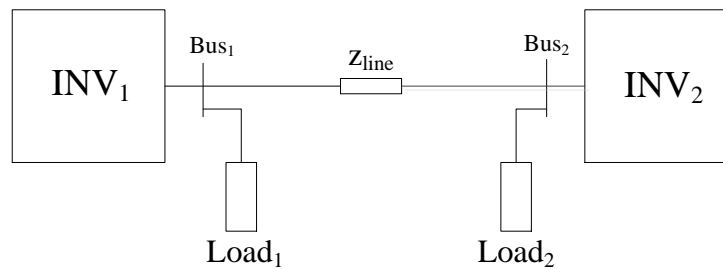

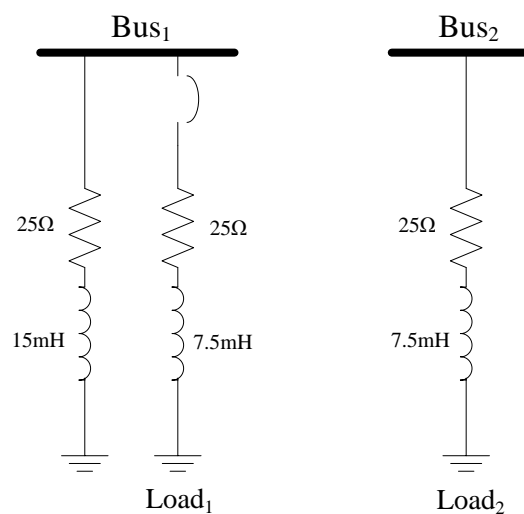Figure 4.2. Microgrid under study

Figure 4.3. Load configuration

Each inverter includes the power hardware and control system shown in Fig. 4.4. This is a relatively standard architecture that is analyzed more thoroughly in [15]. The output stage uses space vector pulsewidth modulation (SVPWM) and an LC filter to achieve high efficiency and low ripple. All three-phase variables (denoted abc) are converted to a rotating reference frame (denoted dq). The rotating reference frame frequency and phase are determined with a phase-locked loop (PLL). Power (active, P, and reactive, Q) is computed and filtered. Droop controllers determine the output frequency from P and the output voltage from Q. Finally, voltage and current control loops are used to determine the voltage vector commands for the SVPWM block.

The complete system in Fig. 4.2 has 33 state variables, including both physical variables and internal control variables. Details are omitted here due to space constraints. Nonlinearity arises primarily in the computation of active and reactive power (p and q respectively),

$$p = \frac{3}{2}(v_{od}i_{od} + v_{oq}i_{oq}) \tag{4.24}$$

$$q = \frac{3}{2}(v_{oq}i_{od} - v_{od}i_{oq}) \tag{4.25}$$

where v_o and i_o are the output terminal voltage and current respectively, and are represented with d and q components in a rotating reference frame. There is also a rotation between the dq frames of the two inverters (by an angle δ) that is nonlinear. The desired linear systems are determined by linearizing the nonlinear model around operating points corresponding to different load conditions.

Fig. 4.5 shows the eigenvalues of the small-signal model when the switched load is turned off. Notice the cluster near the origin, the highly-damped fast modes, and the lightly-damped modes. There are also two eigenvalue pairs at $-6.10 \times 10^6 \pm j375.4$ and $-2.10 \times 10^6 \pm j376.0$, not shown so that the dominant eigenvalues are more visible. The
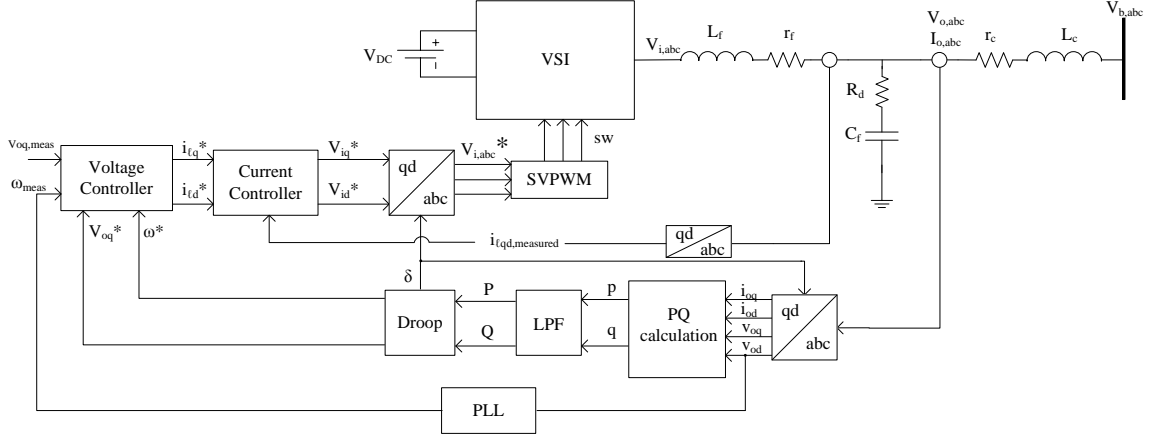
Figure 4.4. Inverter internal details, including power hardware and controller

eigenvalues move when the load switches, but the overall qualitative nature of the eigen-value plot remains the same.

The system may be normalized by dividing all voltages by the rated voltage (170 V), all power values by the rated power (1 kVA), all frequencies by the rated frequency (377 rad/s), and currents and passive elements accordingly. Two load points are considered. The bounds corresponding to (4.8) are

$$||\Phi_1(t,0)|| \leq e^{6.3077 - 4.2577t} \tag{4.26}$$

$$||\Phi_2(t,0)|| \leq e^{6.1668 - 3.9339t} \tag{4.27}$$

The impulse magnitude for the normalized state is $\beta_{max} = 11.505$, found by subtracting the two steady-state operating points. Because of lightly-damped eigenvalues, the bound of (4.16) is extremely loose and not useful. The bound of (4.23), scaled by $\delta_{max} = 13.89$ and $M_{max} = 2.3943$, is shown in Fig. 4.6 for varying transition rate. A transition rate of $\lambda = 2.5s^{-1}$ was chosen, so that the ultimate bound on the magnitude of the normalized state is 85.4.
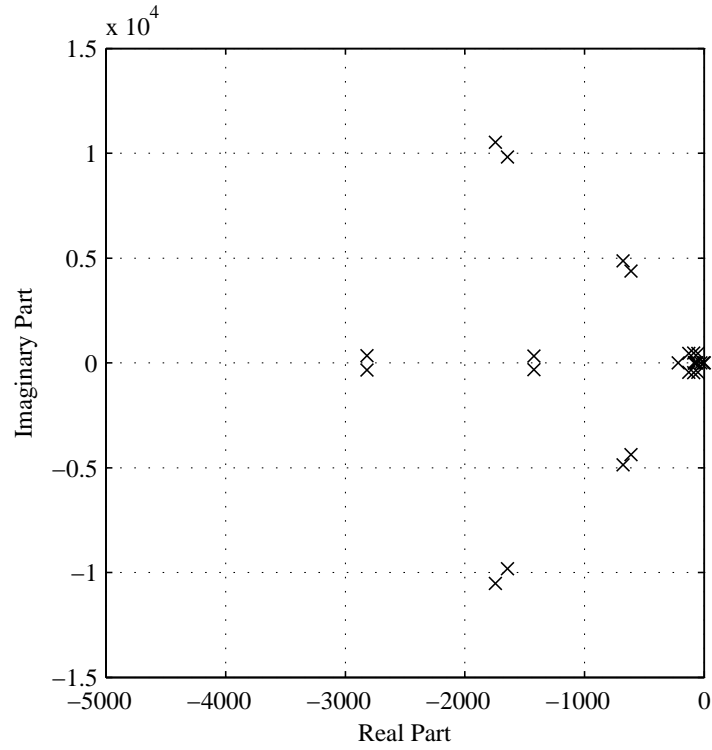
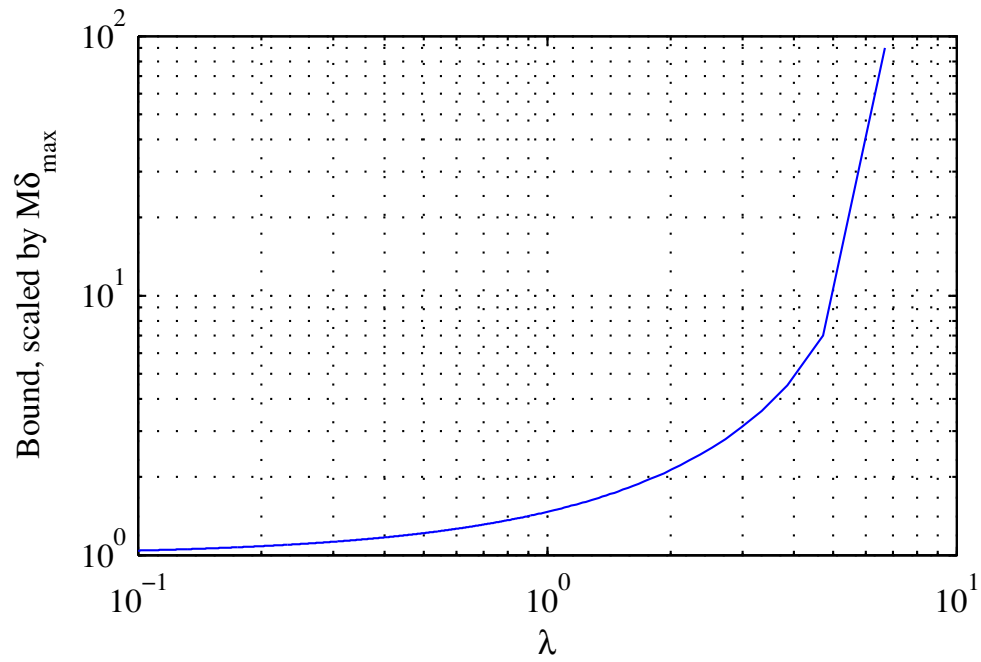Figure 4.5. Eigenvalues for A_1. Two fast, highly-damped pairs have been truncated as noted in the text

Figure 4.6. Variation in the bound on the magnitude of the state as transition rate, λ, varies. Plotted is the scale factor that excludes M_{max} and δ_{max}

A simulation was performed using Simulink. First, a vector of random switching times was constructed using the given λ. At each switching instance, the nominal operating point and the system dynamics were switched. The small-signal, normalized state vector was saved, and its magnitude computed. Fig. 4.7 shows the simulation result compared against the computed bound.

4.4. CONCLUSIONS

A correspondence was established between a microgrid and an impulsive MJLS. The mathematical relationship enables further study and application of results from the control systems community to this emerging application. Furthermore, a bound on the expected value of the continuous state was derived for a generic impulsive MJLS.
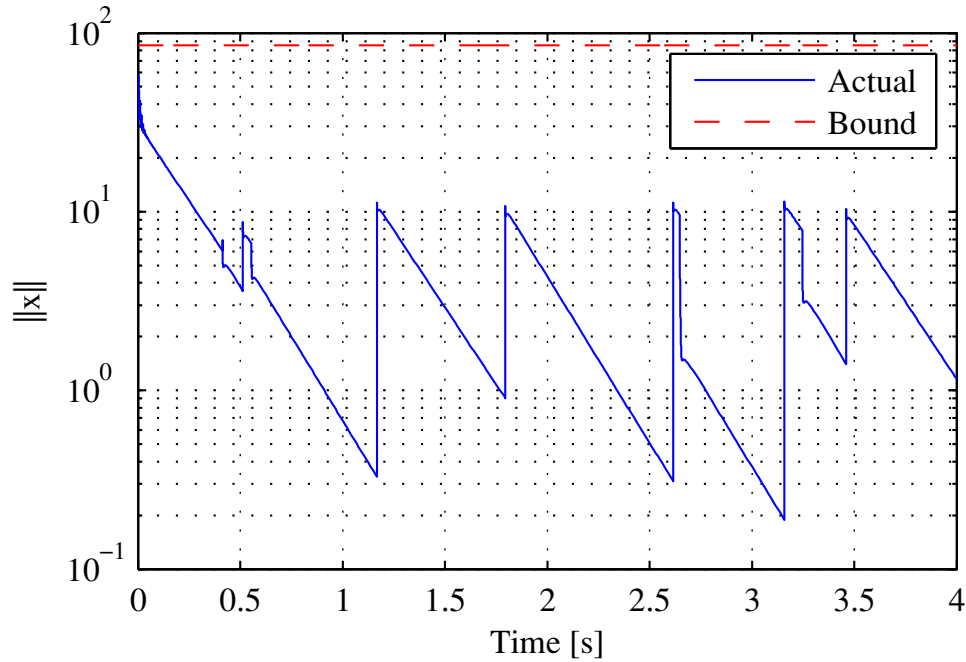

Figure 4.7. Simulated results using one switched load and normalized state vector. The impulses remain below the derived bound

The primary drawback of this approach is the looseness of the bound. Ideally, we would like a bound on terms of the general form $||\Phi_{\sigma_j}(\tau_j, 0)\beta_j||$. Some of the information has been abstracted away in the bounding process. Future work will focus on retaining more information so that the bounds may be made tighter. The results presented here are still useful for systems with highly-damped eigenvalues that are similar in magnitude.

4.5. ACKNOWLEDGMENTS

4.6. REFERENCES

[1] A. Q. Huang, M. L. Crow, G. T. Heydt, J. P. Zheng, and S. J. Dale, "The Future Renewable Electric Energy Delivery and Management (FREEDM) System: The energy internet," *Proceedings of the IEEE*, vol. 99, no. 1, pp. 133–148, Jan. 2011.

[2] T. A. Nguyen and M. L. Crow, "Optimization in energy and power management for renewable-diesel microgrids using dynamic programming algorithm," in *Proceedings of the IEEE International Conference on Cyber Technology in Automation, Control, and Intelligent Systems*, 2012, pp. 11–16.

[3] J. M. Crider and S. D. Sudhoff, "Reducing impact of pulsed power loads on microgrid power systems," *IEEE Transactions on Smart Grid*, vol. 1, no. 3, December 2010.

[4] P. Magne and B. Nahid-Mobarakeh, "Active stabilization of DC microgrids without remote sensors for More Electric Aircraft," *IEEE Transactions on Industry Applications*, in press.

[5] S. V. Iyer, M. N. Belur, and M. C. Chandorkar, "A generalized computational method to determine stability of a multi-inverter microgrid," *IEEE Transactions on Power Electronics*, vol. 25, no. 9, pp. 2420–2432, September 2010.

[6] N. Bottrell, M. Prodanovic, and T. C. Green, "Dynamic stability of a microgrid with an active load," *IEEE Transactions on Power Electronics*, vol. 28, no. 11, pp. 5107–5119, November 2013.

[7] R. Majumder, "Some aspects of stability in microgrids," *IEEE Transactions on Power Systems*, vol. 28, no. 3, pp. 3243–3252, August 2013.

[8] R. Turner, S. Walton, and R. Duke, "A case study on the application of the Nyquist stability criterion as applied to interconnected loads and sources on grids," *IEEE Transactions on Industrial Electronics*, vol. 60, no. 7, pp. 2740–2749, July 2013.

[9] T. A. Henzinger, "The theory of hybrid automata," in *Proceedings of the IEEE Symposium on Logic in Computer Science*, 1996, pp. 278–292.

[10] D. Liberzon, *Switching in Systems and Control*.   Boston: Birkhauser, 2003.

[11] C. Li, M. Z. Q. Chen, J. Lam, and X. Mao, "On exponential almost sure stability of random jump systems," *IEEE Transactions on Automatic Control*, vol. 57, pp. 3064–3077, Dec. 2012.

[12] P. Bolzern, P. Colaneri, and G. De Nicolao, "On almost sure stability of continuous-time Markov jump linear systems," *Automatica*, vol. 42, pp. 983–988, 2006.

[13] ——, "Almost sure stability of Markov jump linear systems with deterministic switching," *IEEE Transactions on Automatic Control*, vol. 58, pp. 209–213, Jan. 2013.

[14] G. Liju and W. Yuqiang, "Exponential stability of impulsive jump linear systems with Markov process," *Journal of Systems Engineering and Electronics*, vol. 18, no. 2, pp. 304–310, 2007.

[15] M. Rasheduzzaman, J. Mueller, and J. W. Kimball, "Small-signal modeling of a three-phase isolated inverter with both voltage and frequency droop control," in *Proceedings of the IEEE Applied Power Electronics Conference 2014*, 2014, pp. 1008–1015.

SECTION

2. CONCLUSION AND FUTURE WORK

This dissertation presents the modeling of microgrid system. The first paper presents an accurate small-signal model of a multiple inverter microgrid system operating in islanded mode. Non-linear dynamical equations describing the system dynamics are presented. These nonlinear equations are linearized around stable operating points to develop the small-signal model of the system. Load perturbation is done to study the system dynamics. The accuracy of the model is assessed through comparison to simulation and experimental results. An eigenvalue analysis is done using the small-signal model to determine the stability of the system. Importance of the passive damping resistor is discussed using the eigenvalue anaylsis.

In the second paper, a small-signal model is developed for a grid-tied system. The system is then reduced applying the singular perturbation algorithm. The reduced order model is compared and its accuracy is assessed using experimental results. The model is then applied to a a modified IEEE-37 node distribution test feeder. The reduced order model eliminates the issue with the 'stiff' solver type and runs much faster than the full order model when simulated.

In the third paper, a reduced order model is developed for the islanded system discussed in the first paper. The reduced system's accuracy is verified against the full order model simulation results. The proposed two-bus system is extended for multi-bus systems. For each of these systems, a comparison of simulation times, taken by different solvers in Matlab/Simulink, are presented. Finally, the reduced order model is applied to a modified IEEE-37 bus system. The islanded system's dynamics are verified against the full

order model. The reduced order grid-tied model, and the reduced order islanded system's model are used to predict the microgrid's dynamic response during the grid-tied to islanded transition event.

In the fourth and the final paper, the stability of the islanded microgrid is studied with the help of MJLS Analysis. A correspondence was established between a microgrid and an impulsive MJLS. The mathematical relationship enables further study and application of results from the control systems community to this emerging application. Furthermore, a bound on the expected value of the continuous state was derived for a generic impulsive MJLS.

The models that are developed in this dissertation could be applied to any standard microgrid system. However, the models suffer from couple of disadvantages. The current controllers are modeled with the conventional PI controllers although they are not completely decoupled. The passive damping resistors improve the system stability but contributes to some loss. This loss could be avoided using the active damping technique. In future, the model needs to account for the active damping. The dq based PLL works better for a balanced system. Different kind of PLL design is suggested to make the model work under unbalanced conditions. The system performance deteriorates under non-linear loading. This needs further investigation in the future work.

VITA

Md Rasheduzzaman (S'12) received the B.S. degree from the Department of Electrical and Electronic Engineering, Chittagong University of Engineering and Technology, Chittagong, Bangladesh, in 2006, and the M.S. degree from the Department of Electrical and Computer Engineering, Purdue University, Calumet, IN, USA, in 2010. He is currently pursuing the Ph.D. degree in electrical engineering with the Missouri University of Science and Technology, Rolla, MO, USA.

His current research interests include power systems and power electronics, application of synchronous generators and inverters in ac microgrid, and design and analysis of microsource controllers for stable operation during grid connected and islanded mode of operations.